Complex Zeros of the Partition Function in Lattice Quantum Chromodynamics

Thesis presented by

Alan James Bell

for the degree of

Doctor of Philosophy

Department of Physics and Astronomy

The University of Glasgow

ProQuest LLC.
789 East Eisenhower Parkway
P.O. Box 1346
Ann Arbor, MI 48106 – 1346

To my family.

Declaration

The first three chapters of this thesis are chiefly a review of the theoretical background and previous work in the field. The work in chapters 4,5 and 6 was done in collaboration with Ian Barbour and, in various combinations, Elyakum Klepfish, Tassos Vladikas and Gaetano Salina. Chapter 7 constitutes a re-analysis of previous results using our new method.

Acknowledgements

I would like to thank those people with whom I have collaborated on various parts of this work: Ely Klepfish, Tassos Vladikas, Gaetano Salina and especially Ian Barbour who initiated the project and supervised my research. I am also grateful for many useful discussions with Christine Davies, Ron Crawford, Simon Hands and David Henty. Ron is also due many thanks for his careful reading of this thesis.

I would also like to thank all those friends who made my stay in Glasgow so pleasant, and of course my family who have been so supportive throughout my studies.

The numerical work was carried out on the IBM 3090 computers at CERN, Rutherford Appleton Laboratory and IBM-ECSEC(Rome) and on the Cray X-MP at RAL.

I am grateful to the Science and Engineering Research Council for a research studentship.

Contents

Abstract

The theory of Lee and Yang, which relates the distribution of the zeros of the partition function to the phase structure of a system, is applied to lattice field theory with dynamical fermions.

A method is described in which the partition function is evaluated as a finite polynomial in either the bare fermion mass or the 'fugacity'. The roots of this polynomial which are relevant to the physics, *i.e.*those close to the real axis, are then studied.

The partition function zeros are first studied in the fermion mass plane for $SU(3)$, $SU(2)$ and $U(1)$ gauge theories with four flavours of staggered fermions in the infinite coupling limit. Differences are observed in the distributions of zeros on finite lattices, but all are consistent with the expected critical point at $ma = 0$ on an infinite lattice. The $SU(3)$ and $U(1)$ calculations are then extended to weaker couplings and, in the $SU(3)$ case, to larger systems.

In Chapter 7 we perform the expansion in the fugacity plane. The Grand Canonical Partition Function is expanded in terms of Canonical Partition Functions for fixed fermion number. The distributions of zeros give strong evidence for the existence, or otherwise, of a phase transition at finite chemical potential.

Chapter 1

Introduction

1.1

Quantum Chromodynamics is the field theory of the strong interactions between quarks and gluons. It is described by the Lagrange density

$$\mathcal{L}_{QCD} = -\frac{1}{2g^2}\,\mathrm{Tr}\,F_{\mu\nu}F^{\mu\nu} + \sum_f \overline{\psi}(i\not{\delta} + \not{A} - m)\psi \tag{1.1}$$

$$F_{\mu\nu} = \delta_\mu A_\nu - \delta_\nu A_\mu + i[A_\mu, A_\nu] \tag{1.2}$$

$$A_\mu = g A^a_\mu T_a \tag{1.3}$$

and T_a is a representation of the Lie algebra of the $SU(3)$ gauge group.

Calculations based on a weak coupling, perturbative expansion around $g = 0$ have been very successful in predicting the high-energy, short distance, behaviour of the theory as probed in collider type experiments. These Feynman diagram techniques are valid in this regime since QCD is an asymptotically free theory. The coupling tends to zero at short distances. Low order perturbative calculations, however, are not valid in the low energy regime where the coupling diverges and we know that quarks are confined in colour singlets.

Renormalisation group calculations predict that hadron masses and $\langle\overline{\psi}\psi\rangle$ will

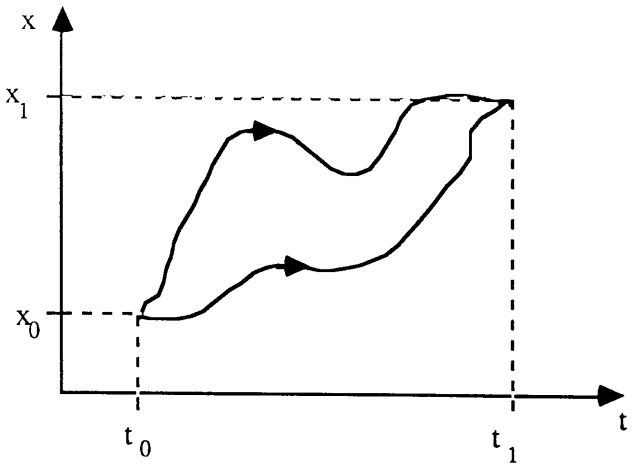

Figure 1.1: Two contributions to the quantum mechanical path integral.

be related to a mass scale introduced by the regularisation scheme.

$$m_H,\ \left\langle \overline{\psi}\psi \right\rangle \sim \Lambda = \text{const. } e^{-\frac{1}{Cg^2(a)}} \tag{1.4}$$

$g(a)$ is the coupling at length scale a. Equation(1.4) has an essential singularity at $g(a) = 0$. This means that it has no perturbative expansion. Hadron masses, chiral symmetry breaking and confinement are therefore inherently non-perturbative and in order to study them we require a non-perturbative regularisation scheme which can be applied directly to the fields, rather than to Feynman diagrams. The lattice gives us such a scheme.

1.2 Introduction to Lattice Gauge Theory

1.2.1 Path Integrals and Statistical Mechanics

The Feynman path integral formulation of quantum mechanics[1] gives us the probability amplitude for a particle at a point $(t_0, \underline{x}_0)$ to propagate to a point $(t_1, \underline{x}_1)$.

$$G(\underline{x}_0, t_0, \underline{x}_1, t_1) = \sum_{\text{all paths}} e^{i\int_{t_0}^{t_1} L(x(t),\dot{x}(t))dt} \tag{1.5}$$

The sum extends over all possible paths between the initial and final points This infinite sum may be replaced by a functional integral over all paths. (Figure 1.1) $L(x, \dot{x})$ is the classical Lagrangian for the system.

We may generalise this to quantum field theory. Let us consider a single scalar field, ϕ. Since the field is simply a function of the space-time coordinates, we may write the partition function — the generating functional for vacuum diagrams — as

$$Z = \int_{\text{field configs}} [d\phi]\, e^{i \int d\tau \int d^3x\, \mathcal{L}(\phi, \delta_\mu \phi)} \tag{1.6}$$

where $\mathcal{L}(\phi, \delta_\mu \phi)$ is the Lagrangian Density function.

Expectation values of time ordered products are calculated with the complex measure

$$\frac{1}{Z} e^{i \int d\tau \int d^3x\, \mathcal{L}} \tag{1.7}$$

$$\langle \Omega | \, T[\phi_1, \phi_2] \, | \Omega \rangle = Z^{-1} \int [d\phi]\, \phi_1 \phi_2 e^{i \int d\tau \int d^3x\, \mathcal{L}(\phi, \delta_\mu \phi)} \tag{1.8}$$

where $|\Omega\rangle$ is the vacuum.

If we now perform the analytic continuation $t \rightarrow i x_4$ ($x_4 \in \Re$) we obtain a *real* measure similar to the Boltzmann factor in statistical mechanics.

$$\frac{1}{Z} e^{- \int d^4x\, \mathcal{L}_E} \tag{1.9}$$

where $\mathcal{L}_E$ is the Lagrangian density function in four Euclidean dimensions.

This is now formally equivalent to a 4-D statistical system of fields in that the time-ordered products of field variables are simply the statistical expectation values of these products with respect to the 'Boltzmann distribution' given above.

It is this equivalence which allows us to calculate these expectation values numerically, as we shall discuss later. It also allows us to make use of many techniques developed for the study of statistical systems.

It must be noted that a naive calculation of expectation values using the above measure will still encounter divergences due to the high frequency components of the fields. We must remove these divergences by imposing a cut off on the momenta associated with the fields.

The analogy with statistical mechanics, and in particular critical phenomena

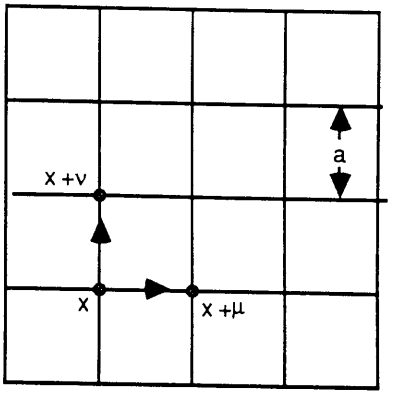

Figure 1.2: Two dimensional slice through a hypercubic lattice

(*e.g.*phase transitions in spin systems), is made closer by the choice of regularisation scheme which we make.

1.2.2 Lattice Regularisation

This regularisation scheme imposes a discrete symmetry on a finite volume of space-time. This usually involves the approximation of continuous space-time by a hypercubic lattice , with lattice spacing a (Figure 1.2).

The imposition of this discrete structure breaks the rotational symmetry of the continuum theory but we hope that this will be restored as we approach the continuum limit ($a \rightarrow 0$).

Consider a single scalar field, ϕ, on a L^4 lattice. If we now Fourier transform this into momentum space we obtain

$$\phi(p) = \sum_{\substack{x_\mu = na \\ n=1,\ldots,L}} e^{ipx}\phi(x). \tag{1.10}$$

$\phi(p)$ is periodic in p with period $p_\mu = \frac{2\pi}{a}$.

The momenta may be restricted to lie in the first Brillouin zone

$$-\frac{\pi}{a} < p_\mu \leq \frac{\pi}{a} \tag{1.11}$$

which gives us the desired ultraviolet cut-off.

We may now restore, in some sense, translational invariance, at scales above a, by imposing periodic boundary conditions in all directions.

1.2.3 the Lattice Action

The Lagrangian density for QCD without fermions is

$$\mathcal{L}_{\text{quen}} = -\frac{1}{2g^2}\,\text{Tr}\,F_{\mu\nu}F^{\mu\nu}. \tag{1.12}$$

Our choice of action , S_L, for the lattice theory must satisfy three requirements.

- $S_L \xrightarrow{a\to 0} \mathcal{L}_{\text{quen}}$
- we require a local action
- S_L must be invariant under local gauge transformations.

The gauge fields may be naturally associated with the lattice links.

$$\begin{aligned} A_\mu(x) \to U_{x,\mu} &= e^{i\int_x^{x+\mu} dx_\mu A_\mu(x)} \\ &\overset{a\to 0}{\simeq} e^{iaA_\mu(x)} \\ &\simeq 1 + iaA_\mu(x) \end{aligned} \tag{1.13}$$

The link variables, $U_{x,\mu}$, are elements of the gauge group, rather than the Lie algebra.

To preserve local gauge invariance, our lattice action must be built up from products of link variables around closed paths on the lattice. The simplest, and most local, choice is the elementary plaquette.[2]

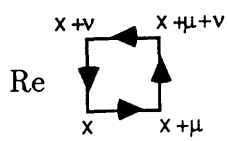

$$\begin{aligned} \text{Re} \quad &= \text{Re}\,\text{Tr}(U_{x,\mu}U_{x+\mu,\nu}U_{x+\mu+\nu,-\mu}U_{x+\nu,-\nu}) \\ &= \text{Re}\,\text{Tr}(U_{x,\mu}U_{x+\mu,\nu}U^\dagger_{x+\nu,\mu}U^\dagger_{x,\nu}) \\ &= \text{Re}\,\text{Tr}\,U_p \end{aligned} \tag{1.14}$$

On the lattice, where derivatives are replaced by finite differences,

$$\delta_\mu A_\nu(x) \to \frac{1}{a}(A_\nu(x+\mu) - A_\nu(x)) \tag{1.15}$$

and

$$\mathrm{Tr}\, U_p \xrightarrow{a\to 0} \mathrm{Tr}(1 - \frac{1}{4}F_{\mu\nu}F^{\mu\nu}) + O(a^6). \tag{1.16}$$

If the lattice action is taken to be

$$S(U) = \frac{6}{g^2}\sum_{x,\mu,\nu}(1 - \frac{1}{3}\mathrm{Re}(\mathrm{Tr}\, U_p)) \tag{1.17}$$

then the correct action is recovered in the continuum limit. The lattice action may be modified by the addition of terms which vanish in the continuum limit but Eqn(1.17) gives the simplest, and most frequently used form.

The lattice partition function becomes

$$Z = \int \mathcal{D}U e^{-S(U)} \tag{1.18}$$

where $\mathcal{D}U$ is the invariant Haar measure of the gauge group. Z, for a finite system, is now well defined, with no divergences.

1.2.4 The Continuum Limit

In order to approach the continuum quantum field theory we must remove the cut-off by letting the lattice spacing shrink to zero. Hadronic physics has a characteristic length scale of around 1fm. Since this is a physical length scale which must remain constant as the lattice spacing becomes smaller, it must become very large when compared to the lattice spacing as $a \to 0$. Since the interactions in the lattice theory are given by finite differences, and thus extend over infinitessimal distances, it requires careful tuning of the parameters in the action so that non-trivial behaviour, with correlations extending over finite distances and hopefully describing physical processes, is obtained.

This tuning is exactly analogous to the tuning required in the approach to the critical temperature in statistical mechanical models.[6]

Ising model	Q.F.T.
$T \to T_c$	$g \to g^*$
$\frac{\xi}{a} \to \infty$	$\frac{\xi}{a} \to \infty$
$\xi \to \infty$, a fixed	ξ fixed, $a \to 0$
$a \sim 1\text{Å}$	$\xi \sim 1\text{fm}$

Table 1.1: Comparison of the critical behaviour of the Ising model and the approach to the continuum limit of lattice gauge theory. ξ is the correlation length in physical units.

Consider an Ising model at a temperature above T_c. correlations between spins will extend over only a few lattice spacings. As the temperature is tuned towards T_c, the correlation length increases towards infinity and the system ungergoes a second order phase transition.

The critical behaviour, as described by the critical exponents, depends only on the spatial dimension and the symmetries of the Hamiltonian. This is in contrast with the correlations above T_c which depend on the lattice structure and the exact form of the interactions.

In quantum field theory, the coupling constant g must be tuned to a critical value, g^*, so that the correlation length diverges when measured in units of the lattice spacing. In this case, however, physical distances must remain finite. Therefore the lattice spacing must be simultaneously tuned to zero.

Perturbative calculations tell us that QCD is asymptotically free[3]. For small coupling, $g(a) \to 0$ as $a \to 0$. The continuum limit is approached by simultaneously tuning g and a to zero while holding physical quantities fixed.

Since the only dimensionful quantity in lattice QCD is the lattice spacing, a,

any mass prediction should take the form

$$M = \frac{1}{a} f(g). \tag{1.19}$$

In a renormalisable theory, as the lattice spacing becomes small compared to characteristic length scales, and so the cut off becomes large, the spacing is no longer expected to affect the physics. This requirement that physical quantities be cut-off independent,

$$a \frac{dM}{da}\bigg|_{a \to 0} = 0 \tag{1.20}$$

leads to the relation

$$f(g) + \beta(g) \frac{df(g)}{dg} = 0 \tag{1.21}$$

where

$$\beta(g) = -a \frac{dg(a)}{da} \tag{1.22}$$

is the Callan-Symanzik beta function.[4]

Equation (1.22) relates the lattice spacing at different values of the coupling by

$$\frac{a(g)}{a(g_0)} = e^{-\int_{g_0}^{g} \frac{dg}{\beta(g)}}. \tag{1.23}$$

In our simulations we typically calculate dimensionless quantities, *e.g.*Ma. If our answer is relevant to the continuum theory then we should find that it scales with the lattice spacing as we perform the measurement at various values of the coupling.

$$M_i a = \text{constant}.\ e^{-\int_{g_0}^{g} \frac{dg}{\beta(g)}} \tag{1.24}$$

irrespective of the form of $\beta(g)$. This leads to the conclusion that we must reduce the coupling until the ratio of two masses , *e.g.*pion and nucleon, becomes constant as g changes.

$$\frac{m_i a}{m_j a} = \frac{m_i}{m_j} = \text{constant} \tag{1.25}$$

As we systematically reduce the lattice spacing we are forced to increase the number of lattice sites so that the physical size of the lattice does not become too

small. It is the extra computation required for these large lattices which makes simulation in this 'scaling regime' very expensive.

The 2-loop perturbative form for $\beta(g)$ is well known[5].

$$\beta(g) = -\beta_0 g^3 - \beta_1 g^5 + O(g^7) \tag{1.26}$$

where $\beta_0 = 11/16\pi^2$ and $\beta_1 = \frac{34}{3}(3/16\pi^2)^2$.

This gives

$$a(g) = \Lambda_L^{-1} e^{-\frac{1}{2\beta_0 g^2}} (\beta_0 g^2)^{-\frac{\beta_1}{2\beta_0^2}} (1 + O(g^2)) \tag{1.27}$$

where Λ_L is a cut off independent mass parameter which sets the scale of QCD. It is an external parameter which must be measured by experiment.

If we are working at sufficiently small coupling, then we expect $\beta(g)$ to approach the 2-loop β-function, $\beta(g) = -\beta_0 g^3 - \beta_1 g^5$. Our *measured* value of ma should have the dependence

$$ma = \text{const. } e^{-\frac{1}{2\beta_0 g^2}} (\beta_0 g^2)^{-\frac{\beta_1}{2\beta_0^2}} \tag{1.28}$$

$$\frac{ma}{a(2-\text{loop})} = \text{const.}\Lambda_L = m \tag{1.29}$$

where a(2-loop) is the value *calculated* from the perturbative formula. This behaviour is known as asymptotic scaling.

If we observe asymptotic scaling behaviour then we can say that we are approaching the perturbative regime which describes so well much of the phenomonology of QCD. The non-perturbative information is the value of the constant in equation (1.29).

1.3 Calculational Methods

1.3.1 Strong Coupling Expansion

The strong coupling expansion of lattice QCD is equivalent to the high temperature expansion of thermodynamic systems. The 'Boltzmann factor' is expanded

in powers of $\beta \equiv 6/g^2$.[7]

$$e^{-S(U)} = 1 - \beta \sum_x (1 - \frac{1}{N_c} \mathrm{Re}(\mathrm{Tr}\, U_p)) + \cdots \tag{1.30}$$

Each factor of β brings with it a product of group variables around a plaquette.

The problem reduces to the computation of chains of group integrals. For $SU(3)$ gauge theory we may use the identities[8]

$$\int \mathcal{D}U = 1 \tag{1.31}$$

$$\int \mathcal{D}U\, U = \int \mathcal{D}U\, U^\dagger = 0 \tag{1.32}$$

$$\int \mathcal{D}U\, UU = \int \mathcal{D}U\, U^\dagger U^\dagger = 0 \tag{1.33}$$

$$\int \mathcal{D}U\, U_{ij} U^\dagger_{kl} = \frac{1}{3}\delta_{il}\delta_{jk} \tag{1.34}$$

$$\int \mathcal{D}U U_{ij} U_{kl} U_{mn} = \frac{1}{6}\epsilon_{ikm}\epsilon_{jln} \tag{1.35}$$

As an example, let us calculate the expectation value of a Wilson loop, $W(r,t)$. The closed loop on the lattice is the simplest object with any physical significance. It can be shown quantum-mechanically that the potential,$V(r)$, between a static quark and antiquark can be defined via

$$< W(r,t) > \overset{t\to\infty}{=} e^{-V(r)t} \tag{1.36}$$

where r and t are the spatial and temporal dimensions of the loop.

Substituting equation (1.30) for the exponential of the gauge action and using equations (1.31)–(1.35), the expectation value picks up its first non-zero contribution from the diagram in which the Wilson loop is 'tiled' using the minimum number of plaquettes. (Figure 1.3)

All link variables now appear in the form $\mathrm{Tr}(UU^\dagger)$. This leads to the result

$$\begin{aligned} < W(r,t) > &= \left(\frac{\beta}{18}\right)^{N_r N_t} \\ &= \left(\frac{1}{3g^2}\right)^{\frac{rt}{a^2}} \\ &= e^{-\frac{\ln(3g^2)}{a^2} rt} \end{aligned} \tag{1.37}$$

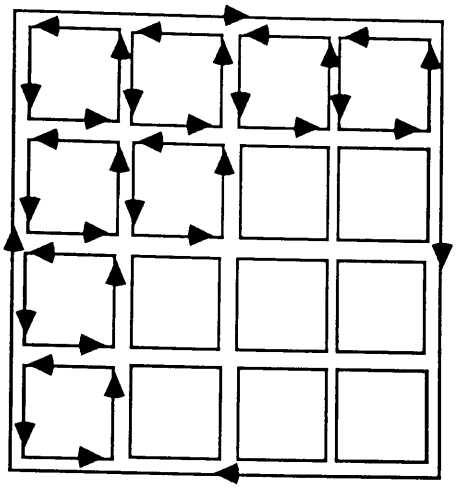

Figure 1.3: The minimally tiled Wilson loop. The lowest order strong coupling contribution to $\langle W(r,t)\rangle$

.

Comparison with Equation (1.36) leads to the linear confining potential

$$V(r) \simeq \sigma r \tag{1.38}$$

with *string tension.*

$$\sigma = \frac{\ln(3g^2)}{a^2}. \tag{1.39}$$

However, this result may not be of direct relevance to continuum QCD. A similar result may be obtained for QED, which is not a confining theory in the continuum. The linear potential may only be lost through a phase transition which should be evident at higher β and higher order in the expansion. Unfortunately, the results of the strong coupling expansion become unclear as we approach the scaling region. We need a more powerful technique if we are to probe continuum physics.

1.3.2 Monte Carlo Method

The path integrals to be evaluated in the calculation of an expectation value are ordinary multiple integrals over the group manifold.

$$< \phi > \; = \; \frac{1}{Z} \int \mathcal{D}U \; \phi(U) e^{-S(U)} \tag{1.40}$$

$$= \frac{1}{Z} \sum_{\text{all config}} \phi(U) e^{-S(U)} \tag{1.41}$$

A naive summation in equation (1.41) is impractical. Even for the simplest possible gauge group, the Z_2 group of the Ising model, on a 10^4 lattice, we have 1.58×10^{12041} configurations. The summation could not be performed in the age of the universe.

All is not lost, however. Due to the Boltzmann factor in equation (1.41), only a small subset of configurations make any significant contribution to the sum. One must generate configurations according to their importance.[8]

$$P([U])[\mathcal{D}U] = [\mathcal{D}U] e^{-S(U)} \tag{1.42}$$

The expectation values then become averages over a large number of configurations taken from the distribution (1.42).

$$< \phi >= \frac{1}{N} \sum_{\text{N configs}} \phi(U) + O(\frac{1}{\sqrt{N}}) \tag{1.43}$$

These configurations may be produced by a *Markov process* in which each configuration is generated from its immediate predecessor with probability $P([U_{x,\mu}] \rightarrow [U'_{x,\mu}])$.

The conditions placed on this probability function will be discussed in the next chapter along with the algorithms used to generate configurations in practice.

1.4 Fermions on the Lattice

If we hope that the lattice theory will reproduce the phenomenological results of QCD, *e.g.*the low lying hadron spectrum, and explain the mechanism by which chiral symmetry is broken, then we must include the effect of quark loops in our calculations.

1.4.1 The fermion doubling problem

The fermion part of the action for continuum QCD is

$$S = \sum_f \int d^4x \, [\overline{\psi}(x)(\not{\partial} + i \not{A} + m)\psi(x)] \tag{1.44}$$

where the sum is over all fermion flavours.

A naive transcription onto the lattice gives, for a single flavour of fermion,

$$S_F = \frac{1}{2a}[\sum_{x,\mu}(\overline{\psi}(x)\gamma_\mu U_\mu(x)\psi(x+\mu) - \overline{\psi}(x+\mu)\gamma_\mu U_\mu^\dagger(x)\psi(x)) + 2ma\sum_x \overline{\psi}(x)\psi(x)] \tag{1.45}$$

For free fermions, when $U_\mu(x) \equiv 1$, we may transform into momentum space using

$$\tilde{\psi}(p) = \sum_n e^{ip.n}\psi(x) \tag{1.46}$$

where the vector n has integer components labeling the lattice sites. $p_\mu = m_\mu \pi / N_\mu$ where N_μ is the length of the lattice in the μ direction and $m_\mu = 0, 1, \ldots, 2N_m - 1$.

The action then becomes

$$S_F = \sum_p \overline{\tilde{\psi}}(p) \sum_\mu (2i\gamma_\mu \sin p_m)\tilde{\psi}(-p) + 2m\overline{\tilde{\psi}}(p)\tilde{\psi}(-p) \tag{1.47}$$

with lattice fermion propagator

$$S(p) = (\sum_\mu \frac{2}{a} i\gamma_\mu \sin p_m + 2m)^{-1} \tag{1.48}$$

For $p_m \ll \pi$ we recover the continuum form

$$S(p) = (\sum_\mu \frac{2i}{a}\gamma_\mu p_\mu + 2m)^{-1} \sim \frac{1}{\not{p} + m} \tag{1.49}$$

However, for p_μ close to π we also recover the continuum form with a new set of γ matrices.

In 4-D, the propagator has 16 poles at the corners of the first Brillouin zone. This means that a single naive Dirac field describes not one but sixteen fermions. This is the *doubling problem* of lattice field theory.

This doubling arises from the periodicity of the sine function in the fermion propagator obtained from the fourier transform of the nearest neighbour form of the lattice derivative. In a continuum theory, a derivative just gives a factor of the momentum. However, if we replace the $\sin p_\mu$ by p_μ in the lattice propagator and then return to position space,we obtain highly non-local fermion interactions.

The doubling problem is also very closely related to chiral symmetry. Suppose that we want to describe a theory with only left-handed particles $\frac{1}{2}(1-\gamma_5)\psi$ and $\overline{\psi}\frac{1}{2}(1+\gamma_5)$. When we put this naively on the lattice, we find that we now have 16 particles, 8 right-handed and 8 left-handed. This is because, at some of the poles of the propagator, we have to modify the γ matrices in such a way that γ_5 changes sign. With the original γ_5, $\frac{1}{2}(1-\gamma_5)\psi$ will now describe a right handed particle at that pole.

This is a general feature of lattice theories which is expressed in a theorem of Nielsen and Ninomiya[9] : A hermitian, local and translationally invariant lattice field theory has an equal number of left and right-handed fermions in every charge sector of the Hilbert space.

We can avoid the doubling only by explicitly breaking the chiral symmetry of the $ma = 0$ action. There are two widely used formulations.

- Wilson fermions, in which the chiral symmetry is completely broken.
- Kogut-Susskind (staggered) fermions which retain a remnant of chiral symmetry at the expense of not completely solving the doubling problem.

1.4.2 Wilson Fermions

Wilson added to the naive action an irrelevant operator, $ar\delta_\mu\overline{\psi}\delta_\mu\psi$, which vanishes in the continuum limit[10]. For the free fermion action on the lattice we

now have

$$S = -\frac{1}{2a}\kappa\sum_{x,\mu}(\overline{\psi}(x)(r-\gamma_\mu)\psi(x+\mu)+\overline{\psi}(x+\mu)(r+\gamma_\mu)\psi(x))+\frac{1}{2a}\sum_x\overline{\psi}(x)\psi(x) \tag{1.50}$$

where

$$\kappa = \frac{1}{2ma+8r} \tag{1.51}$$

is the Wilson hopping parameter.

The free fermion propagator now becomes

$$S(p)^{-1} = 2m+\frac{8r}{a}+\sum_\mu\frac{2i}{a}\gamma_\mu\sin p_\mu-\frac{r}{a}\sum_\mu 2\cos p_\mu \tag{1.52}$$

At $p=(0,0,0,0)$ we recover the continuum form of the propagator. At other corners of the Brillouin zone we have fermions with mass

$$2m+\frac{nr}{a}$$

where n is some integer. Since r is fixed, this represents a divergent mass as $a\rightarrow 0$. this lifts the degeneracy.

r is conventionally taken to be equal to 1, which gives us projection operators $(1-\gamma_\mu)$ and $(1+\gamma_\mu)$. In order that $ma=0$ we must tune κ to a critical value, κ_c.

$$\begin{aligned} 2ma &= \frac{1}{\kappa}-8r \\ \Rightarrow\ \kappa_c &= \frac{1}{8} \end{aligned} \tag{1.53}$$

In the interacting theory,

$$\begin{aligned} S &= \sum_x[\overline{\psi}(x)\psi(x)-\kappa\sum_\mu\{\overline{\psi}(x)(1-\gamma_\mu)U_\mu(x)\psi(x+\mu) \\ &\quad +\overline{\psi}(x+\mu)(1+\gamma_\mu)U_\mu^\dagger(x)\psi(x)\}] \end{aligned} \tag{1.54}$$

κ_c will be a function of the coupling, varying between the free field value, $\frac{1}{8}$ and the strong coupling value of $\frac{1}{4}$.

1.4.3 Staggered Fermions

Kawamoto and Smit [11] reduce the number of degenerate flavours by performing a spin diagonalisation of the action. Define a new field, χ, by

$$\psi(x) = \gamma_1^{x_1}\gamma_2^{x_2}\gamma_3^{x_3}\gamma_4^{x_4}\chi(x), \quad x_4 = t \tag{1.55}$$

The fermion action then becomes

$$\begin{aligned} S(\overline{\psi},\psi,U) &\equiv S(\overline{\chi},\chi,U) \\ &= \frac{a^3}{2}[\sum_{\mu}(\overline{\chi}(x)\eta_\mu(x)U_\mu(x)\chi(x+\mu) - \overline{\chi}(x-\mu)\eta_\mu(x-\mu)U_\mu^\dagger(x)\chi(x)) \\ &\quad + 2ma\overline{\chi}(x)\chi(x)] \end{aligned} \tag{1.56}$$

The fermion signs, $\eta_\mu(x)$, arise from the commutation of γ matrices.

$$\begin{aligned} \eta_\mu(x) &= 1 \text{ if } \mu = 1 \\ &= (-1)^{x_1+\ldots+x_{\mu-1}} \text{ otherwise} \end{aligned} \tag{1.57}$$

The action is now diagonal in the spin degrees of freedom and so describes four single component complex fields.If we retain only one of these fields, we reduce the number of flavours to four.

The action (for $m = 0$) now has a $U(1) \times U(1)$ symmetry

$$\chi_e^o \to e^{i\alpha_e^o}\chi_e^o \tag{1.58}$$

$$\overline{\chi}_e^o \to \overline{\chi}_e^o e^{-i\alpha_o^e} \tag{1.59}$$

where 'e' and 'o' refer to the fields on even and odd lattice sites. χ fields on neighbouring sites have opposite chirality. A mass term couples fields even to even and odd to odd. This forces $\alpha_e = \alpha_o$. This corresponds to the fact that a mass in the continuum Lagrangian couples left handed fields to left handed fields and right to right, forbidding independent rotations of left and right handed components.

It is possible to reconstruct a 4-component, flavoured, Dirac field from the χ field. This field is defined on a lattice of spacing $2a$ with its spin and flavour distributed over an elementary hypercube of the original lattice. The action is that for a naive fermion with an additional term of relative order a which lifts the degeneracy. The 4-momentum is now restricted to the first Brillouin zone associated with the new lattice.

$$\frac{-\pi}{2a} < p_\mu \leq \frac{\pi}{2a} \tag{1.60}$$

The propagator now has,for $m = 0$, only one pole at $p_\mu = (0,0,0,0)$, in each flavour channel, giving four massless flavours.

This action at $m = 0$ has a $U_V(1) \times \tilde{U}_A(1)$ symmetry. The $\tilde{U}_A(1)$ is a remnant of the $SU_A(4)$ symmetry of the naive action, not the $U_A(1)$ chiral symmetry. However, when the $\tilde{U}_A(1)$ is broken spontaneously, we will get a massless 'pion'. We do, therefore, have some remnant of the correct chiral symmetry.

Chapter 2

Algorithms for simulations of QCD

2.1 Introduction

The majority of algorithms for the simulation of QCD with dynamical quarks follow one of two philosophies

- fairly large changes made to one link at a time with an exact calculation of fermion determinant ratios at every link update.This is a very expensive calculation. The most common algorithm of this type is that of Metropolis *et al.*[12].

- approximate methods which update the whole lattice by a small amount using an equation of motion. This requires the calculation of inverse matrix elements only once per lattice update but expectation values must be extrapolated to zero time-step, making multiple runs necessary.

  Examples are the Langevin[13], Microcanonical[14] and Hybrid[16] algorithms.

One algorithm which appears to have the advantages of both these methods is the Hybrid Monte Carlo Algorithm (HMC)[17].

In this method the lattice is updated using one hybrid trajectory. The new configuration is then accepted with probability $p = min[1, e^{\delta\mathcal{H}}]$, where $\delta\mathcal{H}$ is the change in the Hamiltonian during the hybrid trajectory. The Metropolis accept/reject step ensures that this is an *exact* algorithm with no step-size dependence in expectation values.

In this chapter the Metropolis, Langevin, Microcanonical and HMC methods will be briefly discussed. A more detailed description of one formulation for the Hybrid algorithm and the extensions needed to implement the HMC algorithm will then be given.

The last section will give an outline of the algorithms used to calculate the required inverse matrix elements.

2.2 The Metropolis Algorithm

The properties required of a Markov process used to generate field configurations in a Monte Carlo algorithm are

1. ergodicity : for any two configurations $[U_{x,\mu}]$ and $[U'_{x,\mu}]$

$$P([U_{x,\mu}] \rightarrow [U'_{x,\mu}]) > 0 \tag{2.1}$$

2. normalisation :

$$\sum_{[U'_{x,\mu}]} P([U_{x,\mu}] \rightarrow [U'_{x,\mu}]) = 1 \tag{2.2}$$

3. to ensure that we obtain configurations distributed according to the correct probability density

$$\rho([U]) = [dU]e^{-S([U])} \tag{2.3}$$

we require that $\rho([U])$ be a fixed point of our algorithm. *i.e.*

$$\sum_{[U]} \rho([U]) P([U] \rightarrow [U']) = \rho([U']) \tag{2.4}$$

A sufficient condition is that the process satisfies *detailed balance.*

$$\rho([U]) P([U] \rightarrow [U']) = \rho([U']) P([U'] \rightarrow [U]) \tag{2.5}$$

A simple way to implement this is the Metropolis algorithm.

$$\begin{aligned} P([U] \rightarrow [U']) &= min[1, e^{-\delta S}] \\ \delta S &= S([U']) - S([U]) \end{aligned} \tag{2.6}$$

If dynamical fermions are included we must calculate

$$e^{-\delta S} = \frac{detM([U']}{detM([U])} e^{-\delta S_g} \tag{2.7}$$

for every link update. It is not actually necessary to calculate the full determinant each time. The ratio may be rewritten as

$$\frac{detM([U'])}{detM([U'])} = det(1 + M^{-1} \delta M) \tag{2.8}$$

where $\delta M = M([U']) - M([U])$ has non zero elements in only a small block. however, we still have the costly calculation of the necessary inverse matrix elements. This limits exact Metropolis updating to very small lattices.

2.3 Small step-size algorithms

2.3.1 Kramers equation

The Kramers equation[18] for a classical particle of mass m moving in a one dimensional potential $V(x)$ takes the form

$$m \frac{d^2x}{d\tau^2} = -\frac{\partial V}{\partial x} - \alpha \frac{dx}{d\tau} + \left(\frac{2\alpha}{\beta}\right)^{\frac{1}{2}} \eta(\tau). \tag{2.9}$$

This is the Newton equation with the addition of a drag term with coefficient α and a Gaussian noise $\eta(\tau)$ with normalisation

$$\langle \eta(\tau)\eta(\tau') \rangle = \delta(\tau - \tau') \tag{2.10}$$

where, in this case, $\langle x \rangle$ denotes the statistical average of x.

The noise need not actually be Gaussian but must satisfy the above normalisation. The Kramers equation describes the Brownian motion of a particle with the drag term included in the calculation.

The Kramers equation can be rewritten in canonical form by introducing the momentum variable p.

$$\frac{dp}{d\tau} = -\frac{\partial V}{\partial x} - \alpha\frac{p}{m} + \left(\frac{2\alpha}{\beta}\right)^{\frac{1}{2}} \eta(\tau), \quad \frac{dx}{d\tau} = p \tag{2.11}$$

Simulations of this system are performed by discretising τ and introducing a time step, ϵ. If the resulting finite difference equations are solved to first order in ϵ, the equilibrium probability density is found to be

$$P(x,p) = e^{-\beta(\frac{p^2}{2m}+V(x))} + O(\epsilon) \tag{2.12}$$

The Kramers equation thus generates a particle distribution in thermal equilibrium at temperature $T = \frac{1}{k\beta}$, independent of the drag coefficient α.

2.3.2 Langevin Algorithm

The $m \to 0$ limit of the Kramers equation, after rescaling to remove α, becomes

$$\frac{dx}{d\tau} = -\frac{\partial V}{\partial x} + \left(\frac{2}{\beta}\right)^{\frac{1}{2}} \eta(\tau). \tag{2.13}$$

This is the Langevin equation.

For a scalar field theory, the Langevin equation takes the form

$$\frac{\partial \phi(x,\tau)}{\partial \tau} = -\frac{\partial S[\phi]}{\partial \phi(x,\tau)} + \eta(x,\tau) \tag{2.14}$$

where τ is the fictitious time, $S[\phi]$ is the lattice action and $\eta(x,\tau)$ is Gaussian noise normalised by

$$\langle \eta(x,\tau)\eta(x',\tau')\rangle = 2\delta_{xx'}\delta(\tau-\tau'). \tag{2.15}$$

For sufficiently large τ, the configurations $\phi(x,\tau)$ are generated according to the probability distribution

$$P(\phi) = e^{-S[\phi]}. \tag{2.16}$$

This is exactly the required distribution.

For actual numerical simulations, Langevin time must be discretised, giving the following recurrence relations for the fields.

$$\phi(x,\tau_{n+1}) = \phi(x,\tau_n) - \epsilon\frac{\partial S}{\partial\phi(x,\tau_n)} + \sqrt{\epsilon}\eta(x,\tau_n) \tag{2.17}$$

The delta function in the normalisation equation for $\eta(x,\tau)$ (Equation(2.15)) now becomes a Kronecker delta, $\delta_{\tau,\tau'}$ in discrete Langevin time. This leads to an equilibrium probability distribution

$$P(\phi)d\phi = e^{-\overline{S}[\phi]}d\phi \tag{2.18}$$

where $\overline{S}$ is the modified action

$$\overline{S}[\phi] = S[\phi] + \epsilon S_1[\phi] + \cdots \tag{2.19}$$

The $O(\epsilon)$ correction must be eliminated by extrapolation to $\epsilon = 0$.

It can be shown that, for some actions, the $O(\epsilon)$ term can be absorbed into a renormalisation of the bare parameters of $S[\phi]$ giving an effective action $S'[\phi]$. [13]

$$S'[\phi] = S[\overline{\phi}] \tag{2.20}$$

$$\overline{\phi} = \phi - \frac{1}{4}\frac{\partial S}{\partial\phi} \tag{2.21}$$

Discretisation errors can only be absorbed into a renormalisation of the bare couplings and masses in this way if the new action is in the same universality

class as the old one. This is only satisfied for small ϵ and local actions. *e.g.*The pure gauge Wilson action.

This algorithm may be generalised to non-abelian gauge fields in a straightforward manner.

The iterative Langevin scheme

$$U_\mu(x, \tau_{n+1}) = e^{-if_a T_a} U_\mu(x, \tau_n) \tag{2.22}$$

with driving force

$$f_a = \epsilon \partial_a S_0[U] + \sqrt{\epsilon}\eta_a \tag{2.23}$$

is the simplest group invariant discretisation of the differential Langevin equation for a gauge invariant action $S_0[U]$ built up from $U_\mu(x)$ link variables.

The inclusion of fermion loops results in a modification of the driving force.

$$f = \epsilon[\partial S_0 - \frac{1}{2} Re(\xi^\dagger \frac{1}{M} \partial M \xi)] + \sqrt{\epsilon}\eta \tag{2.24}$$

where ξ is a gaussian random vector.

This involves one full matrix inversion per lattice update.This is still quite expensive in computer time.

2.3.3 Microcanonical and Hybrid Methods

The $\alpha \to 0$ limit of the Kramers equation gives the purely deterministic Newton equation.

$$\frac{m d^2 x}{d\tau^2} = -\frac{\partial V}{\partial x} \tag{2.25}$$

This, when written in terms of the canonical variables x and p, is precisely the microcanonical method.[14,15]

$$\frac{dp}{d\tau} = -\frac{1}{2}\frac{\partial V}{\partial x} \tag{2.26}$$

$$p = m\frac{dx}{d\tau} \tag{2.27}$$

As for the Langevin algorithm one can write down a version of the equations for field theories and then proceed to the discretised recurrence relations.

The Kramers equation interpolates between the Langevin and microcanonical (Molecular Dynamics) limits. The Hybrid Molecular Dynamics algorithm used in QCD simulations is not actually the Kramers equation but the philosophy of using a method between the limiting cases is similar.

In the Hybrid algorithm the microcanonical equations of motion are integrated for a few steps. The momenta are then refreshed from a heatbath. *i.e.*several molecular dynamics steps followed by one Langevin step.

This method will converge to the correct equilibrium distribution faster than the Langevin limit. The optimum rate can be obtained by adjusting the length of the microcanonical trajectories – equivalent to tuning α in the Kramers equation.

2.3.4 The Hybrid Monte Carlo Algorithm

The HMC algorithm combines the good points of the exact algorithms with those of the small step-size algorithms. The parallel updating across the lattice which is the advantage of the approximate algorithms is retained but all finite step-size errors are eliminated.

This is achieved by using a hybrid algorithm, rather than local changes, to generate successive configurations in a Markov chain. Each new configuration is then accepted/rejected in a global Metropolis type decision which checks the change in the Hamiltonian of the system.

It is easy to prove [17] that this process of deterministic evolution followed by accept/reject satisfies detailed balance. Ergodicity is ensured by choosing the momenta randomly from a Gaussian distribution at the start of every trajectory.

The distribution of configurations is completely determined by the Hamiltonian in the accept/reject step. In principle one could use any action in the hybrid evolution. In practice it is most efficient to use the same, or a very similar, Hamiltonian for both parts of the algorithm. This point is discussed in more detail for the particular implementation described in the following sections.

2.4 The Hybrid Φ Algorithm

The partition function for QCD in Euclidean space is

$$Z = \int \mathcal{D}\psi \mathcal{D}\overline{\psi} \mathcal{D}U e^{-S_G - \overline{\psi} M \psi} \tag{2.28}$$

which can be written in terms of pseudofermion fields on even sites only.

$$\int \mathcal{D}\psi \mathcal{D}\overline{\psi} e^{\overline{\psi} M \psi} = detM \tag{2.29}$$

$$\begin{aligned} \int \mathcal{D}\phi_e \mathcal{D}\phi_e^\dagger e^{\phi_e^\dagger (M^\dagger M)^{-1} \phi_e} &= \left[det(M^\dagger M)^{-1} \right]^{-\frac{1}{2}} \\ &= detM \end{aligned} \tag{2.30}$$

$$Z = \int \mathcal{D}U \mathcal{D}\phi_e \mathcal{D}\phi_e^\dagger e^{-S_G - \phi_e^\dagger (M^\dagger M)^{-1} \phi_e} \tag{2.31}$$

where M is the fermion matrix for staggered fermions.

$$M_{ij} = m\delta_{ij} + \frac{1}{2} \sum_\mu \eta_{i,\mu} (U_{i,\mu} \delta_{i,j-\mu} - U^\dagger_{i-\mu,\mu} \delta_{i,j-\mu}) \tag{2.32}$$

m is the staggered quark mass, $U_{i,\mu}$ are the link variables and $\eta_{i,\mu}$ are the staggered fermion phases.

Definition of the ϕ fields on even sites only avoids the doubling of quark flavours which would result from the use of $M^\dagger M$ in the action. This is possible since the staggered quark fermion matrix has no elements connecting odd and even sites.

The partition function can be rewritten as [19]

$$Z = \int \mathcal{D}\phi_e \mathcal{D}U \mathcal{D}P e^{-\mathcal{H}_\Phi} \tag{2.33}$$

$$\mathcal{H}_\Phi = \frac{1}{2}\,\mathrm{Tr}\sum P_{i,\mu}^2 + \frac{\beta}{N_c} Re\,\mathrm{Tr}\sum(1 - U_p) + \phi_e^\dagger (M^\dagger M)^{-1}\phi_e \tag{2.34}$$

The traceless, hermitian $P_{i,\mu}$ are interpreted as the momenta conjugate to $U_{i,\mu}$. Since the ϕ_e fields are given no dynamics, they have no conjugate momenta.

The P's are gaussian variables and can therefore be integrated out analytically. The correlation functions of U and ϕ are therefore identical to those obtained using Equation 2.31.

The P variables are initially set by

$$P_{i,\mu} = \sum_{n=1}^{N_c^2-1} r_{i,\mu}^n \lambda_n \tag{2.35}$$

where λ_n are the generators of $SU(N_c)$ and the $r_{i,\mu}^n$ are independent, real, gaussian random variables with variance $\frac{1}{2}$. This gives the distribution of the P variables as

$$p(P) = e^{-\frac{1}{2}\,\mathrm{Tr}\,P^2} \tag{2.36}$$

In order that U remains an element of $SU(N_c)$, the evolution of U must be of the form

$$U(t+\epsilon) = e^{i\epsilon P} U(t) \tag{2.37}$$

$$\Rightarrow \dot{U}(t) = iP\,U(t) \tag{2.38}$$

The ϕ fields are set by defining

$$\underline{\phi} = M^\dagger \underline{r} \tag{2.39}$$

where $\underline{r}$ is a vector of complex, gaussian variables defined on both odd and even sites.

$$P(r) = e^{-r^2} \;\Rightarrow\; P(\phi) = e^{-\phi^\dagger (M^\dagger M)^{-1}\phi} \tag{2.40}$$

It is sufficient to evolve U and P, keeping ϕ fixed. The evolution equations must conserve $\mathcal{H}_\Phi$ and the differential volume element in configuration phase space.

The equation of motion,Eqn 2.37, for U satisfies this requirement. The equation for $\dot{P}$ is obtained by imposing the conservation of $\mathcal{H}_\Phi$ in the motion.

$$i\dot{P}_i,\mu = [-\frac{\beta}{N_c}U_{i,\mu}V_{i,\mu} + 2\tilde{U}_{i,\mu}(\sum_{\nu}\tilde{U}_{i+\mu,\nu}T_{i+\mu+\nu,i} - \sum_{\nu\neq\mu}\tilde{U}^{\dagger}_{i+\mu-\nu,\nu}T_{i+\mu-\nu,i})]_{TA} \quad (2.41)$$

on even sites and

$$i\dot{P}_i,\mu = [-\frac{\beta}{N_c}U_{i,\mu}V_{i,\mu} + 2\tilde{U}_{i,\mu}(\sum_{\nu}T_{i+\mu,i-\nu}\tilde{U}_{i-\nu,\nu} - \sum_{\nu\neq\mu}T_{i+\mu,i+\nu}\tilde{U}^{\dagger}_{i,\nu})]_{TA} \quad (2.42)$$

on odd sites. Where

$$T_{i,j} = \chi_i\chi^*_j \quad (2.43)$$

$$\chi = (M^{\dagger}M)^{-1}\phi_e \quad (2.44)$$

$$\tilde{U}_{i,\mu} = \eta_{i,\mu}U_{i,\mu} \quad (2.45)$$

$[A]_{TA}$ stands for the traceless antihermitian part of A and $V_{i,\mu}$ is the sum of the staples around the link $U_{i,\mu}$.

The integration of the equations of motion is performed using a leapfrog scheme [20].

$$\begin{aligned} P(\frac{1}{2}\epsilon) &= P(0) + \dot{P}(0)\frac{1}{2}\epsilon = P(0) - \frac{\partial S}{\partial U}(0)\frac{1}{2}\epsilon \\ U(\epsilon) &= U(0) + \dot{U}(\frac{1}{2}\epsilon)\epsilon = U(0) + P(\epsilon)\epsilon \quad (2.46) \\ P(\frac{3}{2}\epsilon) &= P(\frac{1}{2}\epsilon) + \dot{P}(\epsilon)\epsilon = P(\frac{1}{2}\epsilon) - \frac{\partial S}{\partial U}(\epsilon)\epsilon \\ &\vdots \quad (2.47) \end{aligned}$$

This integration scheme is one which is reversible and conserves phase space volumes.

The finite step-size errors for a single leapfrog step are $O(\epsilon^3)$ [21]. These errors have been calculated and are seen to have opposite signs for the two possible first order leapfrog schemes: Method 1, where the initial half step is performed on the U fields and Method 2, where the momenta are updated by $\frac{\epsilon}{2}$ as the first step.

The error in a trajectory of $N = \epsilon^{-1}$ steps is $O(\epsilon^2)$. These errors can, to a certain extent, be absorbed into a finite renormalisation of the couplings used in the guidance Hamiltonian used in the Molecular Dynamics equations. This point is discussed in section 2.5 where the various parameters in our final HMC program are tuned.

2.5 The Global Metropolis Step

In the Hybrid Monte Carlo Algorithm, one proposes as a candidate configuration that produced, from the initial configuration, by a single Hybrid trajectory.

$\mathcal{H}_\Phi$ is calculated for the initial and final configurations and the complete lattice update is accepted with probability

$$P_{acc} = e^{-\delta\mathcal{H}_\Phi} = \frac{e^{-\mathcal{H}_\Phi(U',P')}}{e^{-\mathcal{H}_\Phi(U,P)}} \tag{2.48}$$

at the end of the leapfrog sequence.

The entire procedure is thus

1. Refresh momenta and pseudofermion fields from Gaussian distributions.
2. Calculate $\mathcal{H}_\Phi(U,P)$
3. Perform leapfrog sequence.

   (Method 2 is more efficient when performing calculations which include the effects of dynamical fermions.Since the gauge fields are not updated between the calculation of $\mathcal{H}_\Phi$ and the first momentum update, it is not necessary to recalculate $(M^\dagger M)^{-1}\phi_e$ between these steps. The same saving of a matrix inversion can be made at the end of the trajectory.)
4. Calculate $\mathcal{H}_\Phi(U',P')$
5. Perform the Metropolis accept/reject.

The equilibrium distribution of fields is completely determined by the Hamiltonian used in the global Metropolis step. This step is completely independent of the parameters used in the guidance Hamiltonian of the Hybrid evolution. We may, therefore, tune the couplings in the Hybrid Hamiltonian to compensate for the 'renormalisation' caused by the finite step-size errors.

The value of β_{md}, the coupling in the molecular dynamics equations, can be tuned so that the acceptance probability in the Metropolis step is maximised. As one would expect from the signs of the step-size errors, the sign of $(\beta - \beta_{md})$ for the optimal value of β_{md} is opposite for the two leapfrog schemes. This is clearly seen in simulations of pure $SU(3)$ gauge theory[21,22](Fig.1).

The peak in the acceptance rate is much less pronounced in dynamical simulations. There is a peak in the acceptance probability as the quark mass in the guidance hamiltonian is adjusted. However, this peak is very close to $(m_{md} - m) = 0$ and it is, therefore, very close to optimal for the masses to be equal(Fig.2).

2.6 Calculations in Free Field Theory

Analytical calculations on systems of N uncoupled harmonic oscillators have given the HMC acceptance probability as a function of $\delta\tau$ and τ_0 , the step-size and the trajectory length respectively[20].

The Hamiltonian for this system is

$$\mathcal{H} = \frac{1}{2}\sum_{i=1}^{N}(p_i^2 + \omega_i^2 q_i^2) \tag{2.49}$$

For a trajectory consisting of a single leapfrog step – we are in effect considering the Langevin Monte Carlo algorithm – the leapfrog equations are given by

$$p_i(\delta\tau) \;=\; p_i(0) - \omega_i^2 q_i(0)\delta\tau \tag{2.50}$$

$$q_i(2\delta\tau) = q_i(0) + p_i(\delta\tau)\delta\tau \tag{2.51}$$

$$p_i(2\delta\tau) = p_i(\delta\tau) - \omega_i^2 q_i(2\delta\tau)\delta\tau \tag{2.52}$$

for a trajectory of length $2\delta\tau$.

The change in energy for this step is

$$\delta\mathcal{H} = \mathcal{H}(2\delta\tau) - \mathcal{H}(0) \tag{2.53}$$

$$= \sum_i \{2\omega_i^4 q_i p_i \delta\tau^3 + 2\omega_i^4(p_i^2 - \omega_i^2 q_i^2)\delta\tau^4 - 4\omega_i^6 q_i p_i \delta\tau^5 + 2\omega_i^8 q_i^2 \delta\tau^6\} \tag{2.54}$$

The acceptance probability is

$$P_{acc} = \frac{1}{Z}\int d^N q\, d^N p\, e^{-\mathcal{H}(q,p)} min(1, e^{-\delta\mathcal{H}}) \tag{2.55}$$

After several pages of algebra, this reduces to

$$P_{acc} = erfc\left(\delta\tau^3\sqrt{\frac{N\sigma_6}{2}}\right). \tag{2.56}$$

σ_6 is the *spectral average.*

$$\sigma_6 = \frac{1}{N}\sum_{i=1} N\omega_i^6 \tag{2.57}$$

The result for free field theory has the same form with

$$\sigma_6 = \int_0^{2\pi} \frac{dp}{2\pi}[m^2 + 4\sin^2\frac{p}{2}]^3 \tag{2.58}$$

$$= 20 + 18m^2 + 6m^4 + m^6 \tag{2.59}$$

If we increase the number of leapfrog steps to $n = \frac{\tau_0}{\delta\tau}$, the leapfrog algorithm is a linear map on phase space.

$$\begin{pmatrix} q_i(2\delta\tau) \\ p_i(2\delta\tau) \end{pmatrix} = \begin{pmatrix} 1 - 2\omega_i^2\delta\tau^2 & 2\delta\tau \\ -2\omega_i^2\delta\tau(1 - \omega_i^2\delta\tau^2) & 1 - 2\omega_i^2\delta\tau^2 \end{pmatrix} \begin{pmatrix} q_i(0) \\ p_i(0) \end{pmatrix} \tag{2.60}$$

The final expression for the acceptance probability after n steps is

$$P_{acc} = erfc\left(\delta\tau^2\sqrt{\frac{N\bar{\sigma}_4}{2}}\right) \tag{2.61}$$

$$\overline{\sigma}_4 = \frac{1}{8N}\sum \omega_i^4[1-\cos(4\omega_i\tau_0)] \tag{2.62}$$

For free field theory

$$\omega_p^2 = m^2 + 4\sin^2\frac{\pi p}{N} \tag{2.63}$$

In the $N \to \infty$ and $m = 0$ limits

$$\begin{aligned}\overline{\sigma}_4 &= \frac{2}{\pi}\int_0^\pi dx \sin^4 x[1-\cos(8\tau_0 \sin x)] &(2.64)\\ &= \frac{3}{4} - \frac{3}{4}J_0(8\tau_0) + J_2(8\tau_0) - \frac{1}{4}J_4(8\tau_0) &(2.65)\end{aligned}$$

This shows that there are oscillations in the acceptance probability as τ_0 increases for fixed $\delta\tau$ (Fig. 3). This phenomenon has been observed in Hybrid Monte Carlo computations for interacting, four dimensional field theories(Fig. 4).

The optimal trajectory length for a free field system, *i.e.*that trajectory length which will minimise the correlation lengths of observables, has also been calculated and was found to be

$$\tau_0 = \frac{1}{2\omega_{min}} \tag{2.66}$$

This gives a correlation length of $T = \frac{1}{\omega_{min}}$.

This is only true for trajectories with lengths distributed randomly about a mean value of τ_0. For a Hybrid Algorithm with fixed trajectory length the correlation length is found to be infinite.

This is consistent with the numerical results of Mackenzie[23], who found that the relaxation time for a free scalar field was greatly reduced by the use of random trajectory lengths.

A fixed trajectory length was chosen to exactly match the timescale of one momentum mode of the system.This is not so artificial as is sounds since the density of momentum modes above ω_{min} means that it is probable that an arbitrary choice of trajectory length will be close to the period of at least one

mode.The periodicity of the system was evident in the evolution of the action, which relaxed to close to its equilibrium value but then returned to close to its starting value each trajectory.The system did not approach equilibrium even after several hundred trajectories.

The trajectory length was then chosen randomly around the same value. The system approached equilibrium after only a few trajectories.

Our simulations of nearly free $U(1)$ gauge theory did not show the same behaviour of the action. This is probably due to the action being sensitive to only the high momentum modes through the plaquette.

Studies of the Fourier transformed force term in the Hybrid evolution do show the phenomenon well.

On a 2^4 lattice with periodic boundary conditions, we have five momentum modes ; p^2 = 0,4,8,12,16. At each P update , the force term, F_x^μ, is calculated.The fourier transform of this quantity is calculated. We then calculate the gauge invariant observable,

$$\sum_\mu |F^\mu(p)|^2 \propto p^2 \tag{2.67}$$

If we set the number of molecular dynamics steps per trajectory to 1, we can recover the Langevin result.

$$\sum_\mu |F^\mu(p)|^2 = \frac{3p^2}{\beta} \tag{2.68}$$

This agreement is reasonable even from very short runs.

If we repeat the measurements with longer trajectories the agreement is worse, even for longer runs. The autocorrelation function of this quantity was calculated, for lag ,τ, of up to 40 steps, for each non zero value of p^2.

The trajectory length was arranged to match the period of the $p^2 = 8$ mode.

For fixed trajectory length, the p^2 = 4, 12 and 16 modes were seen to decorrelate but the value of the $p^2 = 8$ autocorrelation function was found to

oscillate with period equal to the trajectory length. The value at the end of each trajectory was approximately constant, giving a long, if not infinite correlation length (Fig. 5a).

When the trajectory lengths were chosen randomly from a distribution centred on the length used above, the oscillations were seen to be damped out and the observable did decorrelate (Fig. 5b), albeit more slowly than the other modes. The decorrelation time may be reduced further by increasing the 'randomness' of the trajectory lengths.

A similar effect can be obtained by assigning a 'mass' to each momentum variable in the Hybrid algorithm. These masses are chosen randomly from a distribution centred on unity and are refreshed before each trajectory.

2.7 Matrix Inversion Algorithms

As we have seen, the most computationally intensive part of any simulation of QCD with dynamical quarks is the calculation of matrix elements of the inverse lattice Dirac operator, M^{-1}.It is the time required for this calculation which limits the speed at which new field configurations can be generated.

Due to the large size and sparcity of M, this calculation is best done using an iterative method.

To calculate the i^{th} column of M^{-1} we require the solution, ψ of the equation

$$M\psi = \eta \tag{2.69}$$

where $\eta_j = \delta_{j,i}$. Since the fermion matrix is non-hermitian, we may reformulate the problem as

$$M^\dagger M\psi = M^\dagger \eta \tag{2.70}$$

For the pseudofermion approach used in the Hybrid Monte Carlo we require the solution of

$$M^\dagger M\chi = \phi \tag{2.71}$$

where ϕ are the pseudofermion fields.

With these specific examples in mind, we may state the general problem as

$$H\psi = \eta \tag{2.72}$$

with H a hermitian matrix.

Mimimum Residue Algorithm

The minimum residue algorithm[24] is defined by

$$\begin{aligned} \alpha &= \frac{r_i H r_i}{|Hr_i|^2} \\ \alpha' &= \omega\alpha \\ \psi_{i+1} &= \psi_i + \alpha' r_i \\ r_{i+1} &= r_i - \alpha' H r_i \\ r_1 &= \eta - H\psi_1 \end{aligned} \tag{2.73}$$

ψ_1 is arbitrary, usually chosen to be the null vector. A choice of $1 < \omega < 2$ may improve convergence. If $\omega = 1$, each step minimises $|r_i|^2$ along the direction of r_i. Unfortunately, subsequent minimisations may spoil this minimisation and we may have to repeat the minimisation in the r_i direction at a later stage.

Vectors , p_i, p_j, satisfying $p_i H p_j = 0$ are said to be H-conjugate. minimisations along H-conjugate directions are independent and so a minimum residue algorithm using a sequence of H-conjugate directions, rather than the sequence of residue vectors, would converge exactly in N iterations, for H an $N \times N$ matrix, in exact arithmetic.

Conjugate Gradient Algorithm

The Conjugate Gradient algorithm[24] explicitly minimises along a sequence of H-conjugate directions, defined by the vectors p_i.

$$\alpha = \frac{|r_i|^2}{p_i H p_i}$$

$$\psi_{i+1} = \psi_i + \alpha p_i$$

$$r_{i+1} = r_i - \alpha H p_i$$

$$\beta = \frac{|r_{i+1}|^2}{|r_i|^2}$$

$$p_{i+1} = r_i + \beta p_i \tag{2.74}$$

β is chosen such that $p_{i+1} H p_i = 0$. This ensures that the current step does not spoil the previous one. The remarkable thing about conjugate gradient is that the new direction is actually H-conjugate to *all* the previous p's. In exact arithmetic, we would solve the problem in N steps.

In reality, where we do not have exact arithmetic, the p vectors drift out of H-conjugacy with the early vectors. This does not prevent convergence to a solution, since the only requirement is *local* H-conjugacy, but it will affect the speed of convergence.

The number of iterations required to converge to a given residue depends upon the eigenvalue spectrum of H. although numerical analysis suggests that the convergence time should depend simply upon the condition number, $s = \lambda_{max}/\lambda_{min}$, of H; in practice it is found that the density of small eigenvalues is also important.[24] In fact, it is found in tests using diagonal matrices with known condition number and eigenvalue distribution that the $\sqrt{s}$ behaviour only holds when the eigenvalues are distributed logarithmically.

The fermion matrix becomes more ill-conditioned (s increases), and the number of iterations required to obtain a solution grows, for lattice QCD, in the interesting range of couplings and masses.

Lanczos Algorithm

Another algorithm, and the one used in our programs, is the Lanczos Algorithm. The Lanczos algorithm[25] performs a unitary transformation on a Hermitian

matrix, H, producing a tridiagonal form T. The columns of the unitary transformation matrix are the mutually orthonormal Lanczos vectors x_i. These are calculated using the recurrence relations

$$\alpha_i = x_i^\dagger H x_i$$

$$U = Hx_i - x_{i-1}\beta_{i-1}^\dagger - x_i\alpha_i$$

$$\beta_i^\dagger \beta_i = U^\dagger U$$

$$x_{i+1} = U\beta_i^{-1} \tag{2.75}$$

The α_i and β_i are the diagonal and off-diagonal elements of T.

$$T = \begin{pmatrix} \alpha_1 & \beta_1 & & \\ \beta_1 & \alpha_2 & \beta_2 & \\ & \beta_2 & \ddots & \\ & & & \ddots \end{pmatrix} \tag{2.76}$$

The α_i, β_i and x_i may be used to build up an iterative solution [26] to

$$H\psi = \eta.$$

$$A_{k+1} = -\alpha_{k+1}(\beta_k^{-1})^\dagger A_k + B_k$$

$$B_{k+1} = -\beta_{k+1}(\beta_k^{-1})^\dagger A_k$$

$$y_{k+1} = y_k + A_{k+1}^{-1} t_k$$

$$t_{k+1} = -B_{k+1} A_{k+1}^{-1} t_k \tag{2.77}$$

$$U_{k+1} = U_k + x_{k+1}(\beta_k^{-1})^\dagger A_k$$

$$V_{k+1} = V_k - U_{k+1} A_{k+1}^{-1} t_k$$

$$\psi_k = -V_k(y_k + \frac{\alpha_1}{\beta_1})^{-1} \rightarrow \psi \text{ as } t_k \rightarrow 0$$

where $A_1 = t_1 = 1$, $B_1 = y_1 = 0$

and $x_1 = \eta$, $V_1 = -x_1\beta_1^{-1}$, $U_1 = 0$

The parameter t is related to the residue vector by the relation

$$|r_k|^2 = \left| \frac{t_k}{y_k + \alpha_1\beta_1} \right|^2 \tag{2.78}$$

and we can use this to calculate the norm of the residue without storing the residue vector itself.

Although they have very different philosophies, it can be shown that the conjugate gradient and Lanczos algorithms are equivalent. If ψ_1 is chosen to be the null vector in conjugate gradient then they will give the same residue and solution vector step by step, in exact arithmetic.[26 a]

Rounding errors will result in the Lanczos vectors losing orthogonality but this is not so serious a problem as the loss of H-conjugacy in conjugate gradient. The Lanczos algorithm can be continued until the residue is very small ($< 10^{-70}$). Due to the fact that it explicitly calculates the residue vector, the conjugate gradient algorithm would fail much earlier than this. Although we would never need this degree of accuracy in calculation of fermion propagators in a simulation program, this is important when we want to look at the eigenvalue spectra of fermion matrices.

Block Algorithms

It is often necessary to calculate several columns of the inverse fermion matrix for the same calculation. *e.g.*All the columns affected by a link update when using the Metropolis algorithm. It is possible to reformulate the conjugate gradient and Lanczos algorithms so that these columns may be calculated simultaneously[27].

Taking as our example the Lanczos algorithm, the scalar variables are replaced by full $B \times B$ matrices and the N dimensional vectors by $N \times B$ 'block

vectors'.

The calculation of B columns by this method would , in exact arithmetic. take the same time as the calculation of one column using the conventional algorithm.This factor of B gain is not achieved in practice but the block algorithm does give a considerable saving over using the single algorithm B times.

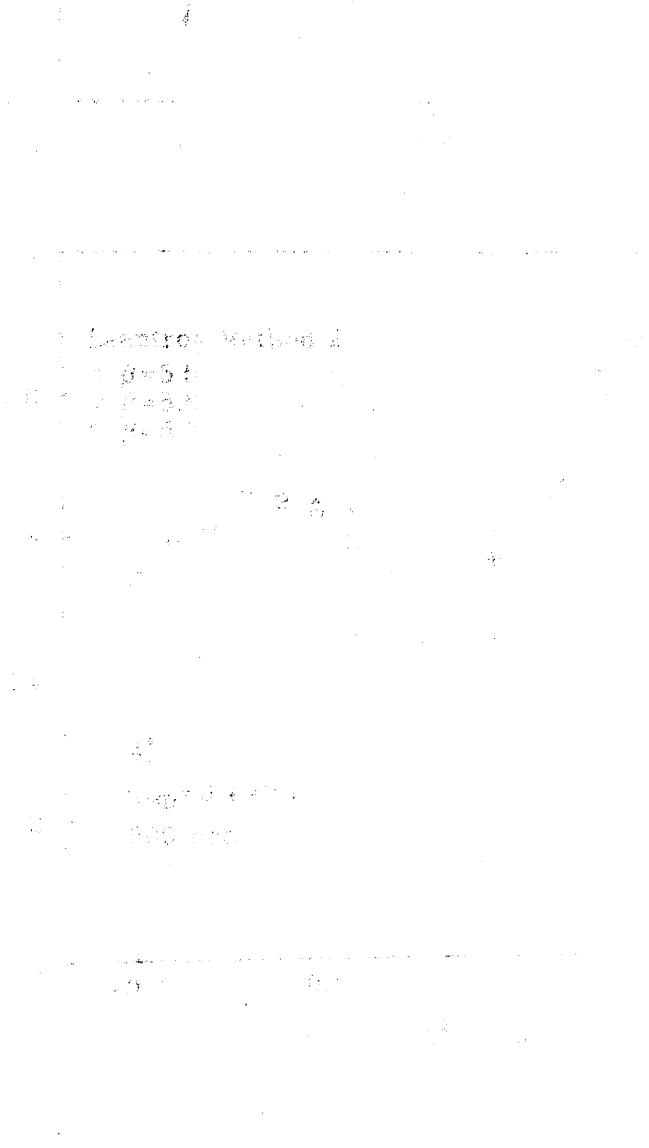

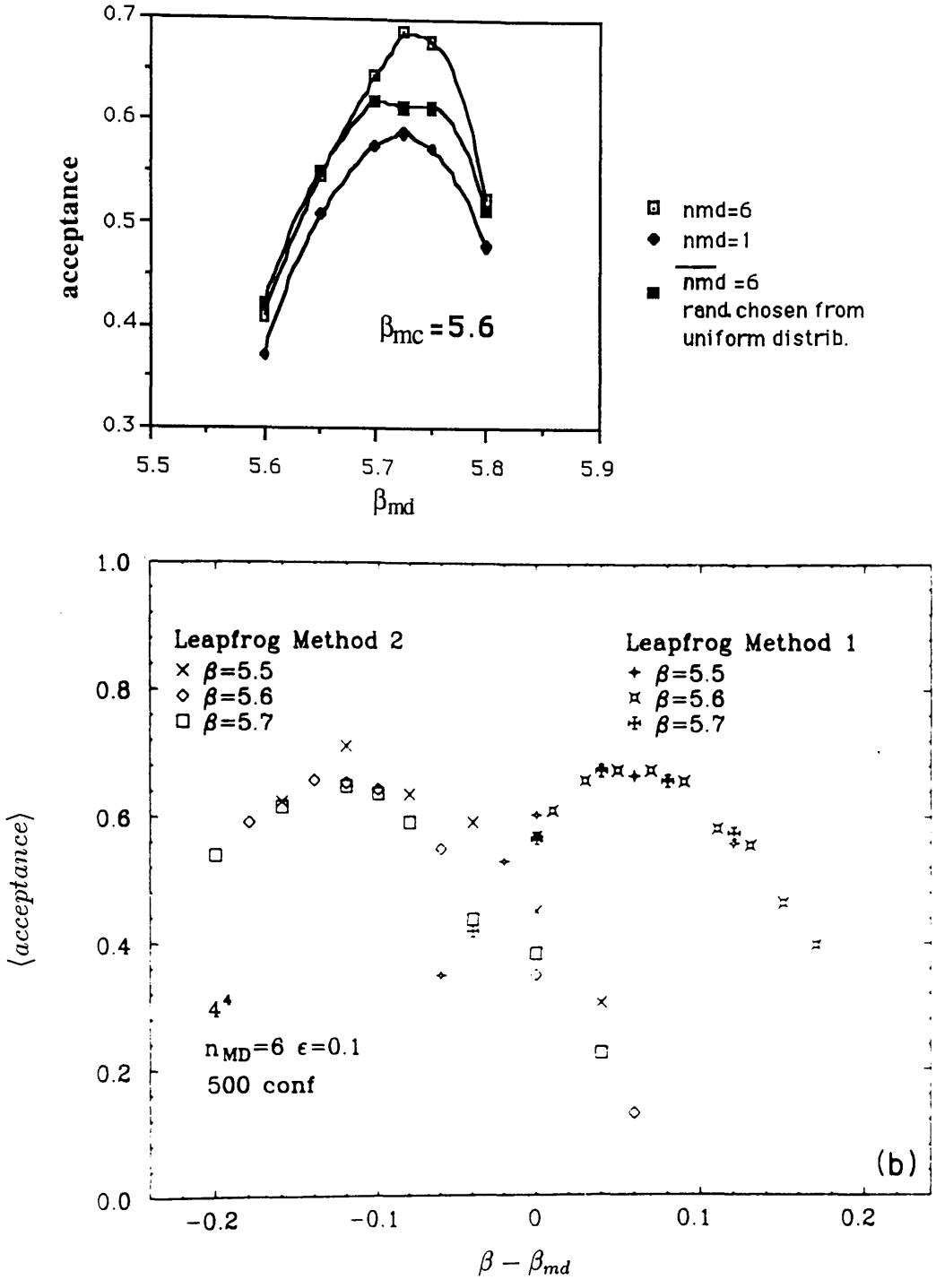

Figure 2.1 : HMC acceptance rate for pure gauge $SU(3)$ as β_{md} is varied at fixed β. The top figure shows results from our program. This corresponds to Method 2 in the lower figure, which is taken from reference [21]

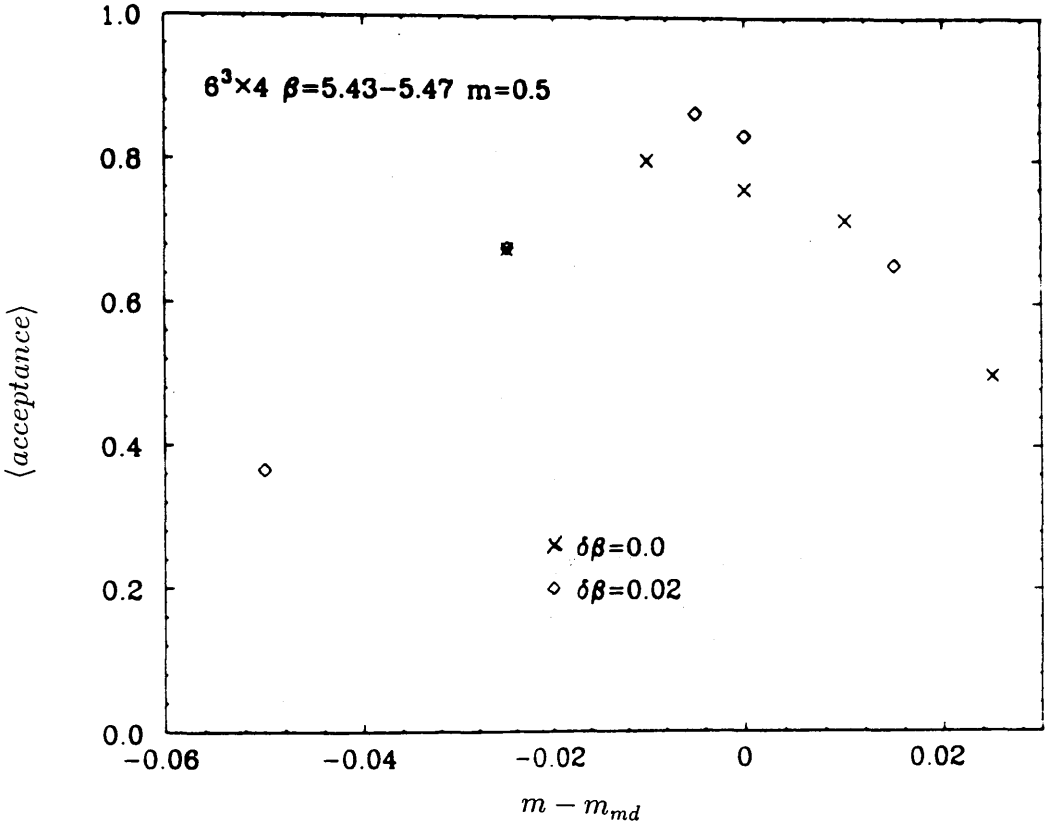

Figure 2.2 : HMC acceptance rate vs $\delta m = m - m_{md}$ for $m = 0.5$, $dt = 0.05$ and $n_{md} = 4$ and $\delta\beta = 0.0$ and 0.02

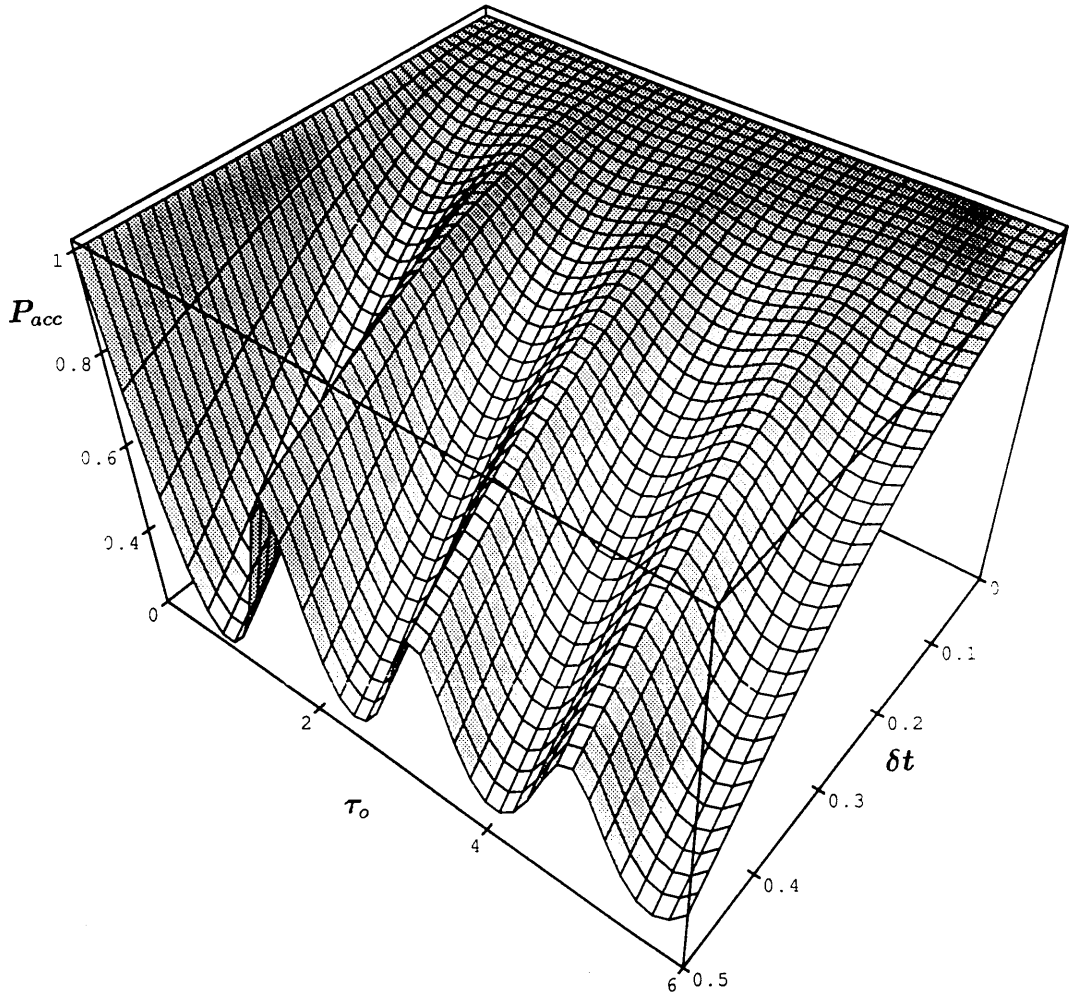

Figure 2.3 : Free field acceptance probability for the HMC algorithm as a function of the step-size δt and the trajectory length τ_0. The $N \to \infty$ expression has been used as an approximation to $\overline{\sigma}_4$ for $N = 256$.

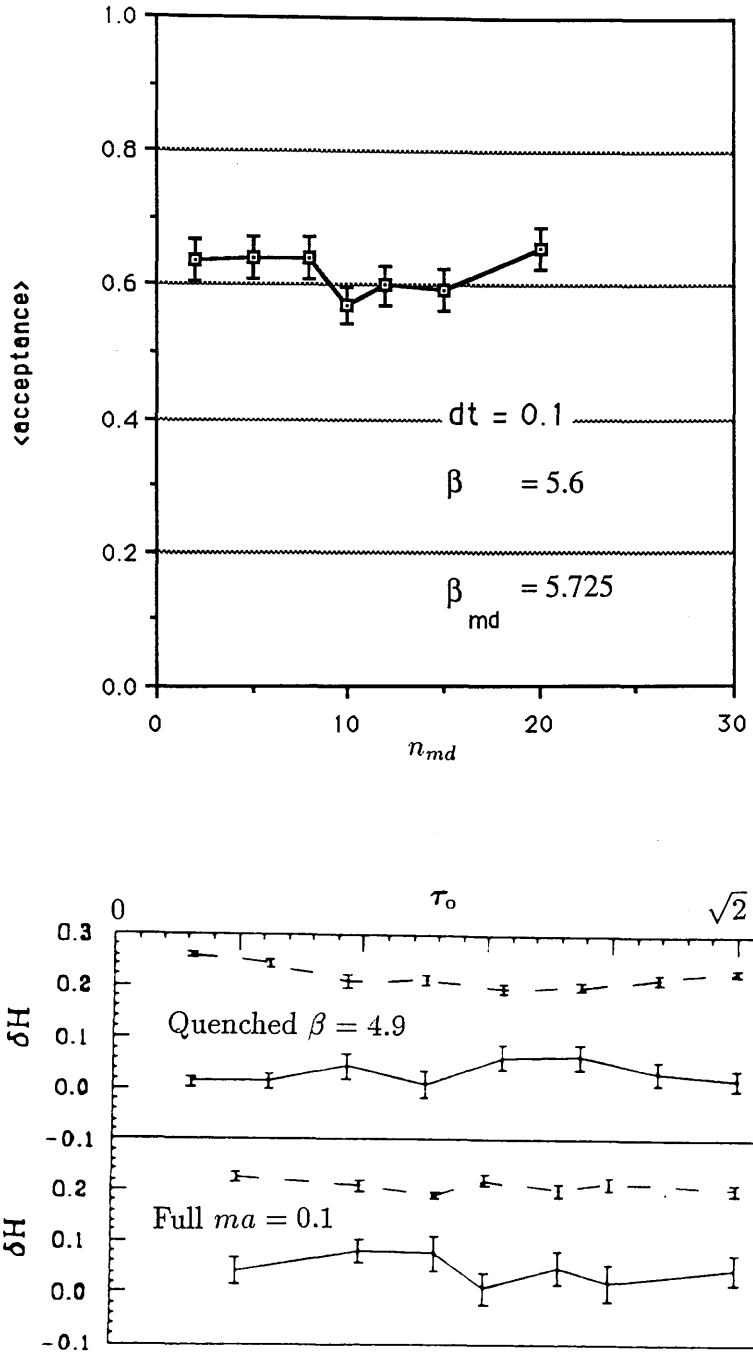

Figure 2.4 : HMC acceptance rate for pure gauge $SU(3)$ as n_{md} is varied at fixed dt. The top figure shows results from our program. The lower figure shows results from reference [22] for pure gauge $SU(3)$ and for QCD with $ma = 0.1$. The average error in the Hamiltonian is also shown (dashed line).

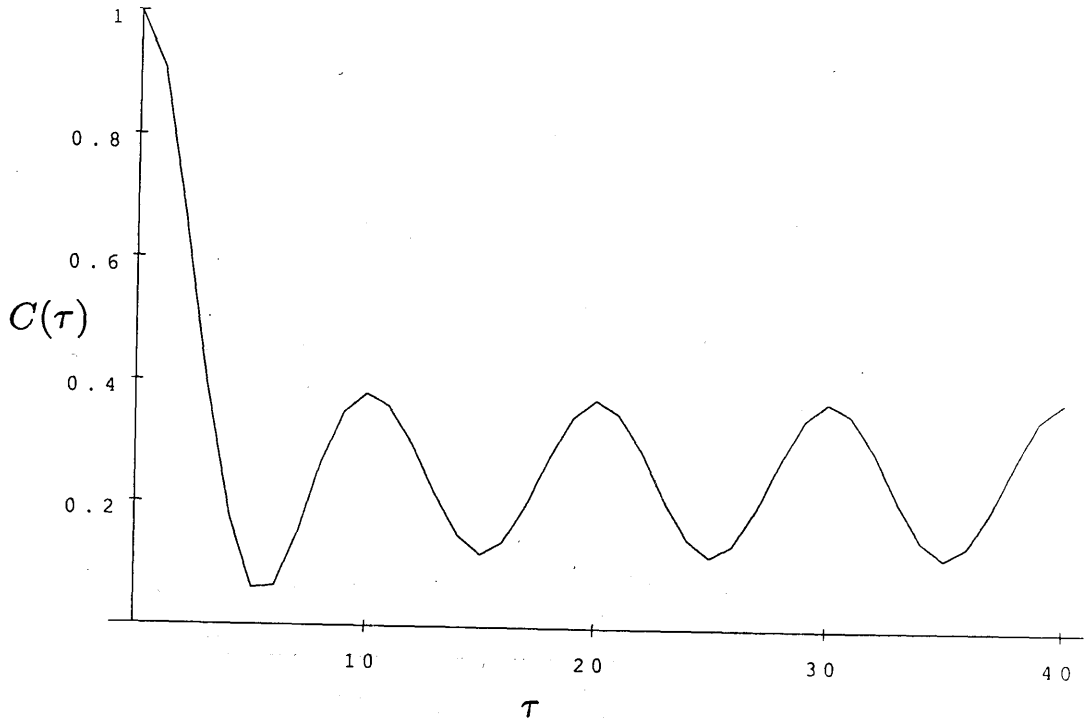

Figure 2.5a : Autocorrelation function of the $p^2 = 8$ Fourier mode of the HMC force term. The timestep, dt, is fixed such that $10dt$ matches the period of the momentum mode. The trajectory length is fixed at $n_{md} = 10$. $C(10)$ therefore gives the correlation between values one full trajectory apart. $\beta = 10.0$

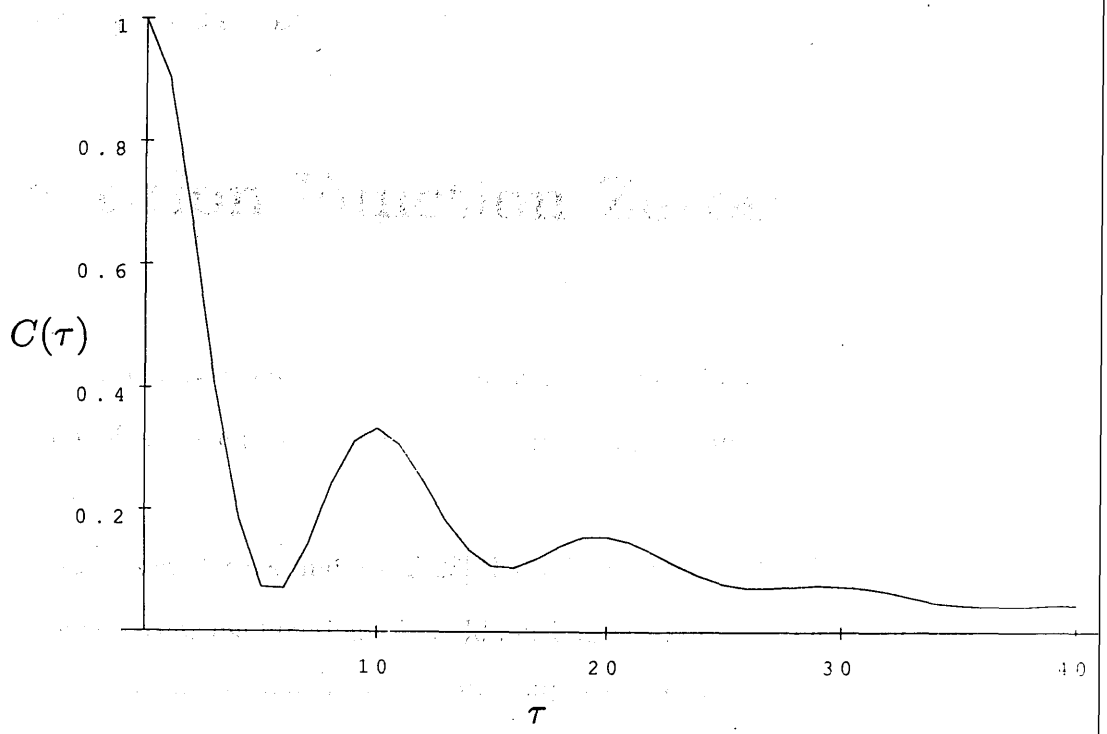

Figure 2.5b : As figure 2.5a except that n_{md} is chosen randomly from the interval (5,15) with average, $\overline{n_{md}} = 10$

Chapter 3

Partition Function Zeros

It is a well known result of statistical mechanics that, if one knows the partition function of a system, then one can, in principle, calculate all thermodynamic quantities.

It was shown by Lee and Yang [28] that a knowledge of the distribution of the zeros of the partition function can yield much information on the phase structure of the system under investigation. We will follow Lee and Yang by using the simple example of a monatomic classical gas in the grand canonical ensemble. This example will illustrate the important features of a method which may then be generalised to more complex, and realistic, systems.

The 'atoms' in our gas have interactions of the form

$$U = \sum u(r_{ij}) \tag{3.1}$$

where r_{ij} is the distance between the ith and jth atoms. We will make three assumptions about the form of these interactions.

1. The atoms have a finite impenetrable core of diameter a.

$$u(r) = +\infty \quad r \leq a \tag{3.2}$$

2. The interaction has a finite range, b.

$$u(r) = 0 \quad r \geq b \tag{3.3}$$

3. $u(r)$ is nowhere $-\infty$

These restrictions may be relaxed and the theory generalised, but we will continue on this simplest path.

Consider this gas confined in a box of volume V and at constant temperature, t. The system can exchange particles with a reservoir at chemical potential μ per atom.

The relative probability of having N particles in the box is

$$\frac{Q_N y^N}{N!} \tag{3.4}$$

where

$$Q_N = \int \dots \int_V d\tau_1 \dots d\tau_N \exp(-U/kt), \tag{3.5}$$

the integration being over the coordinates of the N particles, and

$$y = (2\pi mkt/h^2)^{\frac{1}{2}} \exp(\mu/kt) \tag{3.6}$$

is known as the fugacity.

The grand canonical partition function for the gas in a volume V is then

$$\mathcal{Z}_V = \sum_{N=0}^{M} \frac{Q_N}{N!} y^N \tag{3.7}$$

where M is the maximum possible number of particles in the box.

In thermodynamics we may calculate quantities such as the average pressure and density from the infinite volume behaviour of $\mathcal{Z}_V$.

$$p = kt \mathrm{Lim}_{V\to\infty} \frac{1}{V} \ln \mathcal{Z}_V \tag{3.8}$$

$$\rho = \mathrm{Lim}_{V\to\infty} \frac{\partial}{\partial \ln y} \frac{1}{V} \ln \mathcal{Z}_V \tag{3.9}$$

The existence of the above limits must be established before we may continue.

Lee and Yang proved two theorems regarding the infinite volume behaviour of this theory.

Theorem 1

For all real, positive values of y, $\frac{1}{V}\ln \mathcal{Z}_V$ approaches a limit as $V \to \infty$ which is independent of the shape of V.

This limit is a continuous monotonically increasing function of y.

This obviously solves the problem for Equation(3.8).

The limit in Equation(3.9) may be investigated if we realise that, as a consequence of the hard core of the atoms, we can only squeeze a finite number of atoms into the box and so $\mathcal{Z}_V$ is a polynomial of finite degree in y.

$$\mathcal{Z}_V = \prod_{i=1}^{M}(y_i - y) \tag{3.10}$$

where y_i are the roots of $\mathcal{Z}_V = 0$.

Since all the coefficients, Q_N, are positive, the y_i can never be real and positive. They must either be real and negative or else come in complex conjugate pairs.

Although the only physically meaningful values of y lie along the real axis, we may learn much by studying the distribution of zeros in the complex plane. The distribution of zeros in the infinite volume limit can tell us about the analytic behaviour of thermodynamic functions in the y plane.

Theorem 2

If, in the complex y plane, a region R containing a segment of the positive real axis is always free of roots, then in this region as $V \to \infty$ all the quantities

$$\left(\frac{\partial}{\partial \ln y}\right)^n \frac{1}{V}\ln \mathcal{Z}_V \quad n = 0, 1, 2, 3 \ldots$$

approach limits which are analytic with respect to y. Furthermore the operations $(\partial/\partial \ln y)$ and $\mathrm{Lim}_{V\to\infty}$ commute in R so that, *e.g.*

$$\mathrm{Lim}_{V\to\infty}\frac{\partial}{\partial \ln y}\frac{1}{V}\ln \mathcal{Z}_V = \frac{\partial}{\partial \ln y}\mathrm{Lim}_{V\to\infty}\frac{1}{V}\ln \mathcal{Z}_V \tag{3.11}$$

This gives, together with (3.8) and (3.9),

$$\rho = \frac{\partial}{\partial \ln y}\left(\frac{p}{kt}\right) \tag{3.12}$$

The quantity $(\partial/\partial \ln y)V^{-1} \ln \mathcal{Z}_V$ does not always approach a limit for all values of y. At these values of y the density does not assume a single value — we have a phase transition.

The problem of phase transitions is intrinsically related to the distribution of zeros in the complex y plane.

We will discuss two cases:

1. The zeros of $\mathcal{Z}_V(y)$ do not close on to the real axis of y as $V \to \infty$. There exists a region R, enclosing the whole positive real axis, which is free of zeros.(Figure(1))

   In this case, the two theorems give the result that the pressure and density are analytic, monotonically increasing functions of y in the region R *i.e.* for all real positive values of y.The system exists in a single phase.

2. The zeros of $\mathcal{Z}_V(y)$ close in on to the positive real axis as $V \to \infty$; say at the points y_1 and y_2. There exist three regions R_1, R_2 and R_3 which are free of zeros.(Figure(2))

   By the same reasoning as in the previous case, in each of the segments of the real axis which is free of roots, the system exists in a single phase. At the points y_i the pressure is continuous (by theorem 1) but its derivative, ρ, has in general a discontinuity. It can be shown that the density always increases across the discontinuity.

   As the temperature varies, the points y_2 and y_2 will in general move along the real axis. If at a certain temperature the zeros cease to close in on to one of the points then we are at the critical temperature, t_c for that transition.

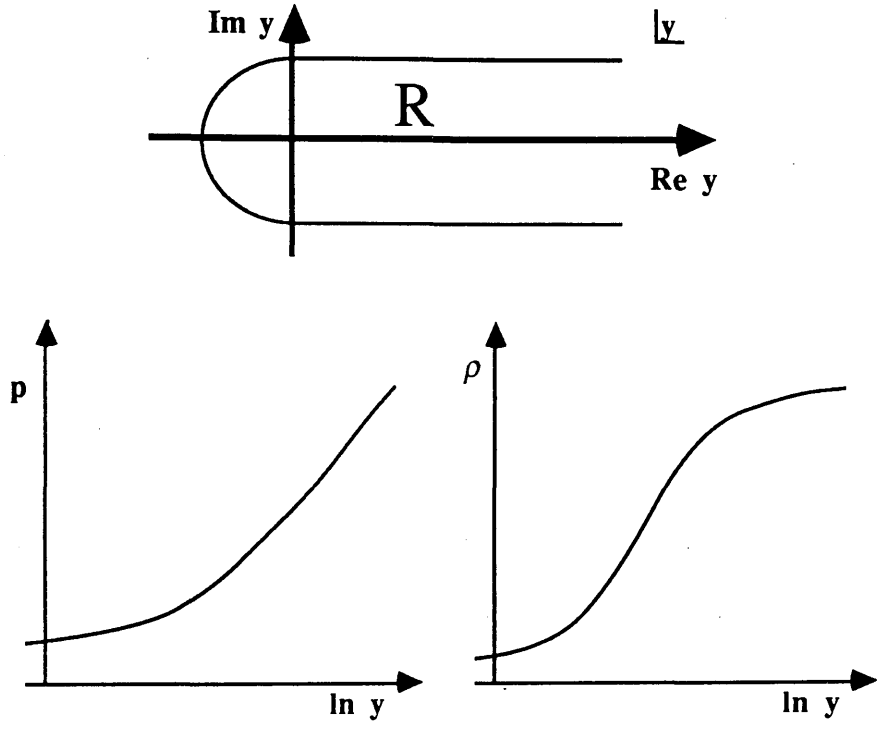

Figure 3.1: Analytic behaviour at a fixed temperature of thermodynamic functions for a single phase system.

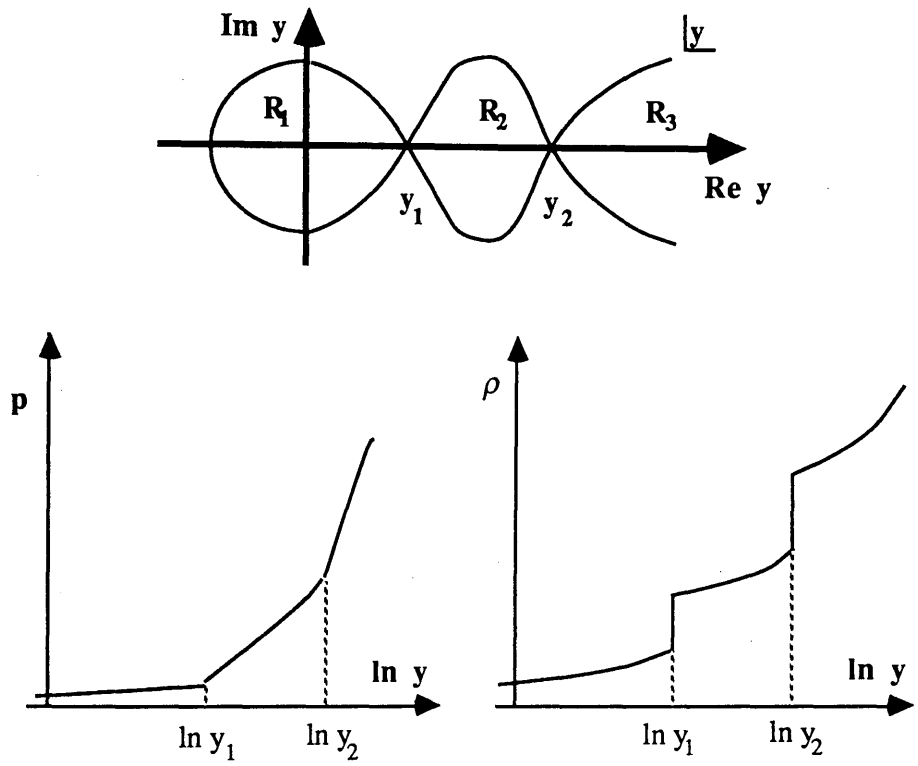

Figure 3.2: Analytic behaviour at a fixed temperature of thermodynamic functions for a system having two phase transitions.

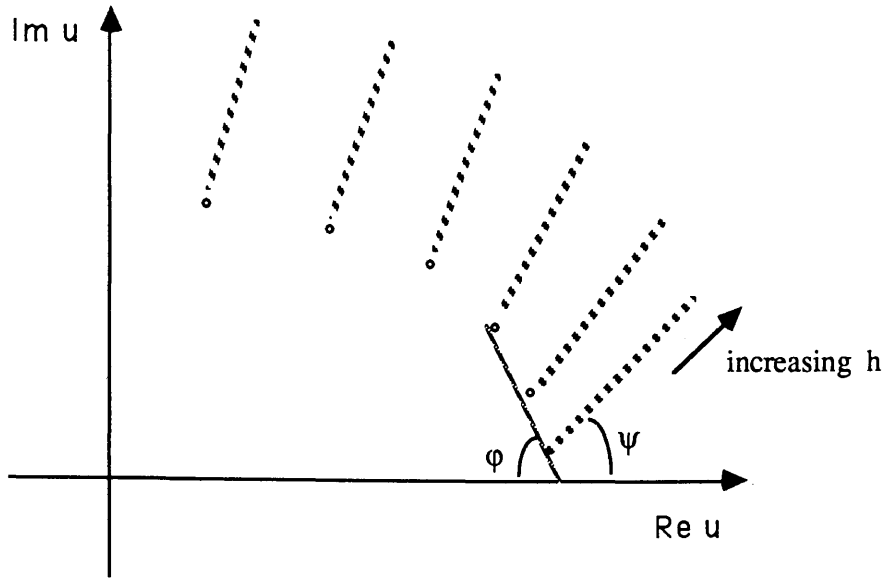

Figure 3.3: Definition of the critical angles φ and ψ for the Ising model

This theory was generalised in a second paper[29] to lattice gas and Ising models in which the zeros are shown to be constrained to lie on the unit circle in the complex y plane (complex h plane in the case of the Ising model with external field h).

The partition function zeros of the Ising model have been studied as a function of temperature, both in zero magnetic field [30] and with a non-zero external magnetic field [31]. In the latter case, an analysis of the finite size scaling behaviour of the zeros was performed. Two critical angles were defined. φ describes the angle between the line of zeros and the real axis in the complex temperature plane, near to the critical point with zero magnetic field. ψ is the angle at which these zeros move off in a real magnetic field. These angles may be related to the usual critical exponents of the system.

$$\tan[(2-\alpha)\varphi] = \frac{\cos(\pi\alpha) - A_-/A_+}{\sin(\pi\alpha)} \tag{3.13}$$

where α is the specific heat critical exponent and A_-/A_+ is the ratio of specific

heat amplitudes above and below the critical temperature. Similarly, the angle ψ is related to the spontaneous magnetisation critical exponent , β, and δ, the exponent which relates magnetic field and magnetisation at critical temperature ($h \sim m^{\delta}$).

$$\psi = \frac{\pi}{2\beta\delta} \tag{3.14}$$

Mean field theory predicts the values $\varphi = 45°$ and $\psi = 60°$. The analysis of Itzykson *et al.*gives $\varphi = 57°$ and $\psi = 58°$.

The critical behaviour of gauge theories without fermions has been studied by looking at the distribution of zeros in the complex $u = \exp(\beta)$ plane, where β is the inverse coupling [32,33]. Plots of these zeros show the type of distribution predicted in the second case discussed above, with the value of β at the critical point in agreement with simulations performed using an order parameter to indicate a phase transition.

Given these previous successes, it seems reasonable to expect that the method should be applicable to lattice QCD with fermions and QCD at finite chemical potential. the latter is a return towards the original idea of Lee and Yang, with the Grand Canonical partition function being expanded in terms of the individual Canonical partition functions.

Chapter 4

The partition function of strongly coupled gauge theories with staggered fermions

4.1 Introduction

Quantum chromodynamics is expected to have a non-trivial phase structure. A phase transition is expected between the low temperature, confining phase which results in the observed spectrum of colour singlet states and a high temperature phase in which the quarks and gluons are deconfined and behave essentially like an ideal gas (Figure 4.1). The transition temperature and the order of this transition are not yet fully determined, even in the pure gauge sector, and calculations on larger lattices on computers with teraflop or even petaflop capability will probably be required to give a definitive answer to these questions. On a finite lattice the physical temperature is determined by the temporal extent of the lattice.

$$T \sim \frac{1}{aN_t} \tag{4.1}$$

The lattice spacing, a, may be related to the coupling by the β-function (Equation 1.22) but the important point is that a decreases as we reduce the coupling. *i.e.*the

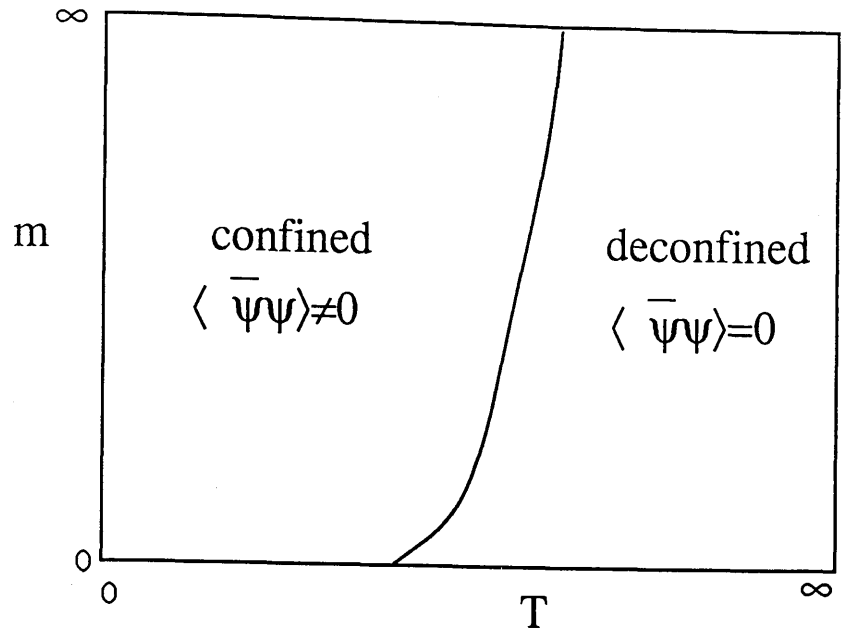

Figure 4.1: Schematic phase diagram for QCD in the temperature/quark-mass plane.

temperature increases as β increases.

Previous studies of the phase structure have concentrated on the search for the critical coupling at fixed bare quark mass. By examining the partition function as a function of the quark mass, we may approach the problem from the opposite viewpoint. At a fixed value of the coupling we may look for the critical quark mass which gives a phase transition.

In the strong coupling regime we have only one critical point, the chiral limit at $ma = 0$. At intermediate values of the coupling we expect to have a finite temperature phase transition at a finite mass which prevents the approach to the chiral limit (Figure 4.1). As the lattice size is increased and therefore the temperature reduced, we expect this critical mass to approach zero since the chiral limit must be attainable in the infinite volume, zero temperature limit which corresponds to our low energy world.

In this chapter, a method is introduced for the study of partition function zeros in gauge theories with four flavours of staggered fermions. The study of partition function zeros allows the investigation of phase transitions and critical behaviour without the need for an order parameter. This is useful in the case of QCD since we have no exact order parameter for the phase transition — $\langle\overline{\psi}\psi\rangle$ is only an exact order parameter in the $ma = 0$ limit and the Polyakov loop is only related to the free energy for the pure gauge ($ma \to \infty$) case.

The partition function can be written as the average value of the determinant of the fermion matrix, with a suitably weighted averaging procedure. For once we make a virtue out of the fact that we are working on a finite lattice since, because the fermion matrix is of finite size, we may expand the determinant exactly as a polynomial in the bare fermion mass.

Preliminary calculations were performed at strong coupling ($\beta = 0$) and on small lattices for $SU(2)$, $SU(3)$ and $U(1)$ gauge groups.. The results are consistent with the expected critical behaviour at $ma = 0$ in all three cases.

4.2 The Method

4.2.1 The Expansion of the Partition Function

The partition function for $SU(N)$ gauge theory with staggered fermions may be written as a function of the bare fermion mass.

$$Z(m) = \int \mathcal{D}U \, \det(M(m)) \, e^{-S_g} \tag{4.2}$$

Since we have the freeedom to define the partition function up to a constant multiplicative factor, we may write

$$Z(m) \;=\; \frac{\int [dU] \, \det(M(m)) e^{-S_g}}{\int [dU] \, \det(M(m_0)) e^{-S_g}} \tag{4.3}$$

$$= \frac{\int [dU] \frac{\det(M(m))}{\det(M(m_0))} \det(M(m_0)) e^{-S_g}}{\int [dU] \det(M(m_0)) e^{-S_g}} \tag{4.4}$$

$$= \left\langle \frac{\det(M(m))}{\det(M(m_0))} \right\rangle_{m_0} \tag{4.5}$$

The average in equation(4.5) is over gauge field configurations, generated using a dynamical quark mass of m_0.

Another self-consistent definition of $Z(m)$ would be

$$Z(m) = \langle \mathrm{Det}(M(m)) \rangle_{\mathrm{quenched}} \tag{4.6}$$

However, many more measurements would be required in order to produce accurate results in this case since the quenched probability distribution,

$$P([U], \beta) \propto e^{S_g([U], \beta)} \tag{4.7}$$

peaks in a region of phase space where there is negligible contribution from the determinant, and vice-versa. This effect is discussed in reference [49]. Quenched updating is only useful on small systems where the reduced updating time allows us to make many measurements in a short time.

We may use the parameter m_0 to deal with this problem. If m_0 is tuned to be in the neighbourhood of the bare mass of physical interest, we will maximise the overlap between our observable and the update probability distribution.

Since the fermion matrix for staggered fermions, M, has the mass only on the diagonal, we may write

$$M(m) = iM' + mI \tag{4.8}$$

where I is the identity matrix.

Using the block odd/even structure of the fermion matrix

$$\det(M(m)) = \det(M^\dagger M)_e \tag{4.9}$$

$$= \det(M'^\dagger M' + Im^2)_e \tag{4.10}$$

$$= \det(M'^2 + Im^2)_e \tag{4.11}$$

where the subscript e denotes the matrix on even sites only.

Since we have a finite lattice, the determinant in Equation(4.11) may be expressed as a finite polynomial in m^2.

$$\det(M(m)) = \sum_{n=0}^{N/2} A_n m^{2n} \tag{4.12}$$

where $N = n_s N_c$ and n_s and N_c are the number of space-time sites and colours respectively.

We may also expand the determinant as a Taylor expansion around m_1, which can be chosen to have any value. The most useful situation is when m_1 is equal to or close to m_0. In this case the statistical errors in the first few coefficients of the expansion will be reduced and we can, therefore, extract the zeros close to m_0 most efficiently.

In the strong coupling simulations described later we ran at a small bare quark mass, $ma = 0.025$. We expanded the polynomial around several *imaginary* values of m_1 and looked for those zeros which were obtained from several of these Taylor expansions.

Configurations are generated using the Hybrid Monte Carlo algorithm described in Chapter 3. Measurements are made at intervals of $\geq O(1)$ in molecular dynamics time, giving configurations which, hopefully, are sufficiently independent. The matrix $M_e'^2$ is then tridiagonalised using the Lanczos algorithm, giving the tridiagonal form, T.

$$T = \begin{pmatrix} \alpha_1 & \beta_1 & & \\ \beta_1 & \alpha_2 & \beta_2 & \\ & \beta_2 & \alpha_3 & \\ & & & \ddots \end{pmatrix} \tag{4.13}$$

Since tridiagonalisation may be performed using a unitary transformation, we now have

$$\det(M(m)) \;=\; \det(U^\dagger M^\dagger M U + U^\dagger I U m^2)_e \tag{4.14}$$

$$= \det(T + Im^2)_e \tag{4.15}$$

Here U denotes the unitary transformation matrix, not a link variable. The coefficients of the polynomial (Equation(4.12)) are now calculated recursively from the tridiagonal form, T.

$$\text{Let} \quad T_p = \begin{pmatrix} \hat{\alpha_1} & \beta_1 & & & \\ \beta_1 & \hat{\alpha_2} & \beta_2 & & \\ & \ddots & & & \beta_{p-1} \\ & & & \beta_{p-1} & \hat{\alpha_p} \end{pmatrix} \tag{4.16}$$

where $\hat{\alpha_i} = \alpha_i + {m_1}^2$.

Then

$$\begin{aligned} \det(T_p + (m^2 - m_1^2)) &= (\hat{\alpha_p} + (m^2 - m_1^2))\det(T_{p-1} + (m^2 - m_1^2)) \\ &- \beta_{p-1}\det \begin{pmatrix} T_{p-2} + (m^2 - m_1^2) & & \vdots \\ & \ddots & \vdots \\ & \beta_{p-2} & \beta_{p-1} \end{pmatrix} \end{aligned} \tag{4.17}$$

The cofactor of the β_{p-2} term in the second determinant is obviously zero since we have a complete column of zeros. We may repeat the step above to obtain

$$\begin{aligned} \det(T_p + (m^2 - m_1^2)) &= (\hat{\alpha_p} + (m^2 - m_1^2))\det(T_{p-1} + (m^2 - m_1^2)) \\ &-\beta_{p-1}^2 \det(T_{p-2} + (m^2 - m_1^2)) \end{aligned} \tag{4.18}$$

We may now insert a polynomial expansion for this determinant.

$$\det(T_p + (m^2 - m_1^2)) = \sum_{n=0}^{p} a_n^{(p)}(m^2 - m_1^2)^n \tag{4.19}$$

$$\begin{aligned} \sum_{n=0}^{p} a_n^{(p)}(m^2 - m_1^2)^n &= (\hat{\alpha_p} + (m^2 - m_1^2)) \sum_{n=0}^{p-1} a_n^{(p-1)}(m^2 - m_1^2)^n \\ &-\beta_{p-1}^2 \sum_{n=0}^{p-2} a_n^{(p-2)}(m^2 - m_1^2)^n \end{aligned} \tag{4.20}$$

This results in a set of recurrence relations for the a_n.

$$a_n^{(p)} = \hat{\alpha}_p a_n^{(p-1)} + a_{n-1}^{(p-1)} - \beta_{p-1}^2 a_n^{(p-2)} \qquad 1 \leq n \leq p-2 \tag{4.21}$$

$$a_{p-1}^{(p)} = \hat{\alpha}_p a_{p-1}^{(p-1)} + a_{p-2}^{(p-1)} \tag{4.22}$$

$$a_p^{(p)} = a_{p-1}^{(p-1)} \tag{4.23}$$

$$a_0^{(p)} = \hat{\alpha}_p a_0^{(p-1)} - \beta_{p-1}^2 a_0^{(p-2)} \tag{4.24}$$

The initial conditions for these recurrence relations are easily obtained.

$$\det(T_1 + (m^2 - m_1^2)) = \hat{\alpha_1} + (m^2 - m_1^2) \tag{4.25}$$

$$\det(T_2 + (m^2 - m_1^2)) = \hat{\alpha}_1\hat{\alpha}_2 - \beta_1^2 + (\hat{\alpha}_1 + \hat{\alpha}_2)(m^2 - m_1^2) + (m^2 - m_1^2)^2 \tag{4.26}$$

giving the initial values

$$\begin{aligned} a_0^{(1)} &= \hat{\alpha}_1 \\ a_1^{(1)} &= 1 \\ a_0^{(2)} &= \hat{\alpha}_1\hat{\alpha}_2 - \beta_1^2 \qquad (4.27) \\ a_1^{(2)} &= \hat{\alpha}_1 + \hat{\alpha}_2 \\ a_2^{(2)} &= 1 \qquad (4.28) \end{aligned}$$

Since the coefficients vary in size by many orders of magnitude, we adopt an exponential parameterisation.

$$a_n = e^{x_n} \tag{4.29}$$

This results in a new set of recurrence relations between the x_n values.

$$x_n^{(p)} = x_n^{(p-1)} + \log(\hat{\alpha}_p + e^{x_{n-1}^{(p-1)} - x_n^{(p-1)}} - \beta_{p-1}^2 e^{x_n^{(p-2)} - x_n^{(p-1)}}) \tag{4.30}$$

The initial conditions become

$$\begin{aligned} x_0^{(1)} &= \log(\hat{\alpha}_1) \\ x_1^{(1)} &= 0 \end{aligned}$$

$$x_0^{(2)} = \log(\hat{\alpha_1}\hat{\alpha_2} - \beta_1^2) \tag{4.31}$$

$$x_1^{(2)} = \log(\hat{\alpha_1} + \hat{\alpha_2})$$

$$x_2^{(2)} = 0 \tag{4.32}$$

As required by Eqn.(4.5) the coefficients are then normalised by dividing out $\det(M(m_0))$.

$$C_n = \frac{a_n}{\det(M(m_0))} \tag{4.33}$$

$$C_n = e^{x_n}(1 \pm \sigma_n) \tag{4.34}$$

where σ_n is the fractional error in C_n.

The coefficients, C_n, are averaged over many configurations and the resulting polynomial is solved for the complex zeros. Since the fermion determinant is real and positive for all real m, the coefficients are real. In the simulations discussed below we always find the C_n to be positive for $m_1 = 0$. It can be easily shown that the coefficients must be positive for all real values of m_1. The determinant may be written in terms of the eigenvalues, $\pm i\lambda$ of M'.

$$\mathrm{Det}M = \prod_{k=1}^{N/2}(m + i\lambda_k)(m - i\lambda_k) = \prod_{k=1}^{N/2}(m^2 + \lambda_k^2) \tag{4.35}$$

$$= \prod_{k=1}^{N/2}((m^2 - m_1^2) + (\lambda_k^2 + m_1^2)) \tag{4.36}$$

The coefficients are thus identified with products of real positive numbers $(\lambda_k^2 + m_1^2)$. This argument holds also if $m_1^2 < 0$ but $|m_1| < \lambda_k \ \forall k$.

4.2.2 Extraction of the zeros from the polynomial

The extraction of the zeros of the averaged polynomial given by Eqn.(4.12) is non-trivial. Fig.(4.2) shows the logarithm of the coefficients $C_n(m_1 = 0)$ obtained from 200 measurements on a 4^4 lattice at strong coupling and update mass $m_0 = 0.025$. The errors shown are statistical.

One immediately notes that, for this lattice size, the coefficients vary in magnitude between e^0 and e^{422} and that their errors (on the logarithmic scale) are small. For small n, they are less than 1% but grow monotonically with n to about 30% at $n = N/2$. This is a consequence of their intrinsic dependence on n and the constraint that

$$\sum_{n=0}^{N/2} \langle C_n \rangle \, m_0^{2n} = 1 \tag{4.37}$$

which follows from Eqn(4.33). Since, in this case, we are updating at a small quark mass, we are minimising the fluctuations in the coefficients which give sizeable contributions to the fermion determinant.For this reason, it is essential to pick an update mass close to the region in which the zeros of the partition function are expected to be. Otherwise many more measurements are required before the errors in the important coefficients are small and the zeros can be determined reliably.

One must also make a good choice for m_1. If $|m^2 - m_1^2|$ is small enough, the last terms of the polynomial will give negligible contributions to the sum. The extraction of the zeros then follows by noting that the distribution of the coefficients as a function of n permits the truncation of the polynomial to order $\hat{N}$ say, finding its zeros by some standard numerical procedure and monitoring their stability as $\hat{N}$ is increased. The zeros obtained by this process are then substituted into the full polynomial and those with small residue are accepted as being true zeros of the polynomial. This procedure can be applied to each of the polynomials arising from different choices of m_1 in order to evaluate the zeros in m close to m_1. The same zeros should appear for adjacent values of m_1 if they are true zeros of the full polynomials. This stability of the zeros should not be confused with their stability with respect to increasing the number of measurements. Essentially, increasing the number of measurements provides a more accurate Taylor's series for the partition function. Hence, as a function of the number of measurements, it is the zeros close to the update mass which will

converge to a constant value first. For the above reasons, it is not possible to determine accurately all the zeros of the partition function. However, the zeros close to the physical region (m real and > 0) can be found and their volume dependence measured.

The shape of the plot of coefficients must be independent of the choice of m_0, this giving only an overall normalisation by a constant multiplicative factor. This has been checked on small lattices.

4.3 Strong Coupling Results

4.3.1 SU(2) and SU(3) Results

Simulations were performed for QCD with SU(2) and SU(3) gauge fields with staggered fermions at $\beta = 0$ and $m_0 = 0.05$ on 2^4 and 4^4 lattices. In the strong coupling limit, we expect only one critical point, the chiral limit at $m = 0$. We therefore expect the relevant zeros of the partition function to be close to $m = 0$.

This is precisely the case in our simulations of $SU(3)$. Here, the zeros are purely imaginary and evenly spaced along the imaginary axis.

$$\text{zero}_n = \pm i(a + nb) \tag{4.38}$$

If we are to recover the expected phase transition at $ma = 0$ as $V \to \infty$ then a and b must scale as V^{-k} with $k > 0$.

The constants a and b appear to scale as L^{-4} as we move from 2^4 to 4^4 lattices. In Fig.(4.3) the imaginary parts of all the zeros on the 2^4 lattice are shown along with the lowest 10 zeros on the 4^4 lattice. The zeros from the 2^4 lattice are scaled by a factor of $2^4/4^4$. The loss of linearity of the zeros on the 2^4 lattice for zeros greater than 0.1 is due to non-negligible errors remaining in the higher coefficients after 800 measurements of the C_n.

For SU(2) the zeros were found to lie in the complex m plane with a non-zero

real part. This is shown in Figs.(4.4 a & b) for 2^4 and 4^4 lattices. The distributions of the zeros in these two cases are similar. A low statistics measurement on a 6^4 lattice at strong coupling confirms that the shape of the distribution does not change greatly with increasing lattice volume, especially in the region close to the real axis. As in SU(3), the imaginary parts of the zeros are evenly spaced and scale with the lattice volume. This is shown in Fig.(4.5) where the imaginary parts of all the zeros on the 2^4 lattice (scaled by a factor $2^4/4^4$) are plotted along with the lowest 20 zeros on the 4^4 lattice. It can also be seen from Figs.(4.4 a & b) that the real part of the zeros close to the real axis scale approximately with the lattice volume. The low statistics run on the 6^4 lattice was in agreement with this scaling behaviour.

We can parameterise the zeros by

$$\text{zero}_n = \pm r_n \pm i(a + nb) \tag{4.39}$$

r, a and b are constants, $n = 0, 1, 2 \ldots$. The real parts, r_n, were observed to scale as L^{-4} on these small lattices. This is consistent with a zero critical mass in the infinite volume limit. The constants a and b are accurately described by a volume scaling behaviour.

Using the distribution (4.38) it is possible to calculate $\langle \overline{\psi}\psi \rangle$ in the infinite volume limit.

$$\ln Z_{SU(3)} = \sum_{n=0}^{3V/2} \ln(m^2 + (a + nb)^2) \tag{4.40}$$

$$= V \int_0^{3/2} \ln(m^2 + (a + Vbx)^2) dx \tag{4.41}$$

where $V = L^4$ is the volume of the lattice. (In the SU(2) case we have

$$\ln Z_{SU(2)} = \sum_{n=0}^{V/2} (\ln((m+r_n)^2 + (a+nb'/V)^2) + \ln((m-r_n)^2 + (a+nb'/V)^2)) \tag{4.42}$$

and the following calculation goes through similarly.)

$$\langle\overline{\psi}\psi\rangle = \frac{1}{V}\frac{\partial}{\partial m}\ln Z \tag{4.43}$$

$$= \frac{2}{Vb}\left[\arctan(\frac{Vbx+a}{m})\right]_0^{3/2} \tag{4.44}$$

Using the finite size scaling behaviour observed in the numerical results, $a = a'/V$, $b = b'/V$ and taking the limit $V \to \infty$,

$$\langle\overline{\psi}\psi\rangle = \frac{2}{b'}\arctan\frac{3b'}{2m} \tag{4.45}$$

If we now take the limit $m \to 0$,

$$\langle\overline{\psi}\psi\rangle \to \frac{\pi}{b'} = 2.01 \pm 0.01 \tag{4.46}$$

using the numerical result $b' = 1.56 \pm 0.01$

A similar calculation in the SU(2) case gives

$$\langle\overline{\psi}\psi\rangle = \frac{2\pi}{b'} = 1.34 \pm 0.03 \tag{4.47}$$

The strong coupling expansion[35], taken to first order in the quark mass gives an expression for the condensate.

$$\langle\overline{\psi}\psi\rangle = \frac{N_c}{\sqrt{2}}\left(\frac{15}{16} - \frac{17}{64}\frac{\beta}{N_c^2} - \frac{5}{32}\frac{\beta^2}{N_c^4} + \frac{m}{\sqrt{8}}(-\frac{3}{4} + \frac{9}{8}\frac{\beta}{N_c^2} + \frac{3}{4}\frac{\beta^2}{N_c^4})\right) \tag{4.48}$$

$$\langle\overline{\psi}\psi\rangle(\beta = 0) = \frac{N_c}{\sqrt{2}}\left(\frac{15}{16} - \frac{3}{4\sqrt{8}}m\right) \tag{4.49}$$

$$= 1.99 - 0.56m \tag{4.50}$$

If we expand the right hand side of Eqn.(4.45) to $O(m)$ we obtain

$$\langle\overline{\psi}\psi\rangle = \frac{2}{b'}\arctan(\frac{3b'}{2m}) \tag{4.51}$$

$$= \frac{2}{b'}(\frac{\pi}{2} - \frac{2m}{3b'}) + O(m^3) \tag{4.52}$$

$$= 2.01 - 0.55m \tag{4.53}$$

The SU(2) results are in similar agreement with the strong coupling expansion.

The distributions of zeros for SU(2) and SU(3) at strong coupling are therefore consistent with chiral symmetry breaking on an infinite lattice but the distributions are different on a finite lattice.

This difference arises from the fact that $SU(2)$ is a pseudo-real group. For $SU(2)$ and $SU(3)$ the partition function is given by an average over the characteristic polynomials, $f_i(m^2)$, each from a single configuration.

$$Z(m) = \frac{1}{N}\sum_{i=1}^{N} f_i(m^2) = \sum C_n m^{2n} \tag{4.54}$$

For staggered fermions, the eigenvalues of the fermion matrix M', on a single configuration, appear in complex conjugate imaginary pairs $\pm i\lambda$ and hence the coefficients of the characteristic polynomials $f_i(m^2)$ are real and positive and consequently the $C_n \geq 0$. Hence $Z(m)$ can have no roots with m^2 real and positive. In addition, since $SU(2)$ is pseudo-real its eigenvalues come in degenerate pairs and we have

$$f_i(m^2) = \left(\sum_j b_j m^{2j}\right)^2 . \tag{4.55}$$

$Z(m)$ for $SU(2)$ is therefore the average of characteristic polynomials, each of which is a perfect square. It can only vanish for m^2 real if *all* the $f_i(m^2) = 0$ at the same value of m^2. However, this cannot be the case since we know that the eigenvalues differ from configuration to configuration. Thus $Z(m)_{SU(2)}$ can have no zeros for any real value of m^2, *i.e.*real *or* imaginary m.

4.3.2 Results for compact U(1)

Simulations were performed of compact $U(1)$ on a 2^4 lattice at $m_0 = 0.1$, 0.8, 1.0 and 1.02 and $\beta = 0.0$. On this small lattice, and with this simple gauge group, the partition function can be calculated analytically as a a polynomial in m^2 [34].

If the polynomial is defined as

$$k(0) + k(1)m^2 + \cdots + k(8)m^{16} \tag{4.56}$$

	ma=0.1	ma=0.8	ma=1.0	ma=1.02
k(0)	1.030	0.990	1.025	0.991
k(1)	28.523	28.166	27.844	27.700
k(2)	179.392	177.867	174.921	174.458
k(3)	438.564	435.607	428.927	427.558
k(4)	511.113	508.347	502.076	499.822
k(5)	310.176	308.652	305.806	304.288
k(6)	99.773	99.316	98.702	98.274
k(7)	16.002	15.949	15.897	15.856
k(8)	1.000	1.000	1.000	1.000

Table 4.1: Normalised coefficients from 2^4 $U(1)$ at various values of the update mass.

then the $k(i)$ are calculated to be as follows.

$$\begin{aligned} k(0) &= 1.0625 \quad & k(1) &= 29 \quad & k(2) &= 182 \\ k(3) &= 444 \quad & k(4) &= 516 \quad & k(5) &= 312 \\ k(6) &= 100 \quad & k(7) &= 16 \quad & k(8) &= 1 \end{aligned} \tag{4.57}$$

When normalised to $k(8)$, the coefficients obtained from the simulations at each update mass were in excellent agreement with each other and with the analytical result (Table 4.1). This must be the case since the update mass contributes only to the overall normalisation of the polynomial.

The zeros were found for each polynomial and were found to be purely imaginary and evenly spaced along the imaginary axis. The zeros from all five polynomials were in agreement to better than 1%. Figure (4.6) shows the imaginary part of $zero_n$ plotted against n.

A strong coupling simulation was then performed on a 4^4 lattice at an update mass of $ma = 0.05$. The zeros were again found to lie evenly spaced along the imaginary m axis. Figure(4.7)

$$zero_n = i(a + nb) \tag{4.58}$$

with $a = 0.014$ and $b = 0.018$

If we repeat the analysis performed on the $SU(3)$ data , assuming, with little justification other than consistency and the desire to have a well defined answer in the infinite volume limit, that the spacing scales as V^{-1} we can obtain an estimate of the chiral condensate.(The 2^4 and 4^4 results show this scaling but this does not constitute a proof.)

$$\left\langle \overline{\psi}\psi \right\rangle = 0.682$$

Again, this is in good agreement with the strong coupling expansion[35].

4.3.3 Analytical Calculations

We may check our simulation by calculating the coefficients of the highest powers of m analytically from Newtons equations. These are a set of recurrence relations which allow the calculation of the coefficients of the characteristic polynomial from the traces of powers of M.

$$\mathrm{Tr}\, M^{2n} + \sum_{i=1}^{n-1} (-1)^i b_i Tr M^{2(n-i)} + 2n(-1)^n b_n = 0 \tag{4.59}$$

$$c(n) = b(N - n) \tag{4.60}$$

The order of coefficients is reversed in Equation(4.60) so that $c(0)$ is the term independent of the mass. Since TrM^2 is independent of the gauge configuration, we may always calculate b_1. The functional integrals over gauge fields is possible in strong coupling, allowing us to calculate b_2 on a 4^4 lattice. With our normalisation

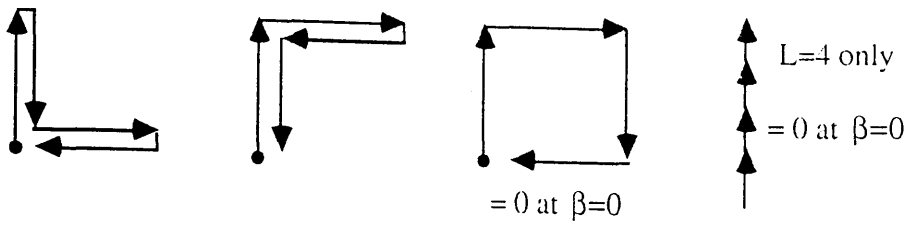

Figure 4.8: Lattice diagrams contributing to $\langle \mathrm{Tr}\, M^4 \rangle$ in strong coupling.

of the fermion matrix,

$$\begin{aligned} \mathrm{Tr}\, M^2 &= 2N_d N_s \frac{1}{4} N_c \\ &= 2N_s N_c \end{aligned} \tag{4.61}$$

where N_d is the dimension of our lattice. In this case $N_d = 4$. The diagrams which contribute to $\mathrm{Tr}\, M^4$ are shown in Figure (4.8). These diagrams have multiplicities $(2N_d)^2$ and $2N_d(2N_d - 1)$ respectively. The Polyakov (Wilson) line and plaquette diagrams, which will contribute on individual configurations, will average to zero on integration over the group manifold, leaving only those terms which are gauge field independent. *i.e.*diagrams in which all links U are matched by the corresponding $U^\dagger$.

This leads to

$$\mathrm{Tr}\, M^4 = \frac{N_s N_c}{16} \left[(2N_d)^2 + 2N_d(2N_d - 1) \right] \tag{4.62}$$

One can similarly calculate $\mathrm{Tr}\, M^6$ and thus obtain analytic values for the last four coefficients.

For $SU(3)$ on a 4^4 lattice we have from equations (4.61 – 4.62)

$$\begin{aligned} \mathrm{Tr}\, M^2 &= 1536 \\ \mathrm{Tr}\, M^4 &= 5760 \\ \mathrm{Tr}\, M^6 &= 26304 \end{aligned} \tag{4.63}$$

This, along with the recurrence relations gives us

$$b_0 = 1 \tag{4.64}$$

$$b_1 = \frac{1}{2}\operatorname{Tr} M^2 = 768 \tag{4.65}$$

$$b_2 = \frac{1}{4}\left(-\operatorname{Tr} M^4 + \frac{1}{2}(\operatorname{Tr} M^2)^2\right) = e^{12.59} \tag{4.66}$$

$$b_3 = \frac{1}{6}\left(\operatorname{Tr} M^6 - \frac{3}{4}\operatorname{Tr} M^4 \operatorname{Tr} M^2 + \frac{1}{8}(\operatorname{tr} M^2)^3\right) = e^{18.125} \tag{4.67}$$

The numerical results, when normalised so that $b_0 = 1$, give 768 , $e^{12.59}$ and $e^{18.125}$. Here we have made the factorisation

$$\langle \operatorname{Tr} M^p \operatorname{Tr} M^q \rangle = \langle \operatorname{Tr} M^p \rangle \langle \operatorname{Tr} M^q \rangle \tag{4.68}$$

since we have to match every U with the corresponding $U^\dagger$. This factorisation breaks down on a lattice of length 2. On a 2^4 lattice, say, sites 1 and 2 will be connected by links U_{12} and U_{21}. $\operatorname{Tr} M^2$ will have terms such as

$$\operatorname{Tr}(U_{12} + U_{21}^\dagger)(U_{12}^\dagger + U_{21}) \tag{4.69}$$

The cross terms will vanish when we calculate $\langle \operatorname{Tr} M^2 \rangle$ but $\langle (\operatorname{Tr} M^2)^2 \rangle$ will have a term $U_{12}U_{21}U_{12}^\dagger U_{21}^\dagger$ coming from these cross terms. Our factorisation will not give the correct result in this case. It will obviously also be invalid for $\langle (\operatorname{Tr} M^4)^2 \rangle$ on all lattice sizes since the plaquette/plaquette† will also contribute at this order and above. However, since this is at the same order as $\langle \operatorname{Tr} M^8 \rangle$ it is beyond the point where we have attempted to enumerate all the contributing diagrams. The factorisation is therefore valid only for the terms which we calculate on the 4^4 lattice.

In principle one could continue this process but since the coefficients which govern the physics are the lowest ones it is not a practical method for the study of the partition function. The number of diagrams contributing to the higher traces

will become very large and the multiplicities will become almost impossible to calculate. Nevertheless, this is a useful check on our method in strong coupling. Since $\mathrm{Tr}\, M^2$ is independent of the gauge field, we may use this known value as a check on our simulations at all couplings.

4.4 Conclusions

Application of our method to the partition function of strongly coupled gauge theories with staggered fermions gives encouraging results. We obtain the expected value for the critical mass, $m_{\mathrm{crit}} = 0$ and can give an estimate of the chiral condensate in the $V \to \infty$, $m \to 0$ limit which is in good agreement with the strong coupling expansion.

The results obtained using this method in the strong coupling case are sufficiently encouraging for an investigation at intermediate coupling to proceed. We expect that the zeros will move out into the complex m plane and indicate a phase transition at a finite value of m for a prescribed value of the coupling, β.

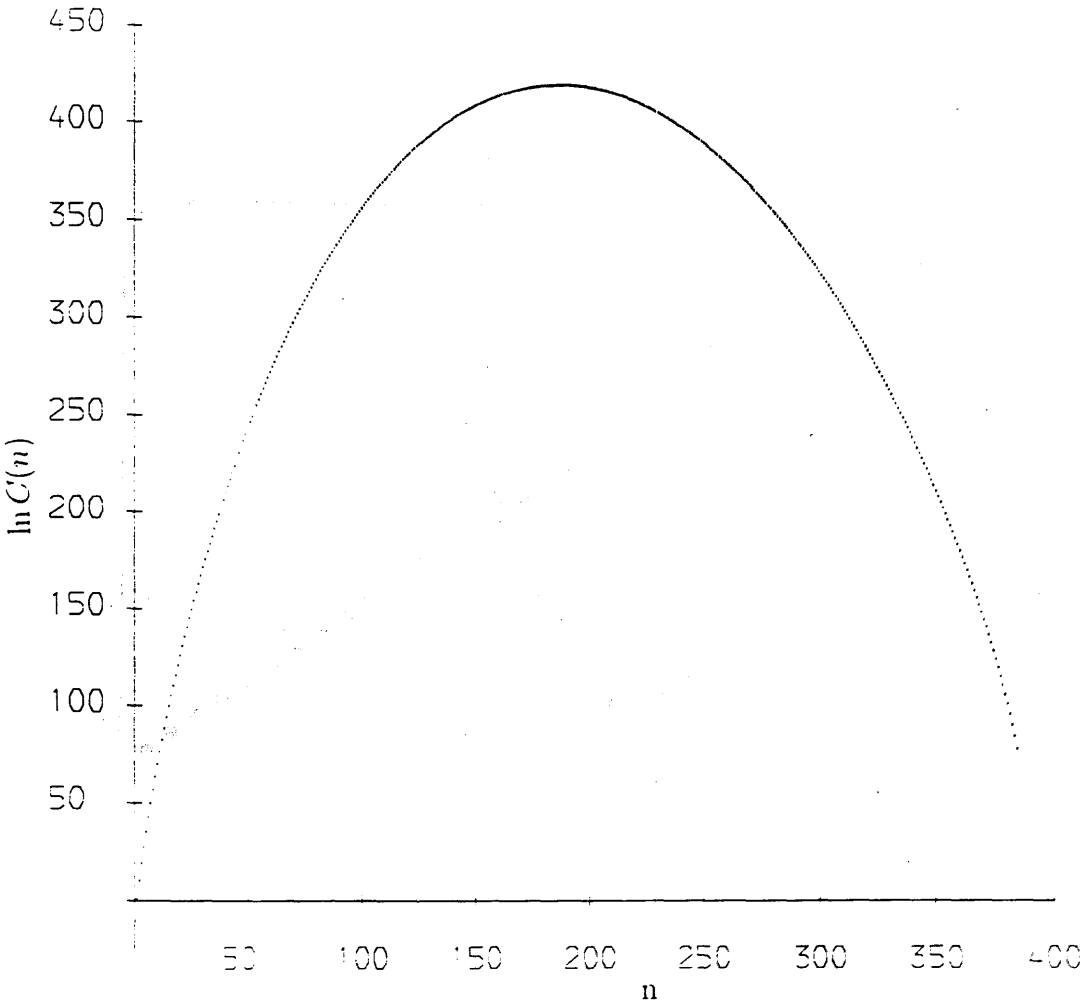

Figure 4.2 : The logarithms of the coefficients of the partition function for $SU(3)$ at $\beta = 0.0$ on a 4^4 lattice. The expansion is around $m_1 = 0.0$ averaged over 200 configurations.

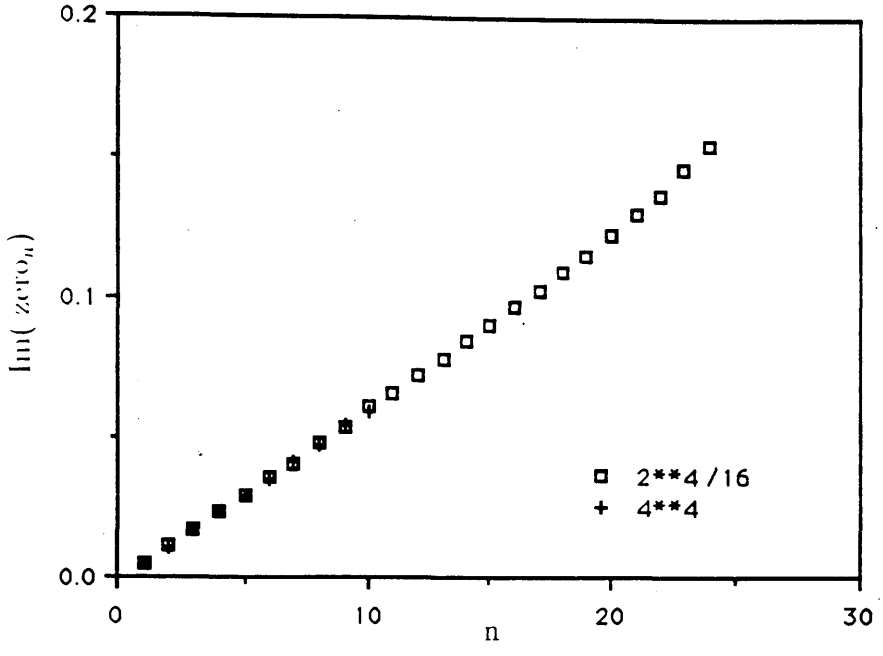

Figure 4.3 : The imaginary part of the n^{th} zero of the partition function, for $SU(3)$ at $\beta = 0.0$ on 2^4 and 4^4 lattices, plotted against n. The 2^4 results are scaled by a factor of $2^4/4^4$.

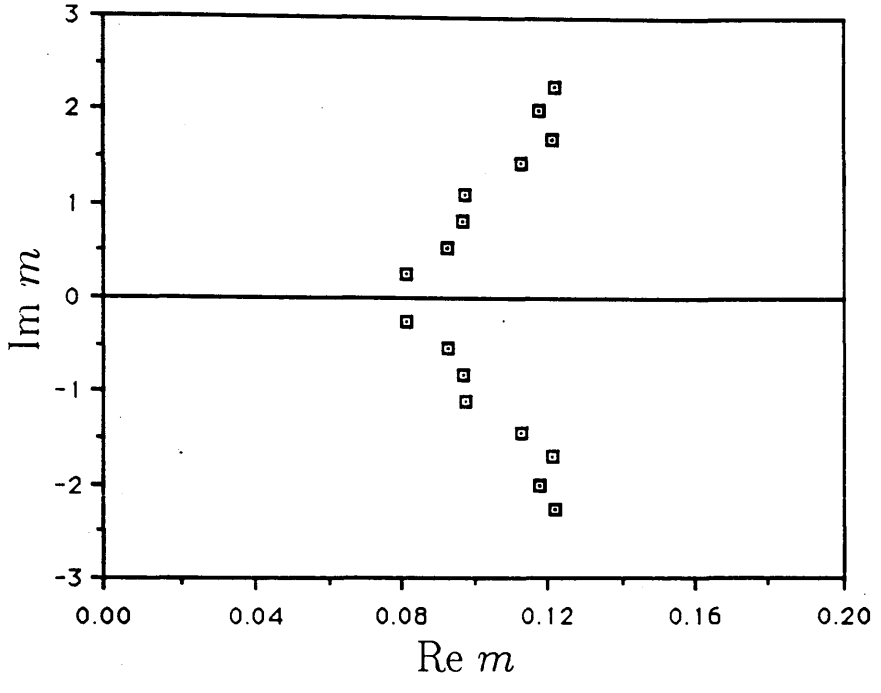

Figure 4.4a : The zeros of the partition function in the complex quark mass plane for $SU(2)$ on a 2^4 lattice. Averages are taken over 10200 configurations. Only those zeros with $\mathrm{Re}(m) > 0$ are plotted as there is a $\pm$ symmetry.

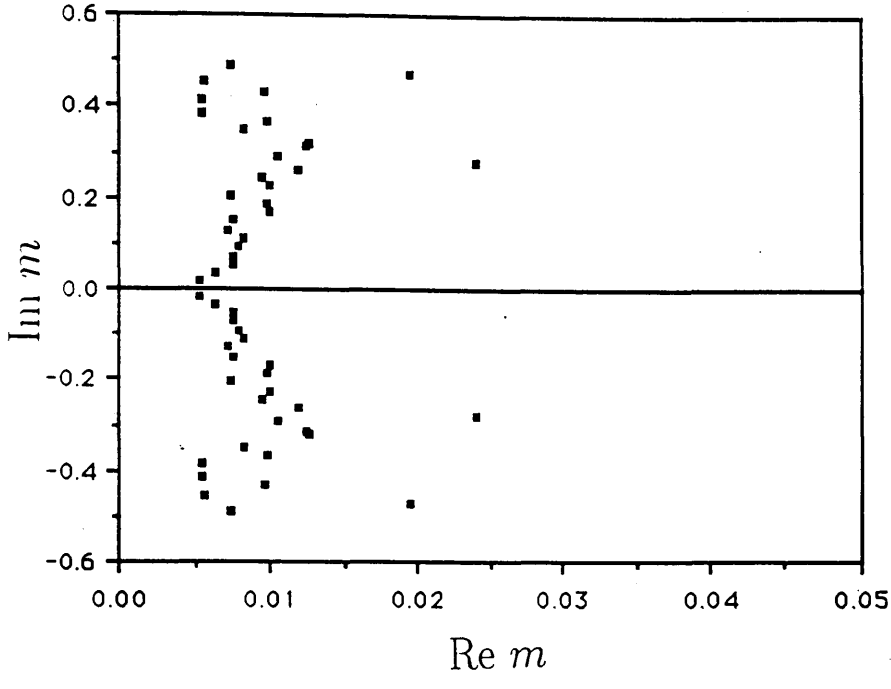

Figure 4.4b : The zeros of the partition function in the complex quark mass plane for $SU(2)$ on a 4^4 lattice. Averages are taken over 1500 configurations.

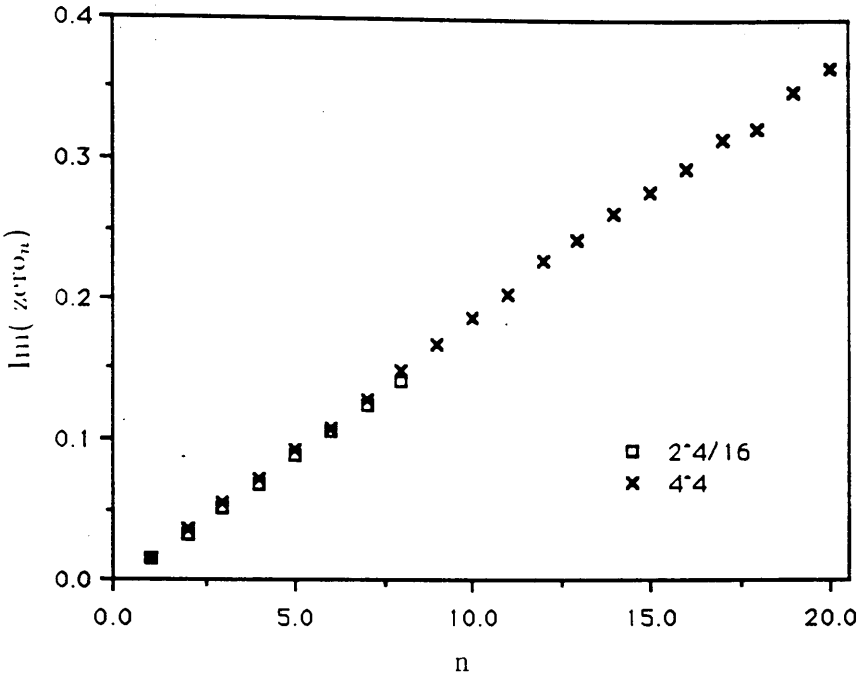

Figure 4.5 : The imaginary part of the n^{th} zero of the partition function, for $SU(2)$ at $\beta = 0.0$ on 2^4 and 4^4 lattices, plotted against n. The 2^4 results are scaled by a factor of $2^4/4^4$.

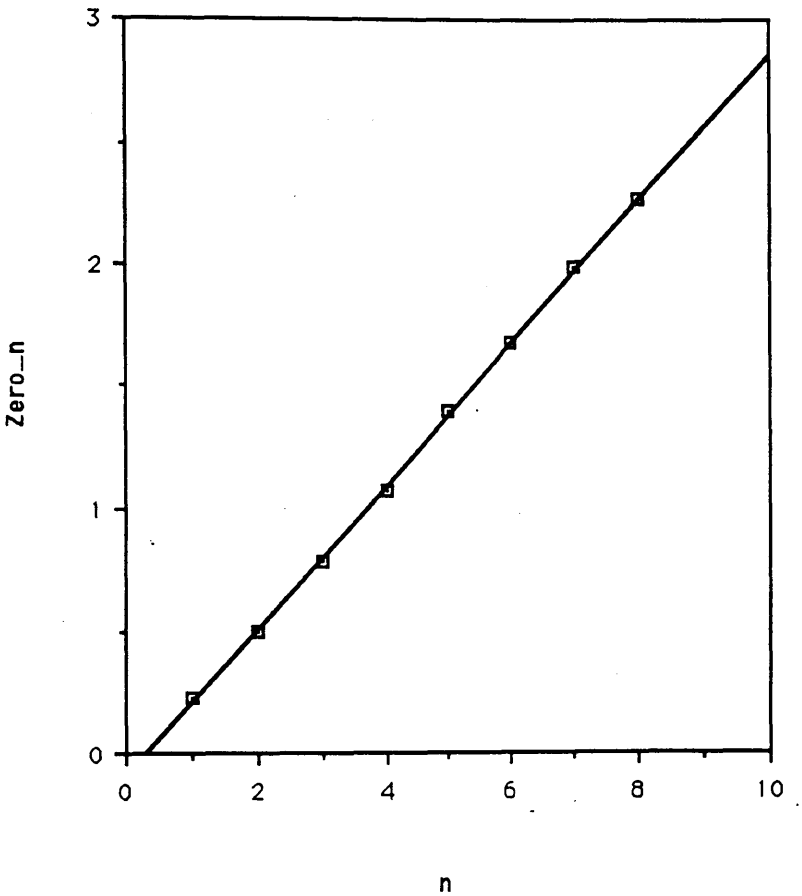

Figure 4.6 : The imaginary part of the n^{th} zero of the partition function, for $U(1)$ at $\beta = 0.0$ on a 2^4 lattice, plotted against n.

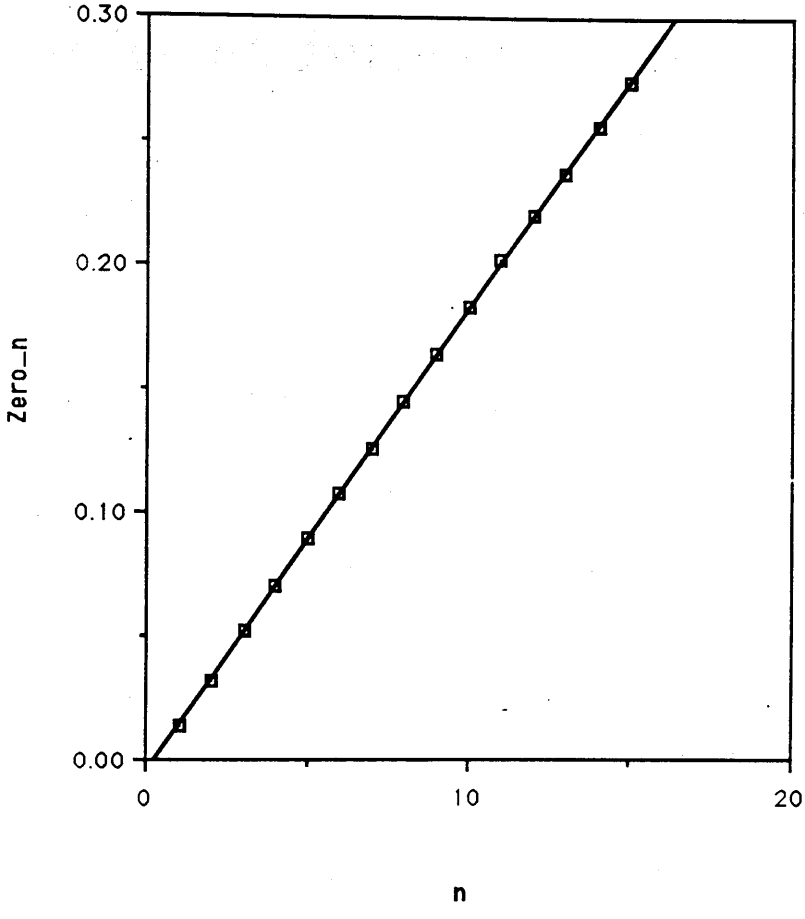

Figure 4.7 : The imaginary part of the n^{th} zero of the partition function, for $U(1)$ at $\beta = 0.0$ on a 4^4 lattice, plotted against n.

Chapter 5

Results at Intermediate Couplings

5.1 Introduction

In this chapter we generalise the method of Chapter 4 to weaker couplings. We expect to find a phase diagram qualitatively similar to Figure (4.1), with $m_c a = 0$ at low β and a critical line extending from $ma = 0$ at some value of β and interpolating between the chiral phase transition at $ma = 0$ and the pure gauge deconfinement transition at $ma = \infty$. It is still an open question as to whether the critical line is continuous across the whole range of quark masses. Some investigations[36,39] have concluded that the phase transition disappears for masses above a certain value . This corresponds to a break in the critical line for intermediate masses (Fig.(5.1)).

Previous investigations of this phase diagram have looked for a critical coupling at fixed ma. Some evidence has been found for a phase transition up to $ma = 1.0$ on lattices with temporal extent,$n_t = 4$ [46]. There is strong evidence that this phase transition is first order for small bare quark masses, but weakens and eventually becomes a continuous cross-over for larger values of ma.[37] The

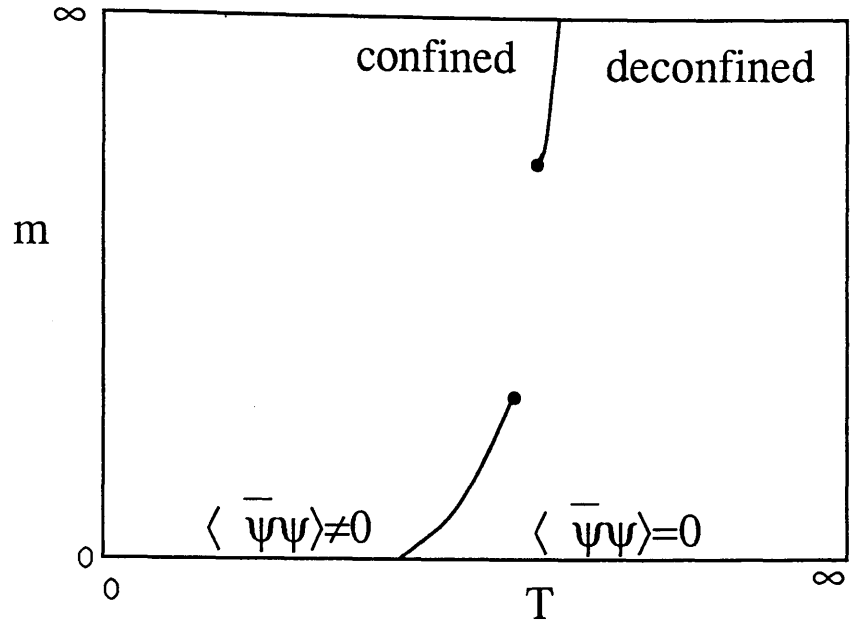

Figure 5.1: Another proposed phase diagram for QCD at finite temperature. Compare with Fig.(4.1).

behaviour of the maximal mass for which the transition is first order as the lattice size, particularly in the time direction, is increased should tell us if the transition persists for finite masses in the continuum.

A modified measurement method, which will allow the extension of the method to larger lattices, is decribed. This new method, along with our original method, is used to investigate the phase diagram of QCD on a 4^4 lattice at four values of β. These simulations give four points on the critical line which are in agreement with previous published data.

At one of these values of β, the behaviour of the zeros is studied as the lattice size is increased to $6^3.4$.

5.2 Avoiding Reorthogonalisation

5.2.1

Our measurement algorithm, as described in Chapter 4, suffers from a huge memory requirement which will ultimately prevent us from continuing to larger lattices. This results from our need to calculate all the Lanczos α's and β's before we can construct our polynomial. In order that we can do this we must artificially maintain orthonormality of the Lanczos vectors, lost due to rounding errors. For this purpose we must store all the Lanczos vectors at each stage. This means that we need extra storage for $N_s N_c/2$ complex vectors, each of length $N_s N_c/2$. On a 4^4 lattice this amounts to almost 2.5Mb and, on a 6^4 lattice, to over 60Mb.

We can avoid this problem by allowing the Lanczos vectors to drift out of orthonormality as we iterate the algorithm. In order that the Lanczos vectors still span the N-dimensional space of the eigenvectors we will now have to perform $M > N$ iterations of the Lanczos algorithm. We may now use the method of Sturm sequences (See section 5.2.2) to find the eigenvalues of the $M \times M$ matrix and sort out those which are also eigenvalues of the original $N \times N$ matrix. We know that the sum of the eigenvalues of $(M^\dagger M)_e$ is a constant, $2N_s N_c$, since $\mathrm{Tr}\, M^\dagger M$ is gauge field independent, so we can easily check that we have found all the correct eigenvalues.

We may then use the eigenvalues to calculate the coefficients of the characteristic polynomial.

$$A_N = \begin{vmatrix} \lambda_1 + m^2 & & & \\ & \lambda_2 + m^2 & & \\ & & \ddots & \\ & & & \lambda_N + m^2 \end{vmatrix} \tag{5.1}$$

$$A_N = A_{N-1}(\lambda_N + m^2) \tag{5.2}$$

$$\sum c_n^N m^{2n} = \sum c_n^{N-1} m^{2n}(\lambda_N + m^2) \tag{5.3}$$

$$\tag{5.4}$$

$$c_n^N = \lambda_n c_n^{N-1} + c_{n-1}^{N-1} \tag{5.5}$$

This method takes approximately the same time as the method with reorthogonalisation on a 4^4 lattice and gives a considerable memory saving.

5.2.2 Sturm Sequences

Let B_r be the $r \times r$ matrix formed by taking the first r rows and columns of an $N \times N$ hermitian matrix. Define the polynomials $P_0(\lambda) \ldots P_N(\lambda)$ as the characteristic polynomials of $B_0 \ldots B_N$.

$$P_0(\lambda) = 1 \tag{5.6}$$

$$P_r(\lambda) = \mathrm{Det}(B_r - \lambda I) \tag{5.7}$$

Then, for any real value of λ, the number of sign changes in the sequence $\{P_0(\lambda), P_1(\lambda), \ldots, P_N(\lambda)\}$ equals the number of eigenvalues of B_N less than λ.

For a tridiagonal matrix we may calculate the $P_r(\lambda)$ using a recurrence relation.

$$P_r(\lambda) = (\alpha_r - \lambda)P_{r-1}(\lambda) - \beta_{r-1}^\dagger \beta_{r-1} P_{r-2}(\lambda) \tag{5.8}$$

It is usually more convenient to calculate the ratios of successive terms in the sequence.

$$r_r(\lambda) = \frac{P_r(\lambda)}{P_{r-1}(\lambda)} = \alpha_r - \lambda - \frac{\beta_{r-1}^\dagger \beta_{r-1}}{r_{r-1}(\lambda)} \tag{5.9}$$

$$r_0(\lambda) = 0 \tag{5.10}$$

The number of eigenvalues less than λ is now given by the number of negative terms in the sequence $\{r_0(\lambda), \ldots, r_N(\lambda)\}$.

By successive bisections of an interval which is known to originally contain all the eigenvalues, we may home in on the k^{th} eigenvalue.

If an eigenvalue of the $N \times N$ matrix lies in the interval $(\lambda - \delta, \lambda + \delta)$ then we may also check to see if it is also an eigenvalue of the $(N-1) \times (N-1)$ matrix. The most convenient way to do this is to look at $r_N(\lambda - \delta)$ and $r_N(\lambda + \delta)$. If these terms have the same sign then there is also an eigenvalue of the smaller matrix in the interval $(\lambda - \delta, \lambda + \delta)$.

The *shift* of an eigenvalue is defined as the smallest δ for which the eigenvalue remains in the interval on the removal of the last α and β.

Real eigenvalues of the smaller matrix, $M^\dagger M$, will have a small shift since the eigenvectors will have small entries after the first $N_s N_c/2$ places. In contrast, the eigenvectors of spurious eigenvalues will have large entries and so will be sensitive to the removal of the last α and β, resulting in a large shift.

Another problem which must be dealt with is the duplication of real eigenvalues. If we continue the algorithm long enough for the slowly converging eigenvalues to be obtained, those eigenvalues of $M^\dagger M$ which converge quickly may appear several times as eigenvalues of B_N. We therefore assume nondegeneracy of the eigenvalues and demand that successive eigenvalues differ by more than some cut-off.

5.3 Results at Intermediate Couplings on a 4^4 lattice

5.3.1 $\beta = 3.0$

At a coupling of $\beta = 3.0$ QCD is still in the strong coupling regime. The lowest zeros of the partition function,in the complex quark mass plane, are still evenly spaced along the imaginary axis. The imaginary part of the n^{th} zero is plotted against n in Fig.(5.2).

The spacing in this case is greater than in the $\beta = 0.0$ case. Thus, if the

chiral condensate is calculated by the same method as in Chapter 4, one obtains a lower value in the infinite volume limit. This is what we expect as we make the coupling weaker.

$$\left\langle \overline{\psi}\psi \right\rangle (\beta = 3.0) = 1.60 \tag{5.11}$$

$$\left\langle \overline{\psi}\psi \right\rangle (\beta = 0.0) = 2.01 \tag{5.12}$$

5.3.2 $\beta = 5.04$

It is only as one weakens the coupling to the vicinity of the finite temperature phase transition that one expects the zeros to migrate off the imaginary axis and move onto the complex m plane. This is illustrated in Fig.(5.3b) where we show the zeros of the partition function in the complex mass plane at $\beta = 5.04$ on a 4^4 lattice. Configurations were generated using an update quark mass of $m_0 = 0.025$ and 3060 measurements (using the original method, including reorthogonalisation.) of the coefficients of the characteristic polynomial were averaged. The shape of the coefficients, C_n, when plotted as a function of n,(Fig. (5.3a)), is visually similar to that at strong coupling (Fig.(4.2)) but a strong signal was found for the complex nature of the zeros (Fig(5.3b)).

The positions of the zeros were monitored every 50 measurements during the simulation. The imaginary parts of those zeros close to the real axis were seen to stabilise very quickly, but many more measurements were required before the real parts stopped increasing and began to converge towards stable values. This is shown in Fig.(5.4) where we plot the lowest zeros as a function of the number of measurements averaged over. The lowest three zeros are very close to convergence. Again, since the characteristic polynomial is in m^2, there are corresponding zeros in the unphysical Real(m) < 0 plane.

The zeros form a distribution which is qualitatively similar to the ideal case described in Chapter 3 (Fig.(3.2)). The zeros approach the real m axis at on

one point, indicating that the system on a finite lattice must be attempting to simulate a 'phase transition' at m_c close to 0.05 . *i.e.*for $m < 0.05$ the system will simulate the chirally restored phase and for $m > 0.05$ it will be in the broken phase. Since the zeros have still not fully converged to constant values, we can put a good lower bound on the value of m_c but the upper bound can only be obtained from a fit to the data. The bound obtained from this fit is obviously dependent on the functional form we fit to. We therefore give a fairly conservative error estimate on m_c.

$$m_c(\beta = 5.04) = 0.045 \begin{array}{l} +0.01 \\ -0.003 \end{array} \tag{5.13}$$

5.3.3 $\beta = 4.9$

In this case, the coefficients of the expansion of the partition function were averaged over 3260 measurements at a coupling of $\beta = 4.9$ on the 4^4 lattice. The simulation again had an update quark mass of 0.025.

The behaviour of the zeros is slightly different in this case, probably because we find we are simulating in the chirally broken phase whereas at $\beta = 5.04$ we were in the restored phase.

The final distribution has the same basic shape as the previous case, with the 'pinch' onto the real axis occurring at $ma \simeq 0.01$. (Fig.(5.5)) The difference between the two cases is not in the final distribution: this must be independent of the update mass and thus independent of which phase we are simulating. The difference occurs in the way the zeros approach their final values. In this case, complex zeros appear after around 200 measurements and then *decrease* towards a constant value. (Fig.(5.6 a & b)) Again, the imaginary parts stabilise much more quickly than the real parts.

Simulation at such a low bare quark mass, $ma \sim 0.01$, is very difficult and expensive in computer time since the matrix inversion required in the update

process becomes much more ill conditioned. Our method allows the extraction of information relevant at this quark mass without encountering the problems of simulating there.

5.3.4 $\beta = 5.2$

The measurement method without reorthogonalisation was used to perform 1200 measurements at $\beta = 5.2$ with m_0 =0.18.

The zeros again form a 'cavity' around the low m part of the real axis, (Fig(5.7)) but in this case the approach of the zeros towards the real axis at the 'critical' mass is much less pronounced. We find the critical mass to be at around $m = 0.2$.

This is consistent with a weakening of the transition at this mass and coupling. Estimates of the largest bare quark mass at which one would see a discontinuity in $\langle\overline{\psi}\psi\rangle$ as β is increased indicate that this is above or at least around that value, am_{max}. S. Gottlieb, in Lattice 90, estimates $am_{max} \simeq 0.07$ [37] for lattices with $n_\tau = 4$. In the same proceedings, A. Vaccarino estimates $0.05 \leq am_{max} \leq 0.2$ [38].

5.4 Extension to larger lattices

The removal of the requirement that the Lanczos vectors be stored for reorthogonalisation allows us to increase the size of the system under consideration. This extension could follow either of two paths.

The lattice could be enlarged isotropically and the zeros monitored as we move towards the infinite volume, zero temperature limit. In this case, we would expect the zeros to approach the real m axis, indicating a sharpening of the transition, and simultaneously the point of closest approach should move towards $\mathrm{Re}(m) = 0$. This would indicate a true critical point at $m = 0$ in the $V \to \infty$ limit.

The second option, and the one chosen here, is to increase the spatial size of the lattice while keeping the temporal extent constant. Provided the coupling , and hence the lattice spacing, is kept constant our system remains at a constant physical temperature. Here we expect (hope?) that the lowest zeros will approach the real axis but with approximately constant real part.

5.4.1 Results on the $6^3 4$ lattice

Simulations were performed at $\beta = 5.04$ on a lattice of size $6^3 4$. In the light of the results from the 4^4 lattice, the update mass was chosen to be $ma = 0.04$. We hope that the zeros closest to the real axis will still lie close to this point on the larger lattices. A Taylor expansion of the partition function around the update mass will have small statistical errors in the first few coefficients. If the zeros of interest do indeed lie close to this point then we should be able to obtain estimates of their values after many fewer measurements.

It should be stressed again that our choice of update mass does not affect the positions of the zeros. It merely influences which zeros we can obtain after a certain number of measurements.

The position of the smallest zero (*i.e.*the zero closest to the real axis) was monitored as a function of the number of measurements made on the $6^3 4$ lattice. When the simulation was stopped, after 225 measurements, the lowest two zeros had converged to stable values. The exact positions of other zeros could not be determined, although the general area covered by them could be estimated from the positions of less well determined zeros obtained from expansions around various values of the mass. (Fig.(5.8))

The lowest zero was seen at $(Re(m), Im(m)) = (0.0424, 0.0093)$. The real part of the zero is slightly smaller than in the 4^4 case. This is consistent with the corresponding increase of β_c in traditional finite temperature simulations as the spatial size of the lattice is increased.

As expected, the lowest zero is seen to approach the real axis as we increase the lattice size.

The method was also applied to a system of size $8^3.4$ at a coupling of $\beta = 5.04$. In this case, due to limits on computer time — one update and measurement requires $\sim 1\frac{1}{2}$ Cray XMP hours.— it was only possible to perform 100 measurements. The zeros obtained from this simulation do not appear to have converged to their physical values (Figure(5.9)). No agreement is seen between zeros obtained using different values of m_1. No signal is seen, however, that the method is breaking down on this lattice size. This appears to be yet another lattice problem which simply requires more cpu time or preferably more Mega(or Giga)Flops. The problem of non-agreement between different expansions is a sign that we have pushed our root-finder to its limit. The range of magnitudes covered by the coefficients means that, even using suitable changes of variables, we can only use 170 of the 3073 coefficients. Some zeros are found which appear to be relatively insensitive to the level of truncation on individual expansions. However, if we are to obtain agreement between different expansions, we will have to solve much larger polynomials. This will probably require the development of a specialist algorithm of the type used by Karliner, Sharpe and Chang [32].

5.4.2 Infinite volume and continuum limits

The above results , showing the approach of the partition function zeros to the real axis as L_s increases, would indicate a real phase transition at finite m as the spatial size of the lattice goes to infinity. This $L_s \to \infty$ limit at fixed β does not describe continuum QCD but some explicitly lattice theory with *fixed* and *finite* lattice spacing.

It would be interesting to see the behaviour of the transition point as the continuum limit is approached. In particular, is there a phase transition which extends to $m_q > 0$ in the continuum?

The approach to the continuum limit would be obtained by increasing β, thereby reducing the lattice spacing, and simultaneously increasing the number of sites in the time-like direction, n_τ, in such a way as to keep the temperature, $T = 1/an_\tau$, constant. Obviously, this process would require a prohibitive cost in computer time. It is, however, interesting to speculate as to possible results.

Since we are changing the coupling, we have one more level of complication. The quantity we can measure is $m_c a$, while the physical object is m_c. We can deal with this in the following way.

Consider the ratio of the two physical quantities T and m_c.

$$\frac{m_c}{T} = an_\tau m_c \tag{5.14}$$

We can measure am_c and n_τ and so we know the value of m_c/T. If we can keep the temperature constant, while increasing n_τ, we can investigate the behaviour of m_c.

As we increase β we must monitor the reduction in a by calculating correlation lengths. We must be in the scaling region of course. We then increase n_t to keep the temperature constant. In this way the behaviour of m_c could be studied. As we get deeper into the scaling regime, we would hope that m_c/T would approach the continuum value , $m_c(continuum)/T$.

The analysis of Gottlieb [37] predicts the maximum value of ma at which we can have a first order transition. This value, am_{max}, is seen to decrease as the lattice size increases, n_τ going from 4 to 6 to 8. Since this transition must be taking place at the same physical temperature on all three lattice sizes we may use Equation(5.14) to look for scaling behaviour. The results are shown in Table(5.1). Substantial violation of scaling occurs between $n_\tau = 4$ and $n_\tau = 6$. As we go from 6 to 8, however, the behaviour is much better. Using estimates of $m_{max}(continuum)/T_c$ and of T_c we can obtain a value for $m_{max}(continuum)$.

$$m_{max} = \frac{m_{max}}{T_c} T_c \simeq 0.120 \times 100\text{MeV} \simeq 12\text{MeV} \tag{5.15}$$

n_τ	am_{max}	$m_{max}/T_c = am_{max}n_\tau$
4	0.073	0.292
6	0.021	0.126
8	0.015	0.120

Table 5.1: Scaling behaviour of m_max. Taken from S. Gottlieb in Lattice 90.

Thus, for some values of the coupling, such that $T \simeq T_c$, we might expect m_c to approach a non-zero value in the continuum limit.

5.5 Comparison with previous published data

There have been several studies of finite temperature QCD on lattices with $N_t = 4$. The spatial sizes of these lattices varies from 4^3 to 12^3. These simulations used several different update algorithms— Exact updating [40,41], Langevin[46], Hybrid[44,45] and Hybrid Monte Carlo [43,42]— but all look for β_c at a fixed value of m.

The results for β_c are in general insensitive to the spatial size of the lattice, with the exception of the 4^34 simulations which give results which, while comparable, are consistently slightly lower than the larger lattices at the same value of the quark mass.

Fig.(5.10) shows a comparison of our results with results from several other sources. The agreement, considering the radically different method of measurement, is very good. Our results on 4^34 lattices are , in fact, consistently closer to the $L_s \geq 6$ results than are previous 4^34 simulations. This may be due to finite size effects affecting the two methods in different ways.

5.6 Conclusions

The method described above can be seen in two ways. It can be considered as an alternative method for finite temperature lattice field theory. As such it gives results which are in agreement with previous methods.

A second use, which is equally applicable on isotropic lattices, is in investigating the smallest dynamical quark mass which should be used on any particular lattice at given coupling. If one makes the bare quark mass too small then the thermodynamics of the system will be altered. The system will be in the wrong phase and *e.g.*the masses of hadronic excitations could be drastically different.[47] Ideally one would like to approach the chiral limit, $ma = 0$, or at least work with quark masses which are comparable to the masses of the light up and down quarks which form the lowest hadronic states. The measurement of hadronic masses requires much lower bare masses than are used at present.

Study of the zeros of the partition function may give some information regarding the allowable values of ma in future simulations and on the size of lattice required in order that 'physical' quark masses can be simulated.

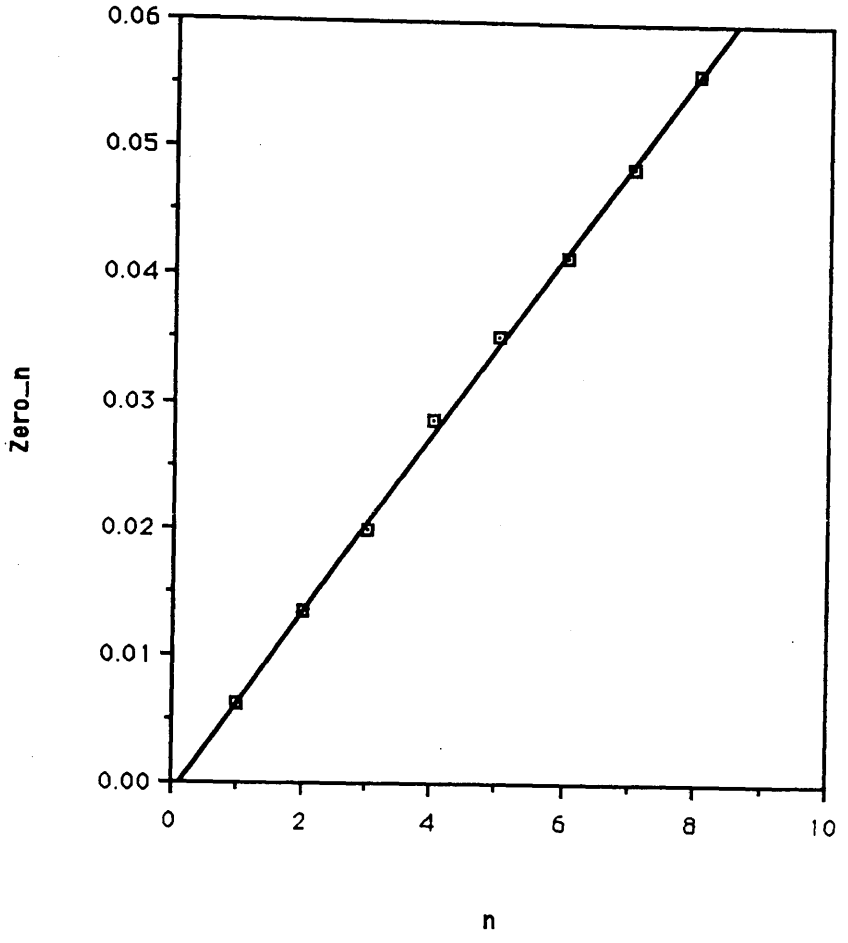

Figure 5.2 : The imaginary part of the n^{th} partition function zero, for $SU(3)$ at $\beta = 3.0$ on a 4^4 lattice, plotted against n.

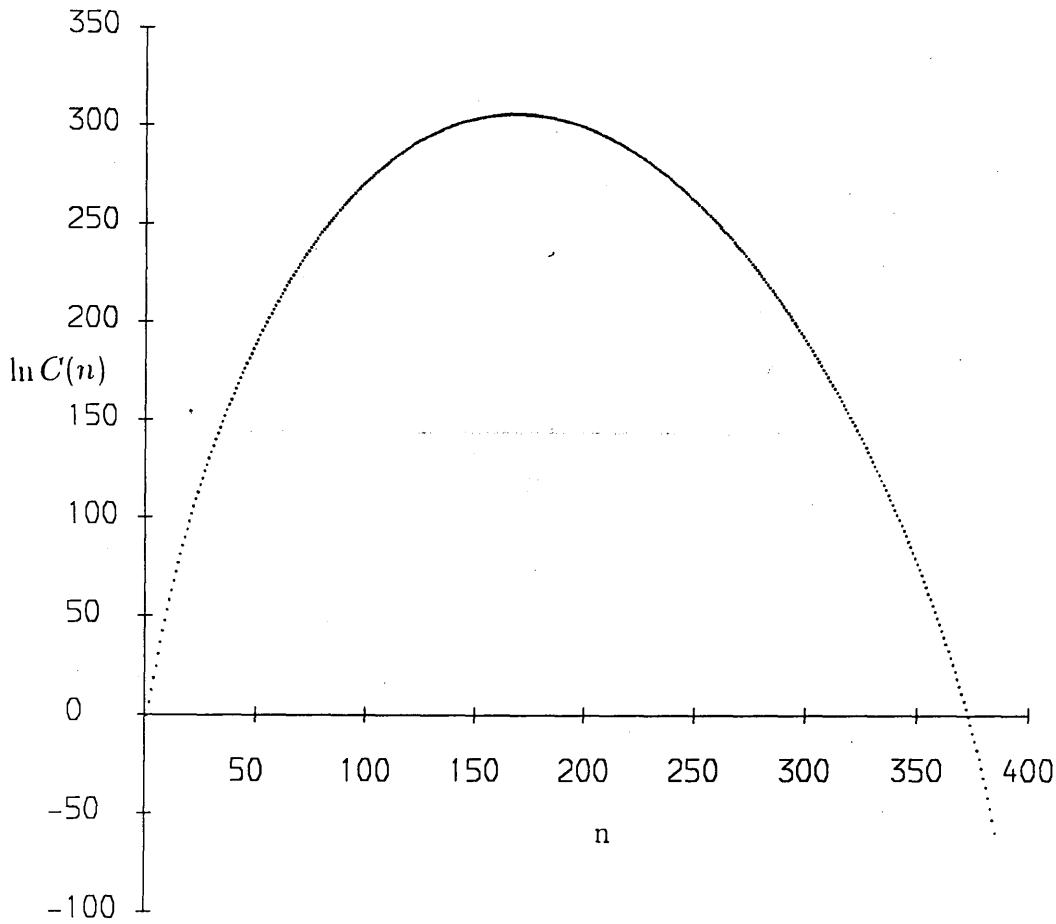

Figure 5.3a : The logarithms of the coefficients of the partition function expanded in the bare quark mass for $SU(3)$ at $\beta = 5.04$ on a 4^4 lattice. Averages are taken over 3060 configurations.

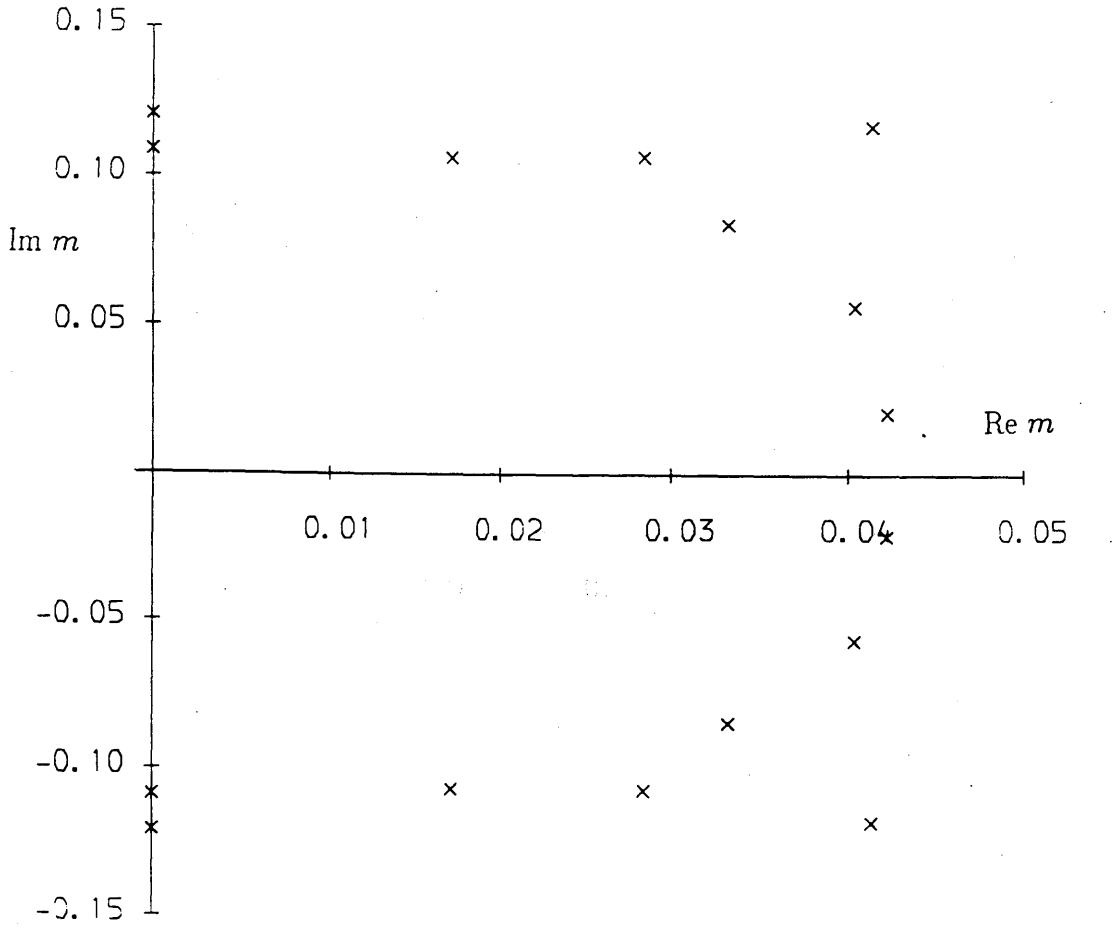

Figure 5.3b : The partition function zeros in the complex quark mass plane for $SU(3)$ at $\beta = 5.04$ on a 4^4 lattice. Averages are taken over 3060 configurations.

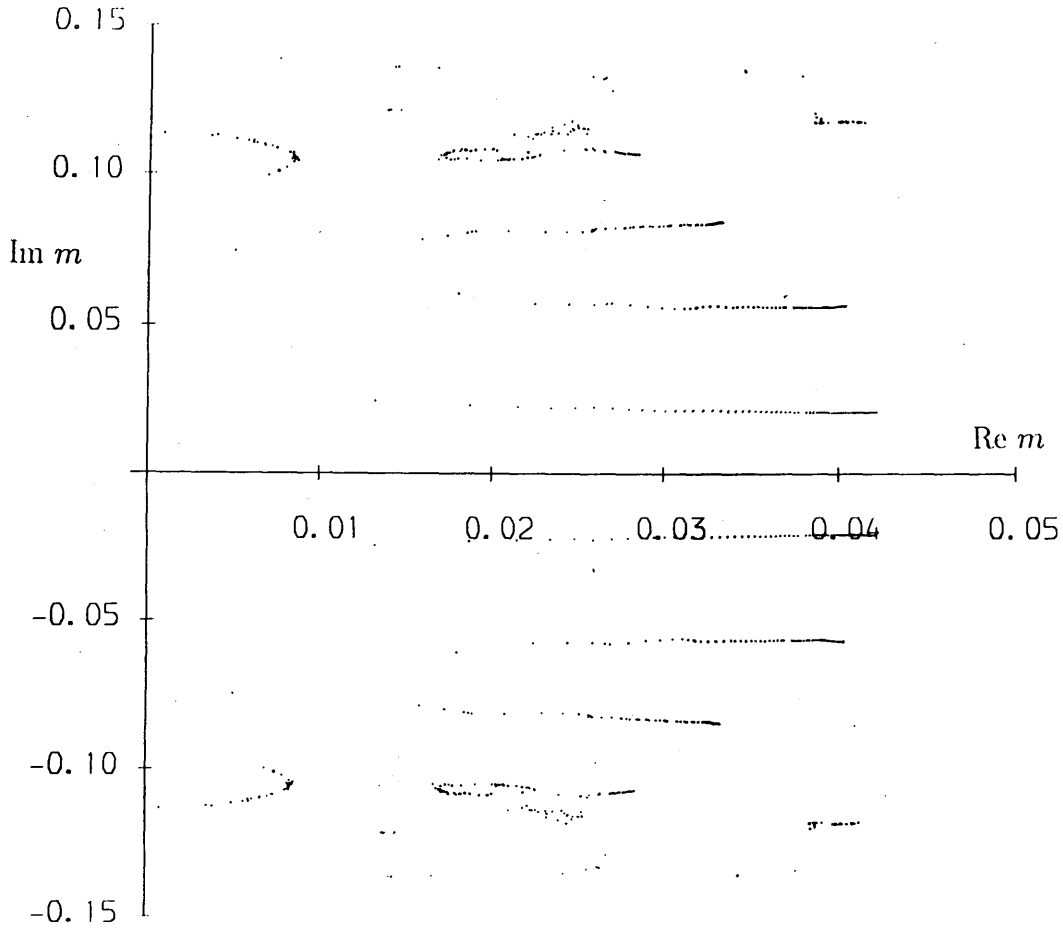

Figure 5.4a : The evolution of the lowest zeros for the same system as Fig.(5.3). The zeros are plotted every 50 measurements.

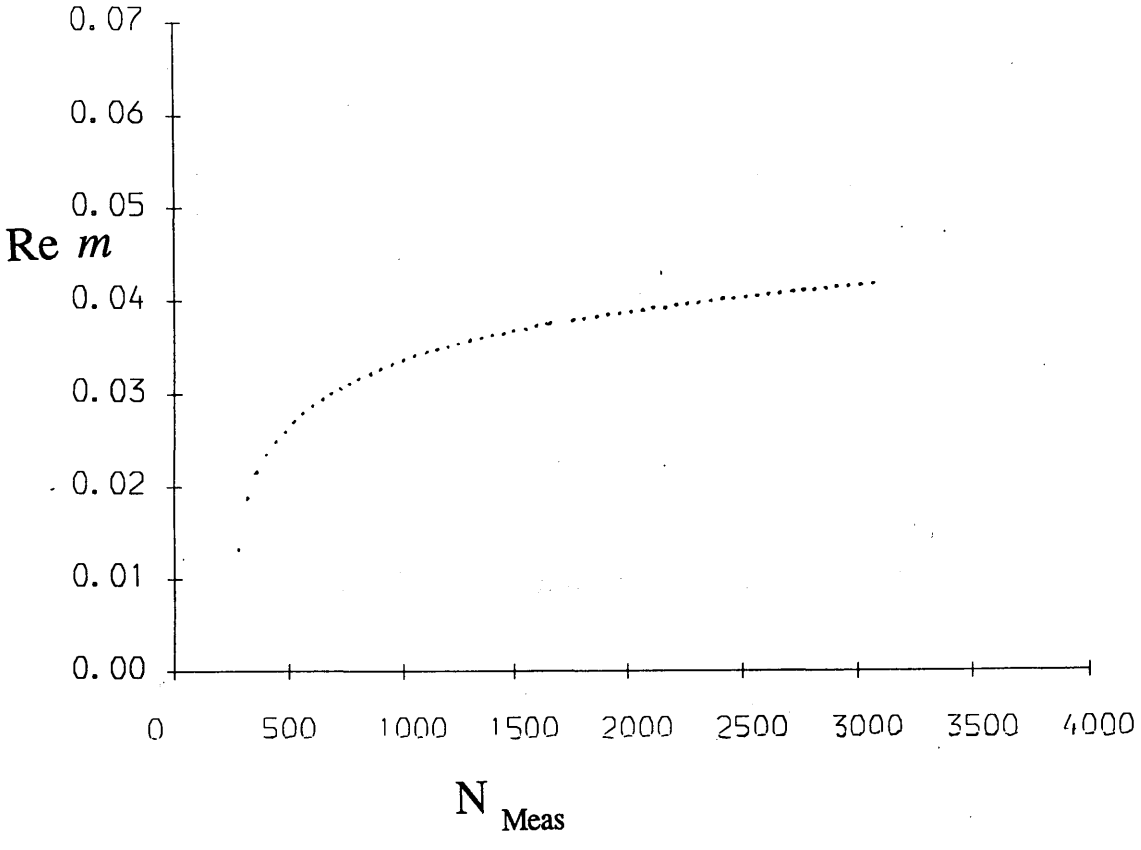

Figure 5.4b : The real part of the zero closest to the real axis plotted against the number of measurements made.

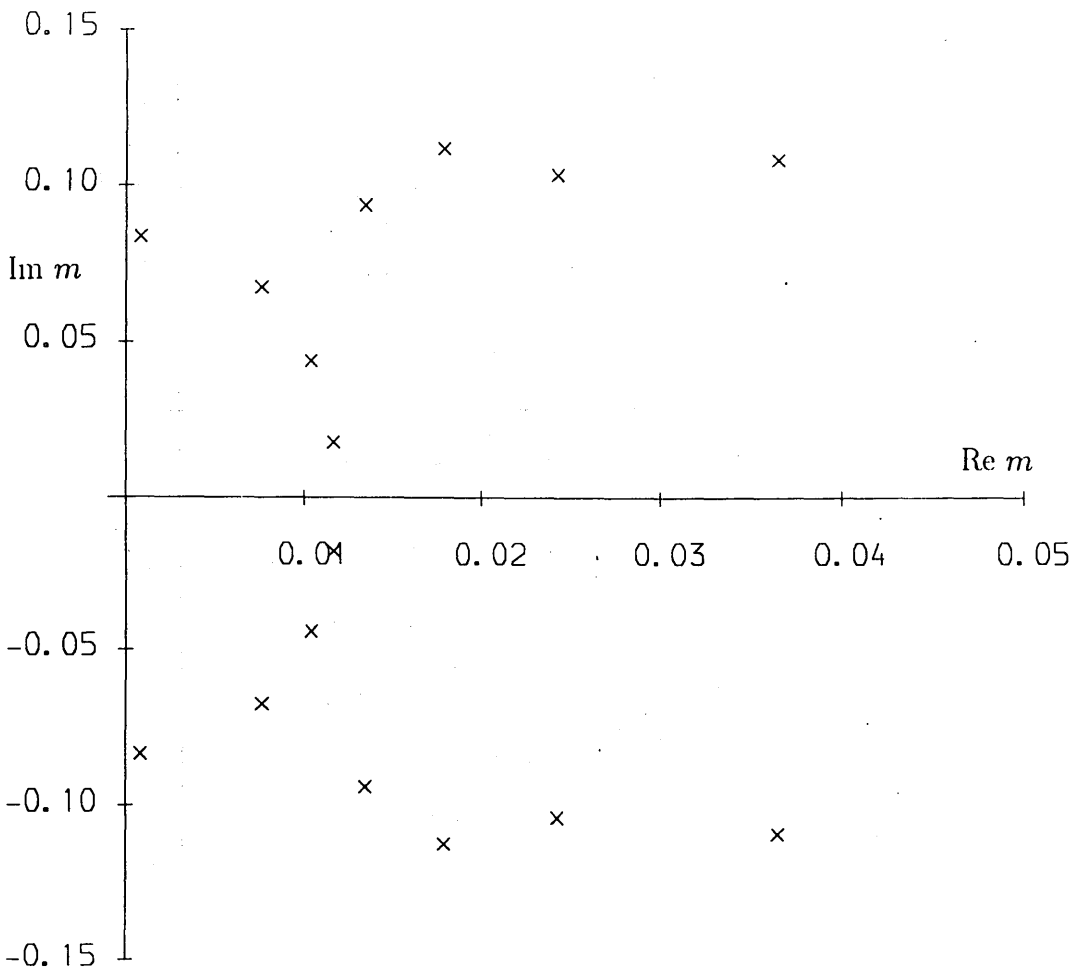

Figure 5.5 : The partition function zeros in the complex quark mass plane for $SU(3)$ at $\beta = 4.90$ on a 4^4 lattice. Averages are taken over 3260 configurations.

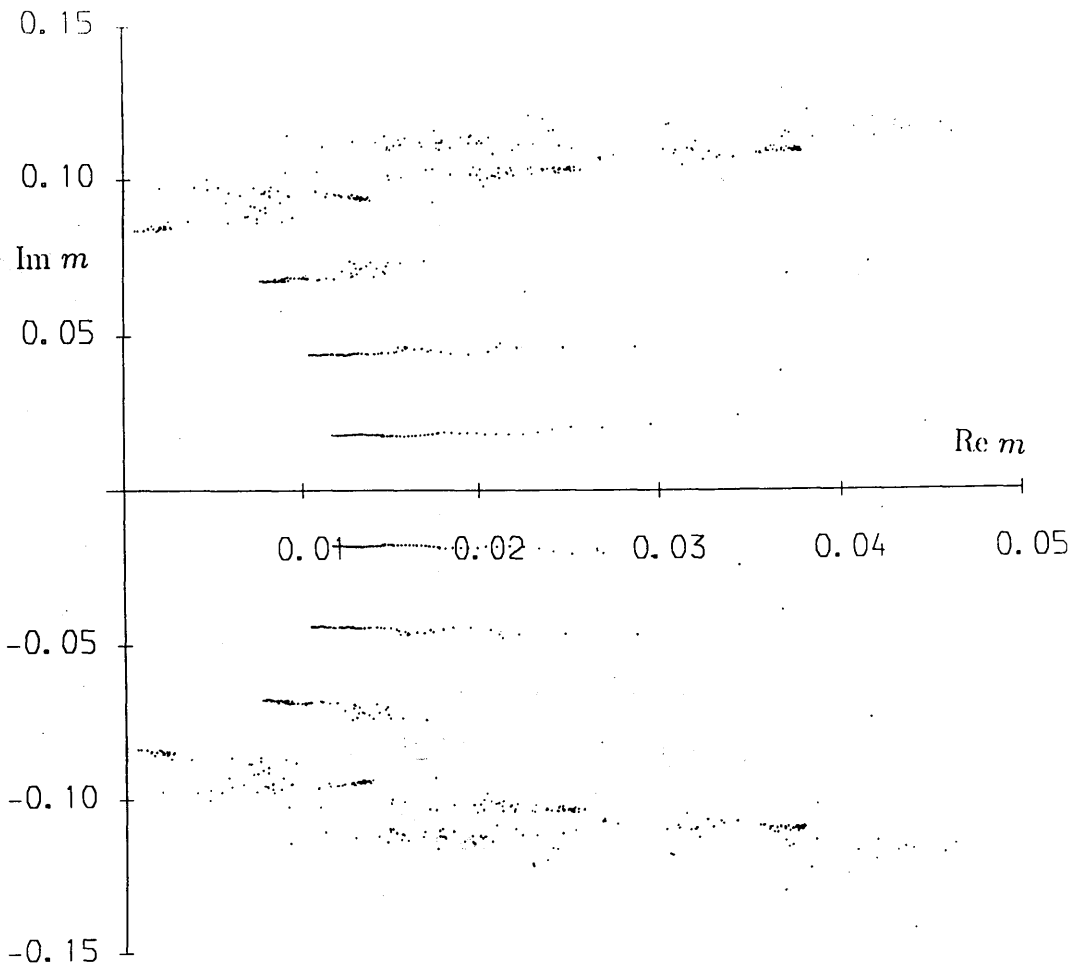

Figure 5.6a : The evolution of the lowest zeros for the same system as Fig.(5.5). The zeros are plotted every 50 measurements.

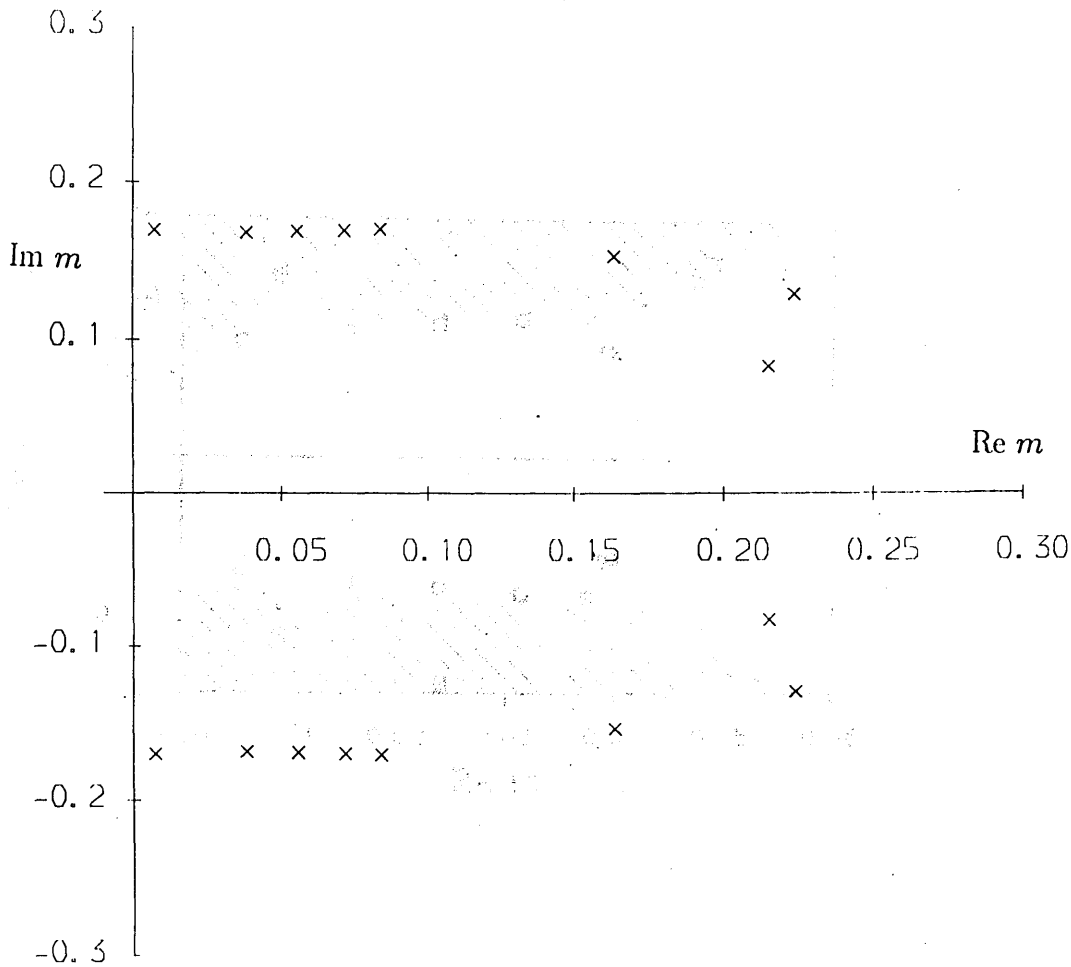

Figure 5.7 : The partition function zeros in the complex quark mass plane for $SU(3)$ at $\beta = 5.20$ on a 4^4 lattice. Averages are taken over 1200 configurations.

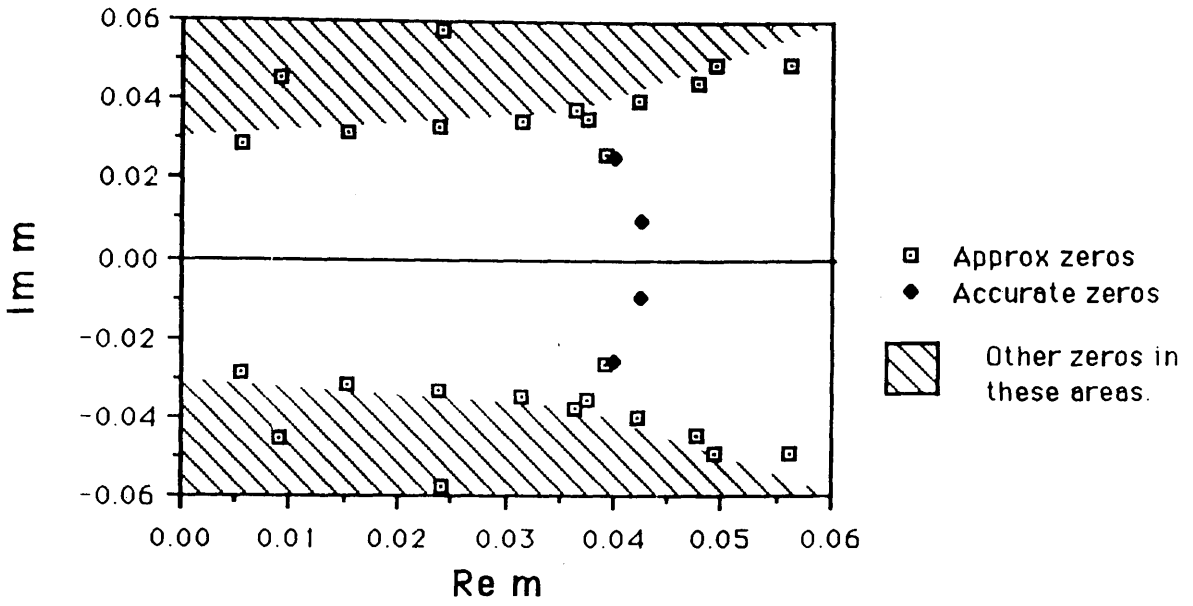

Figure 5.8 : The partition function zeros in the complex quark mass plane for $SU(3)$ at $\beta = 5.04$ on a $6^3.4$ lattice.

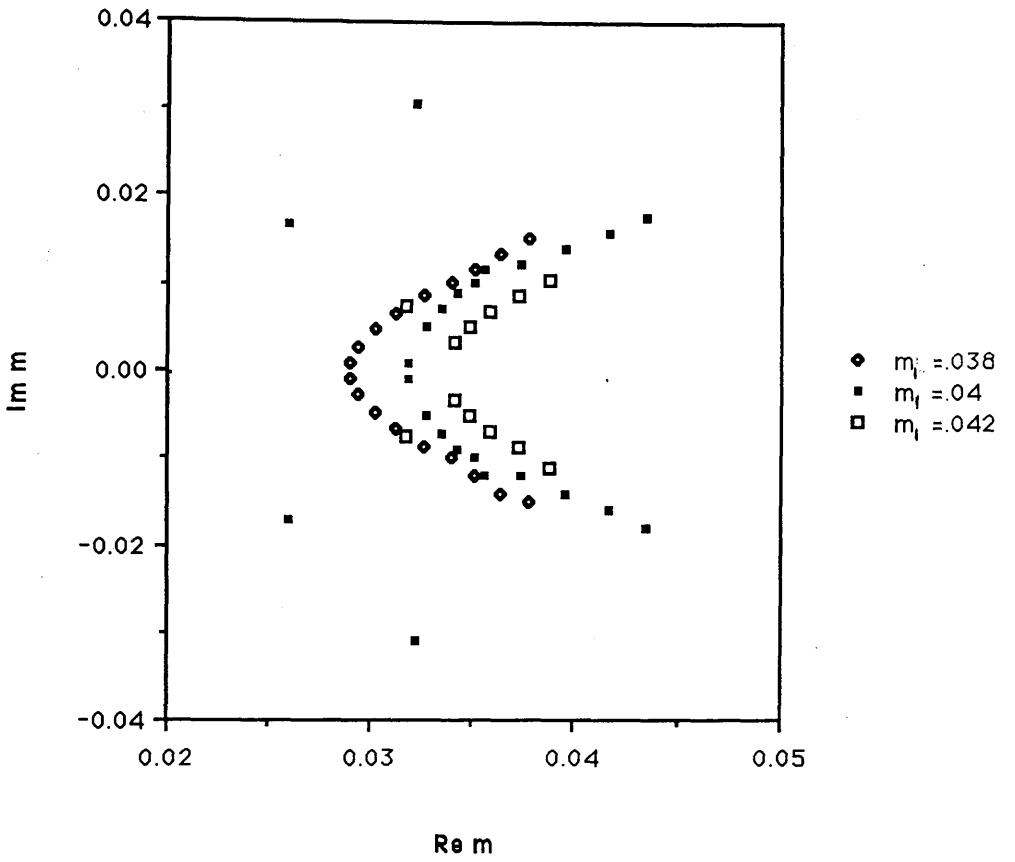

Figure 5.9 : The partition function zeros in the complex quark mass plane for $SU(3)$ at $\beta = 5.04$ on an $8^3.4$ lattice. These zeros have not yet converged to their physical values.

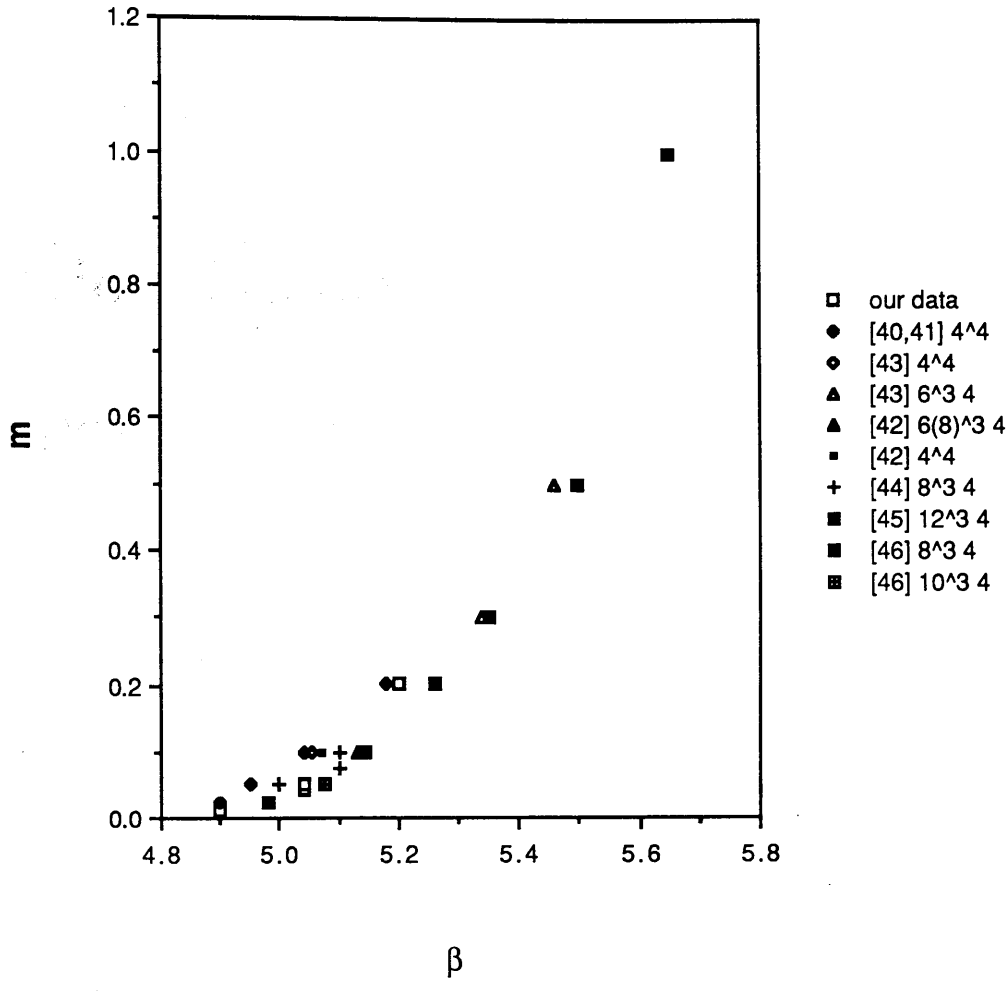

Figure 5.10 : Points of phase transition (or crossover) in the β–ma plane for lattice QCD on lattices with $n_\tau = 4$.

Chapter 6

Partition Function Zeros for Compact Lattice QED.

In this chapter we use the method of previous chapters to study the critical behaviour of compact lattice QED. The comparative simplicity of this model— our $U(1)$ gauge field variables are single complex numbers rather than complex valued matrices — and the resultant saving in computation time means that it is possible to perform a much more detailed investigation than was possible with $SU(2)$ or $SU(3)$ gauge fields. A further time saving could have been made by working with the real phases, $\theta_{x,\mu}$ rather than the link variables $U_{x,\mu} = e^{i\theta_{x,\mu}}$. It was decided, however, that, considering the time and effort required to rewrite the Hybrid Monte Carlo code in this form, the original code, modified to eliminate matrix multiplications, would be fast enough for the size of systems under investigation.

Our study is again in some sense 'orthogonal' to previous work on the critical behaviour of the theory. Previous studies worked at a fixed value of the bare fermion mass, chosen to make the simulation stable and either looked for a discontinuity in $\langle\overline{\psi}\psi\rangle$ as the coupling is varied, or for evidence of coexisting phases at a critical coupling [48] or else attempted to evaluate the fermionic determinant

as a function of the energy of the system [49]. We perform simulations at several values of β and try to estimate the critical value of the mass in each case. The scaling properties of the partition function zero closest to the real axis should give some information on the order of the phase transition.

We have been able to perform simulations at 10 values of β in the range $0.0 \leq \beta \leq 1.5$. Systematic errors have been controlled by repeating some of the simulations using different update masses.

6.1 Results

Results for compact $U(1)$ at $\beta = 0.0$ on 2^4 and 4^4 lattices were presented in Chapter 4. In this section we present the results obtained for weaker couplings.

In each simulation the system was evolved through 600 thermalisation sweeps from either a random or ordered start. This should ensure that when measurements are taken the configurations used are generated with the correct weight. Measurements of the coefficients were made after every hybrid Monte Carlo sweep. (A sweep consists of several trajectories and the molecular dynamics time between measurements, weighted by the HMC acceptance, is of O(1)) The zeros were calculated every 400 measurements up to 3200. This gives us eight sets of zeros from each run, which will give us some indication of the stability of the zeros obtained.

In every case, the coefficients form a curve very similar to that shown in Figures (4.2) and (5.3a) for QCD. The similarity between the distributions of the coefficients for different values of β, and even for different gauge groups, makes the study of these graphs uninformative. For this reason the reader is referred to Figure(4.2) as the generic example rather than showing several indistinguishable figures.

Despite this apparent similarity, if one looks at the numerical values of the coefficients, rather than the general shape of the curve, one can see some interest-

ing behaviour. In Figure(6.1) we show the behaviour of the first few coefficients , $\ln C_n$ $(n = 1, \ldots, 9)$ with varying β. They are all normalised so that $C_0 = 1$. We note that all the coefficients are characterised by a rapid, almost simultaneous, transition at $\beta \sim 0.8 - 0.9$. This, as we shall see later, is the range of couplings where we see evidence for critical behaviour.

In Figures(6.2 a–j) we show the corresponding behaviour of the partition function zeros as β is increased. We have already seen (Chapter 4) that at infinite coupling, $\beta = 0.0$, the zeros are purely imaginary (Figure(6.2 a)). This behaviour persists up to about $\beta \simeq 0.8$, where some zeros begin to migrate into the complex plane. (Figures(6.2 b & c)) For these values of β the real axis is 'pinched' at the origin, suggesting a critical mass value $m_c a = 0.0$.

As we move towards weaker couplings, the zeros migrate into the complex plane and pinch the real axis. For $\beta \sim$0.8–0.9 the pinch occurs at $m_c \sim$ 0.1–0.4 (Figures(6.2 d–g)). In the weak coupling regime, $\beta \gtrsim 1.0$, there is no evidence for a critical value of the bare fermion mass (Figures(6.2 h–j)).

6.2 Systematic Error

Having obtained the main features of the theory's behaviour, we now turn to a systematic analysis of the stability of our results. Results in this section should also be applicable to the work presented in Chapters 4 and 5 where such a thorough investigation was not possible.

The first question which must be addressed is the independence of the results on the choices of m_1 and m_0.

In these simulations m_1 has always been chosen to vary in the intervals [0,0.4] on the real axis and [-0.4,0.4] on the imaginary axis. Since it is not possible to obtain all the zeros of the polynomial we must ensure that the zeros which we do obtain are not influenced by our choice of m_1. The root finding routine

will preferentially find those roots close to m_1 but if we have two values of m_1 reasonably close to the root in question, the root should be found in both cases, with no systematic shift due to the different values of m_1. The zeros which are accepted as true zeros of the partition function are those which appear for more than one value of m_1. The fact that we always have m_1^2 real means that the root finder can easily find roots close to the axes, but has difficulty coping when the zeros are far away in the m-plane. This explains the scarcity of zeros found at large values of β. This problem could be made less serious by the use of complex values for m_1. However, this would result in complex valued coefficients in the polynomial and a more sophisticated root finding routine would have to be implemented. Since the physically interesting zeros are those close to the real axis, this is not a serious problem when it comes to understanding the physics.

Our results should be independent of the update mass, m_0, since this only gives an overall multiplicative factor in the partition function. Figures (6.3 a & b) show the zeros obtained after 3200 measurements with two different masses at each of two β values. Those zeros which we would expect to be calculated accurately are seen to be independent of m_0.

As a check that the zeros we calculate have converged to stable values, *i.e.*we have performed enough measurements, we look at the zeros obtained as the number of measurements increases. In Figure (6.4) we show the zeros at $\beta = 0.85$ after 2400, 2800 and 3200 measurements. The zeros close to our values of m_1, those close to the axes, have converged to stable values. The zeros further from our expansion points are less stable.

6.3 Conclusions

The physics observed for compact $U(1)$ gauge theory with dynamical staggered fermions is summarised in Figure (6.5). The real part of the zero closest to the

real axis is plotted for the values of β considered. The critical mass, m_c, is compatible with zero in the strong coupling area. For values of β in the range 0.8 – 0.9 the critical mass is strongly β dependent. In the weak coupling regime, $\beta > 1.0$, there is no sign that the theory displays critical behaviour at any mass.

The fact that $U(1)$ is cheaper to simulate than QCD has allowed us to examine the systematics of our method very thoroughly. The partition function zeros are, as expected theoretically, independent of the updating mass in the simulation. Work is currently in progress to investigate the dependence of the zeros on the lattice boundary conditions. Runs are being done using identical parameters with both periodic and antiperiodic boundary conditions in all directions.

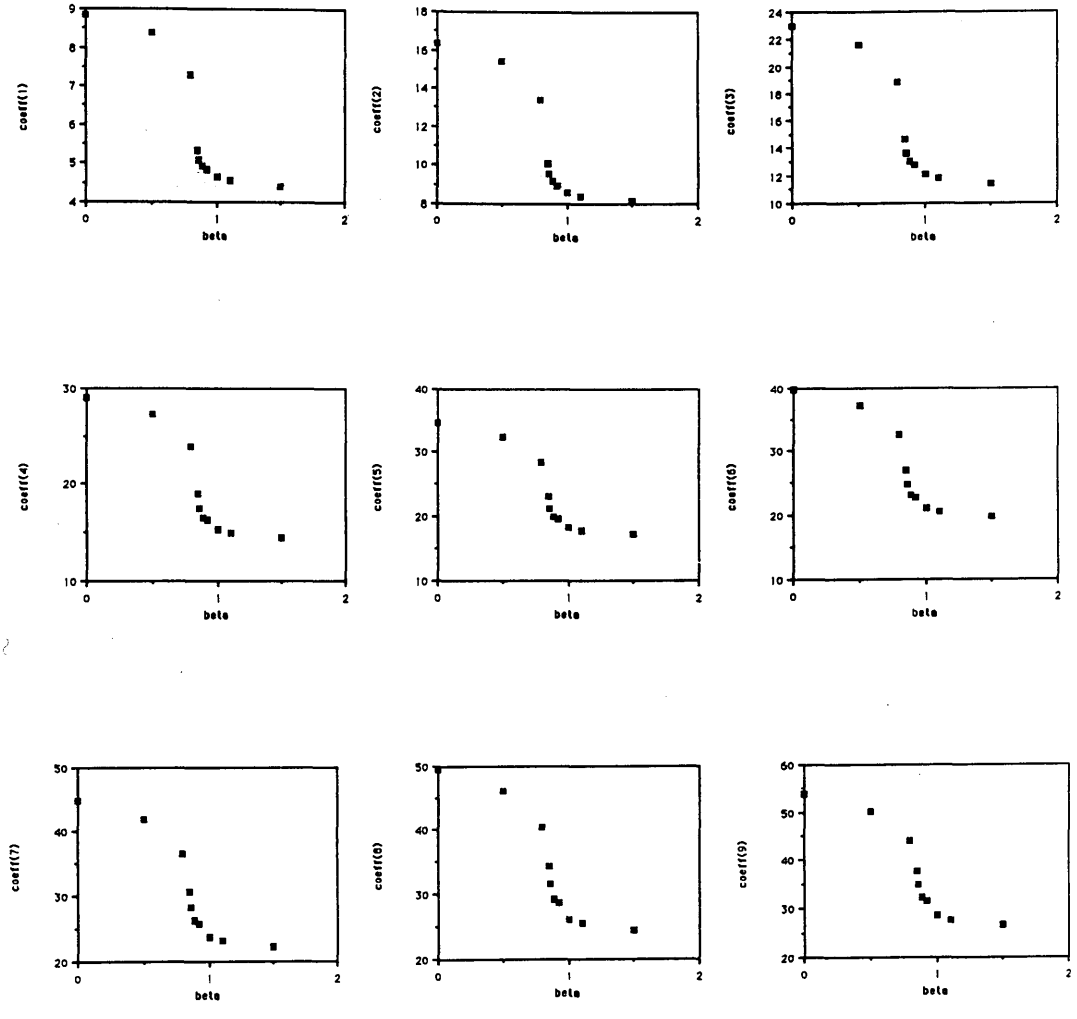

Figure 6.1 : Logarithms of the first nine coefficients in the expansion of the partition function for $U(1)$ on a 4^4 lattice as β is varied. All coefficients are normalised such that $C_0 = 1$.

Figure 6.2 : Partition function zeros in the complex fermion mass plane for $U(1)$ on a 4^4 lattice.

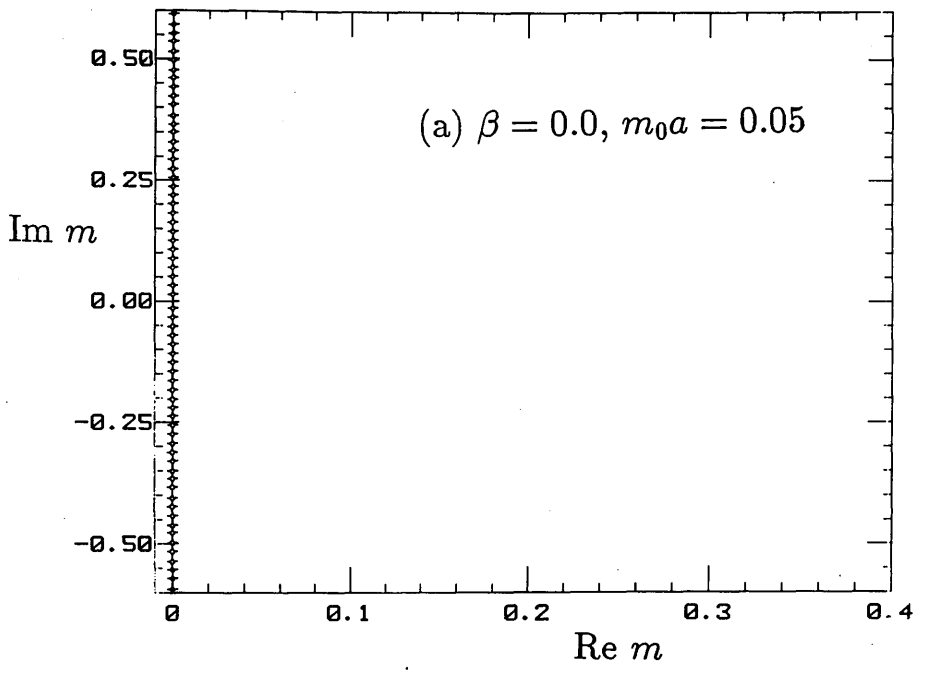

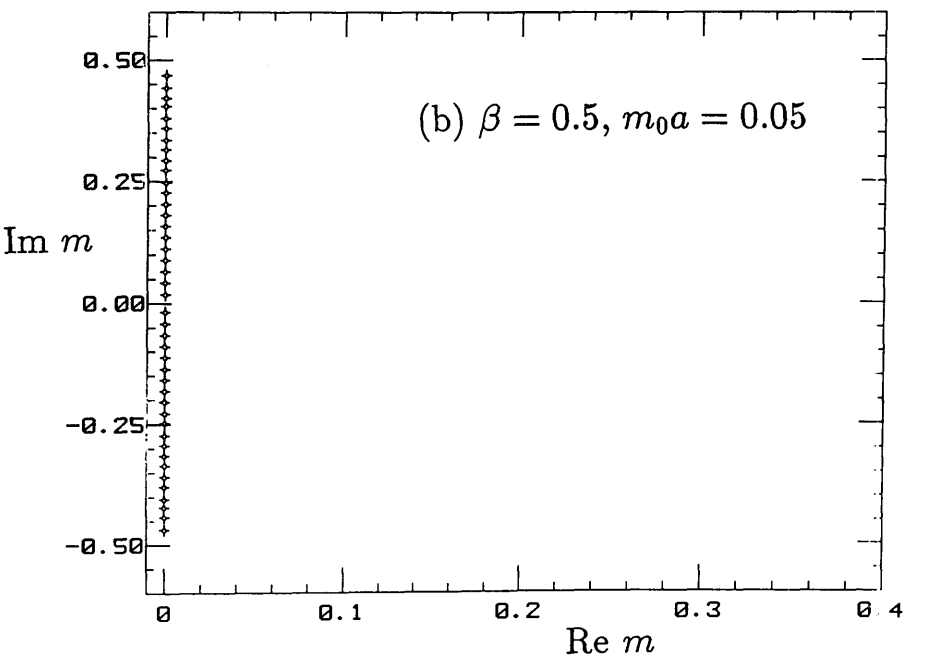

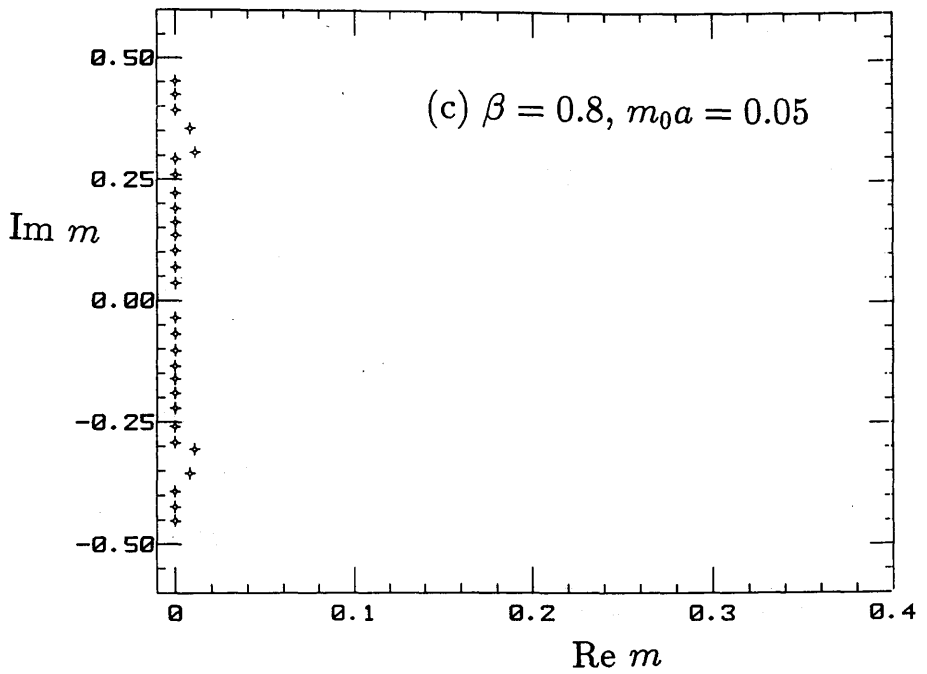
(c) $\beta = 0.8$, $m_0 a = 0.05$
0.50
0.25
0.00
-0.25
-0.50
Im m
0
0.1
0.2
0.3
0.4
Re m

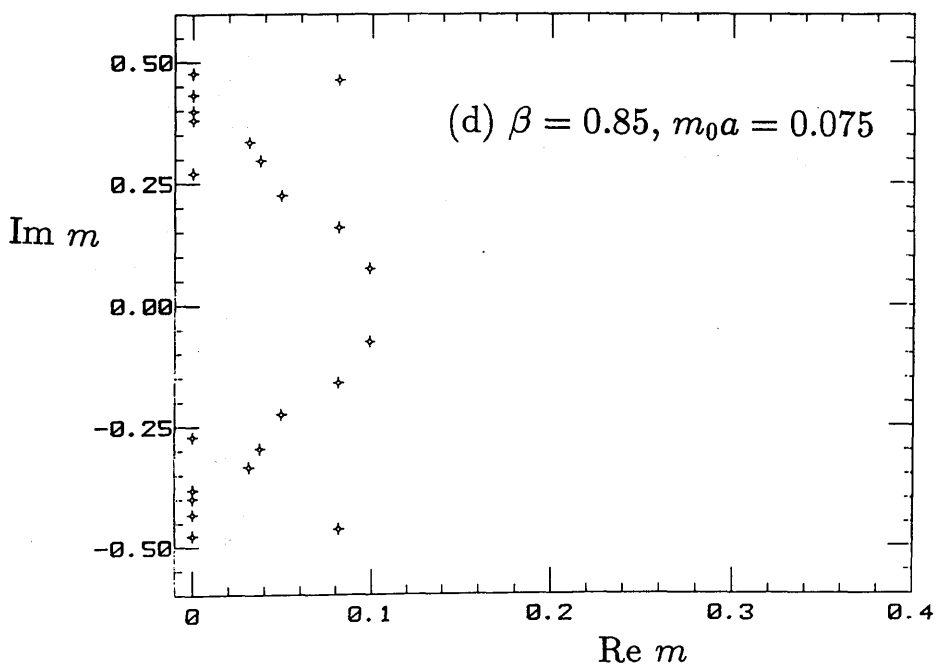
(d) $\beta = 0.85$, $m_0 a = 0.075$
0.50
0.25
0.00
-0.25
-0.50
Im m
0
0.1
0.2
0.3
0.4
Re m

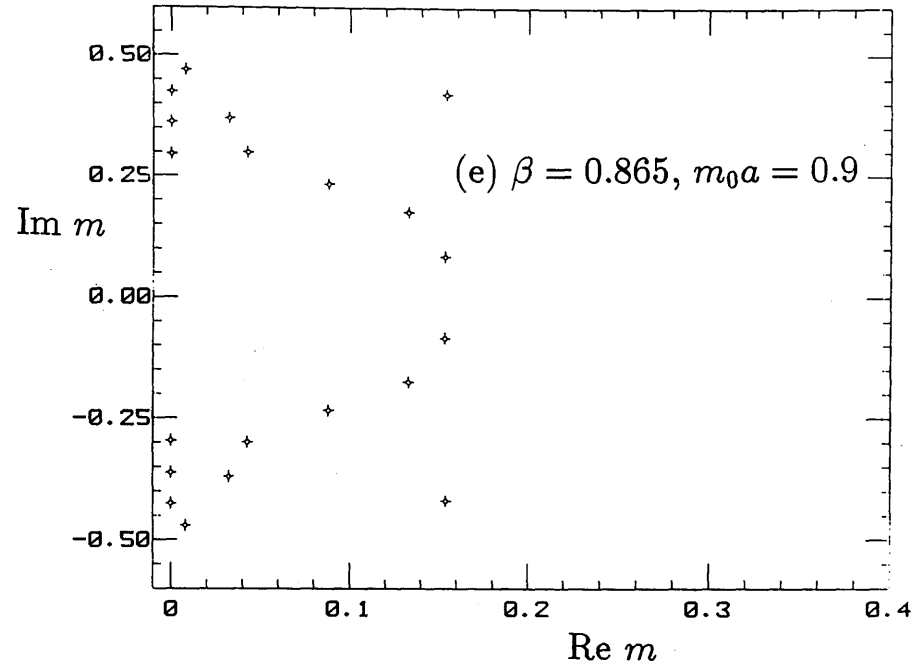
(e) $\beta = 0.865$, $m_0 a = 0.9$
Im m
Re m
0.50
0.25
0.00
-0.25
-0.50
0
0.1
0.2
0.3
0.4

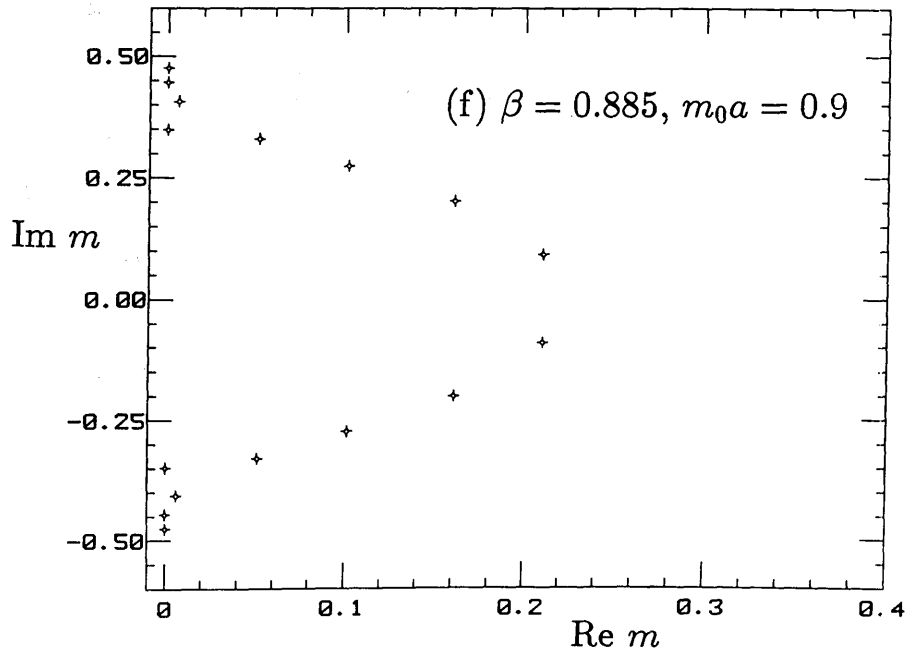
(f) $\beta = 0.885$, $m_0 a = 0.9$
Im m
Re m
0.50
0.25
0.00
-0.25
-0.50
0
0.1
0.2
0.3
0.4

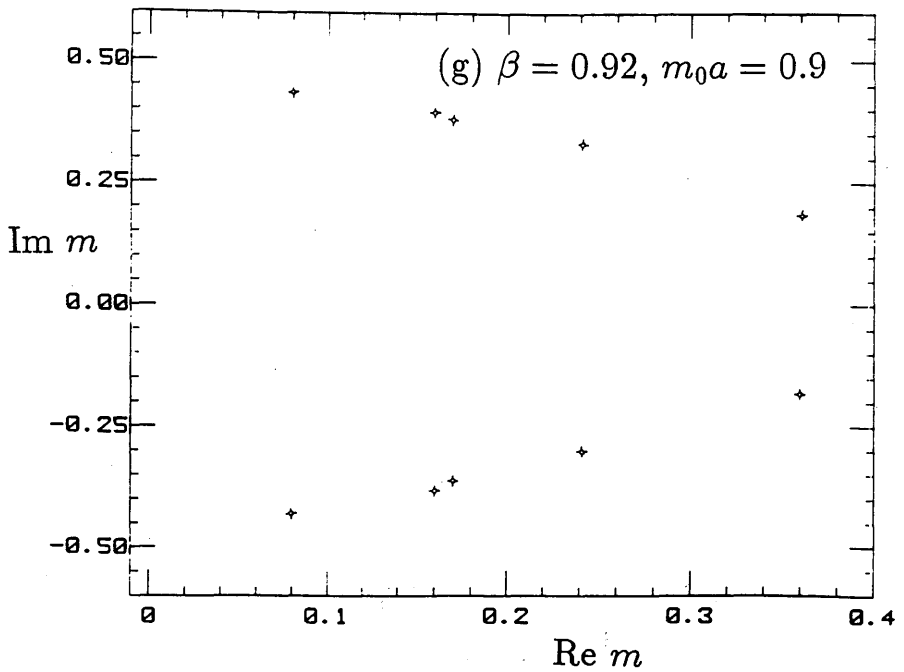
(g) $\beta = 0.92$, $m_0 a = 0.9$
0.50
0.25
0.00
-0.25
-0.50
Im m
0
0.1
0.2
0.3
0.4
Re m

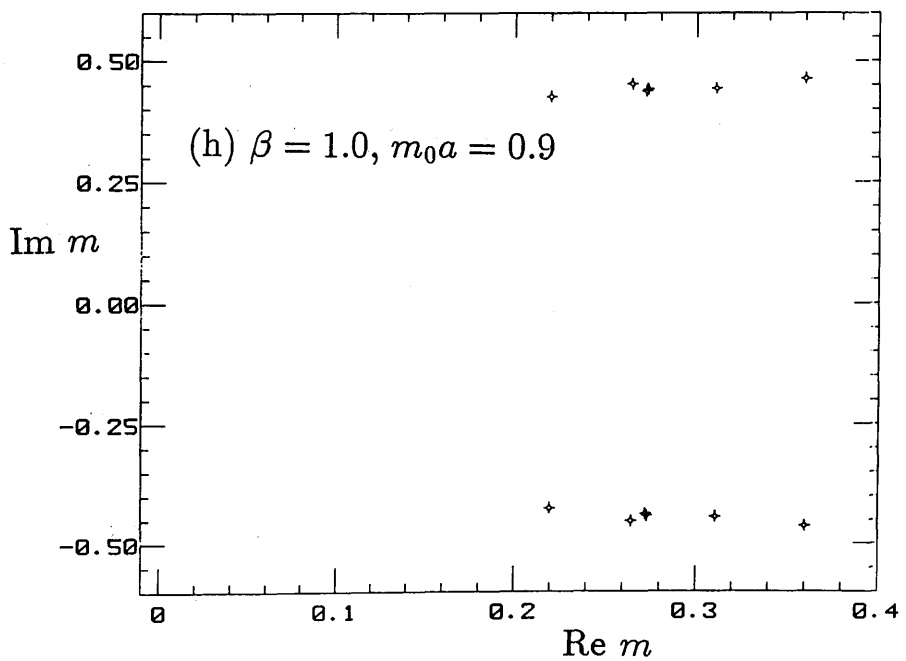
(h) $\beta = 1.0$, $m_0 a = 0.9$
0.50
0.25
0.00
-0.25
-0.50
Im m
0
0.1
0.2
0.3
0.4
Re m

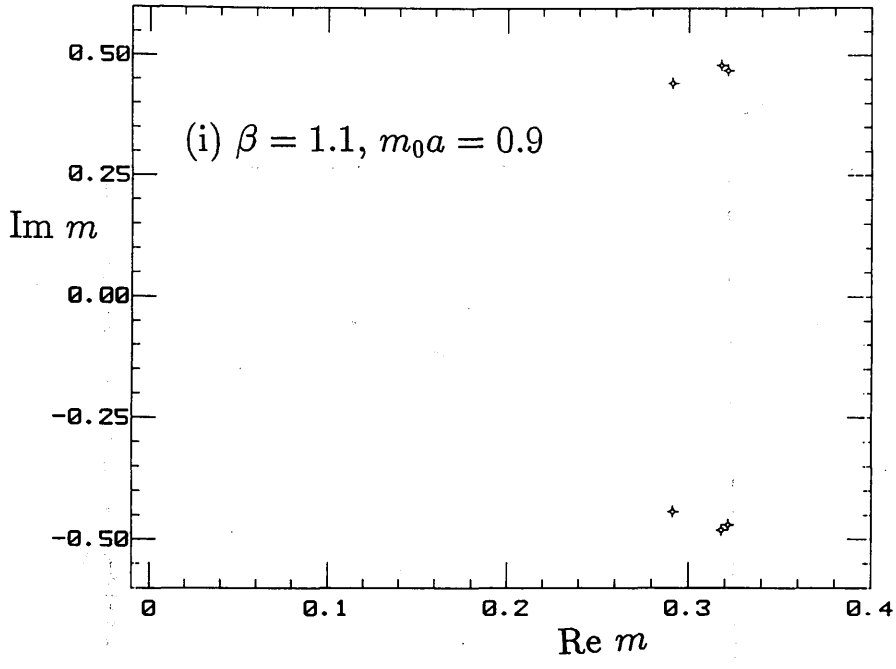
(i) $\beta = 1.1$, $m_0 a = 0.9$
0.50
0.25
0.00
-0.25
-0.50
Im m
0
0.1
0.2
0.3
0.4
Re m

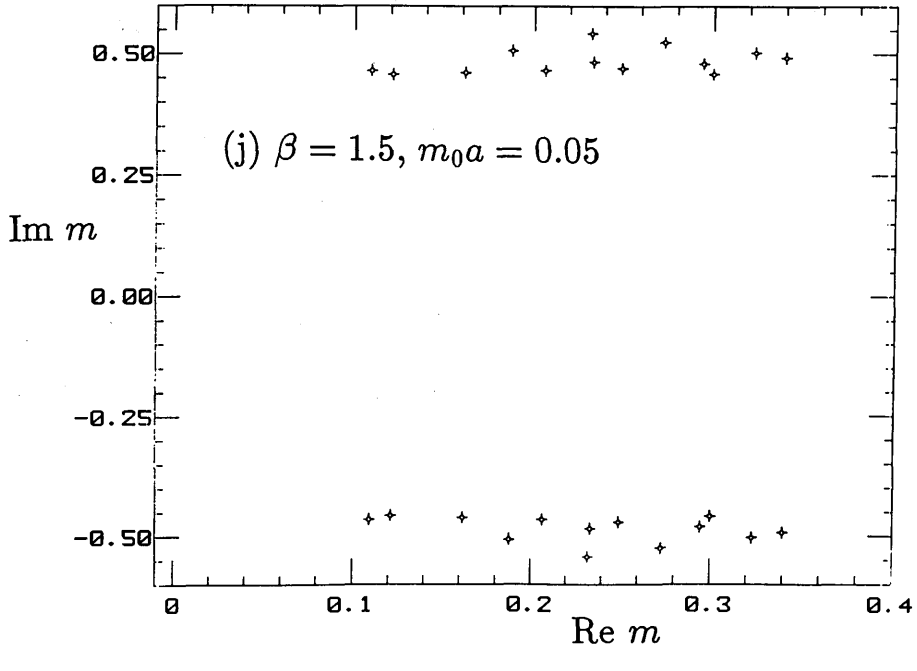
(j) $\beta = 1.5$, $m_0 a = 0.05$
0.50
0.25
0.00
-0.25
-0.50
Im m
0
0.1
0.2
0.3
0.4
Re m

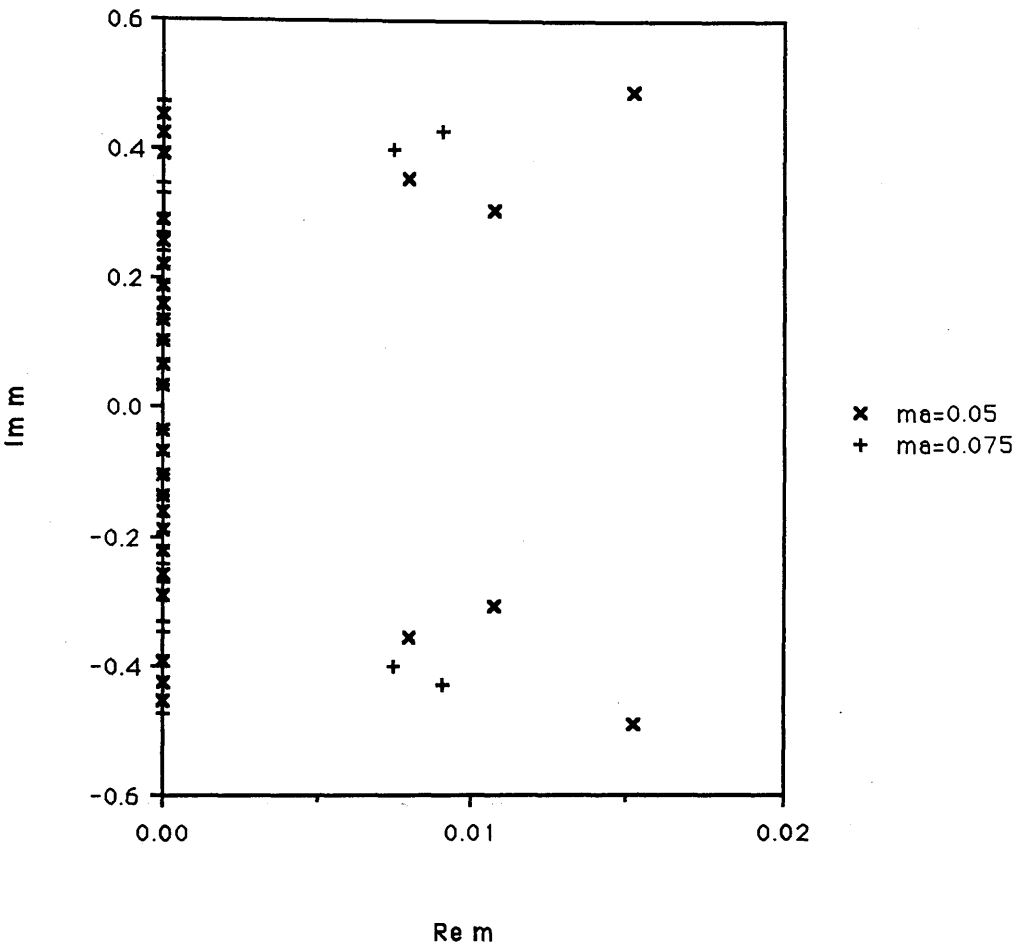

Figure 6.3a : Partition function zeros for $U(1)$ on a 4^4 lattice at $\beta = 0.8$. Zeros are plotted for runs with updating mass 0.05 and 0.075.

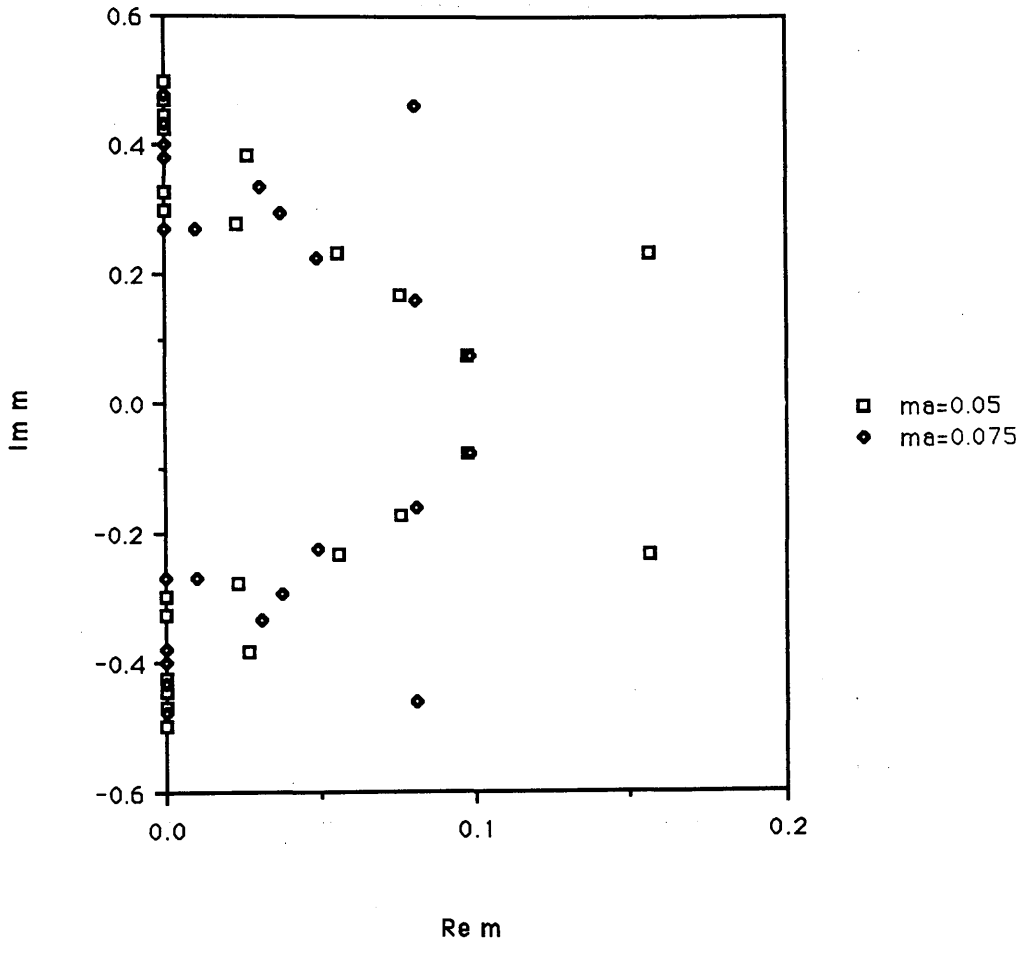

Figure 6.3b : Partition function zeros for $U(1)$ on a 4^4 lattice at $\beta = 0.85$. Zeros are plotted for runs with updating mass 0.05 and 0.075.

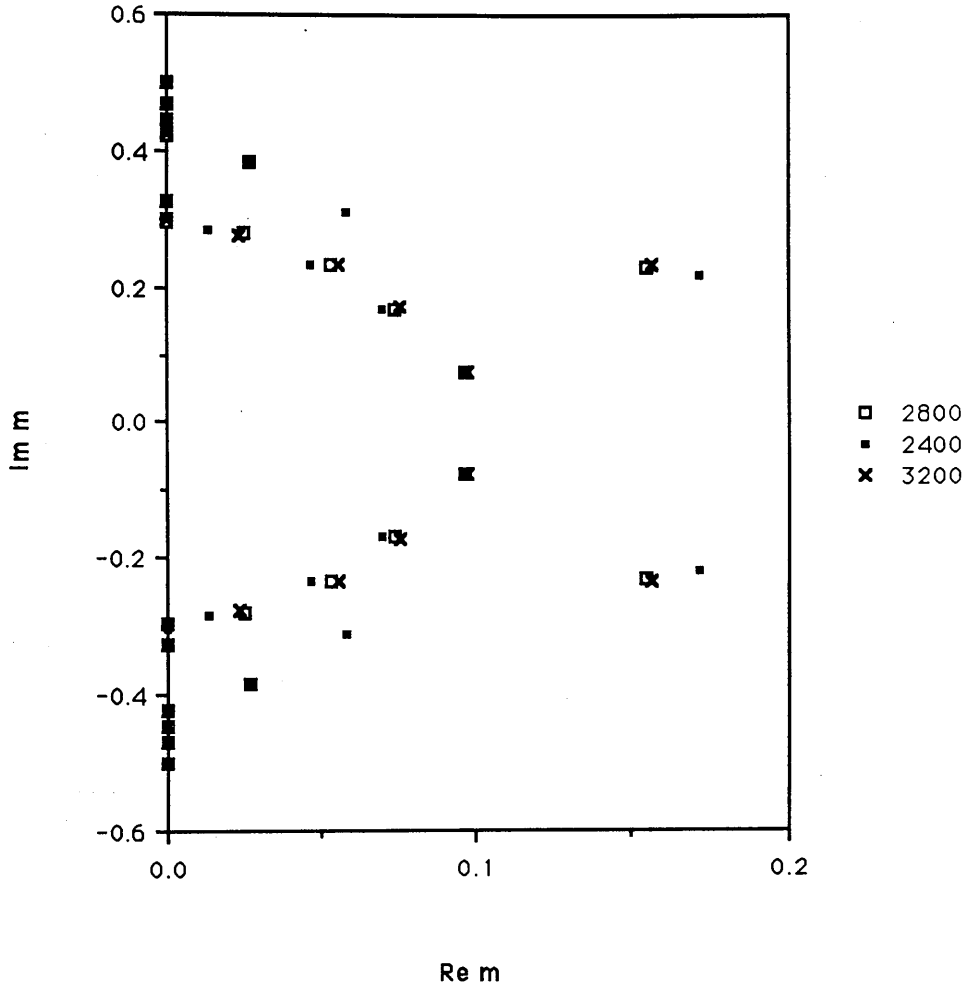

Figure 6.4 : Partition function zeros for $U(1)$ on a 4^4 lattice at $\beta = 0.85$ plotted after 2400, 2800 and 3200 measurements.

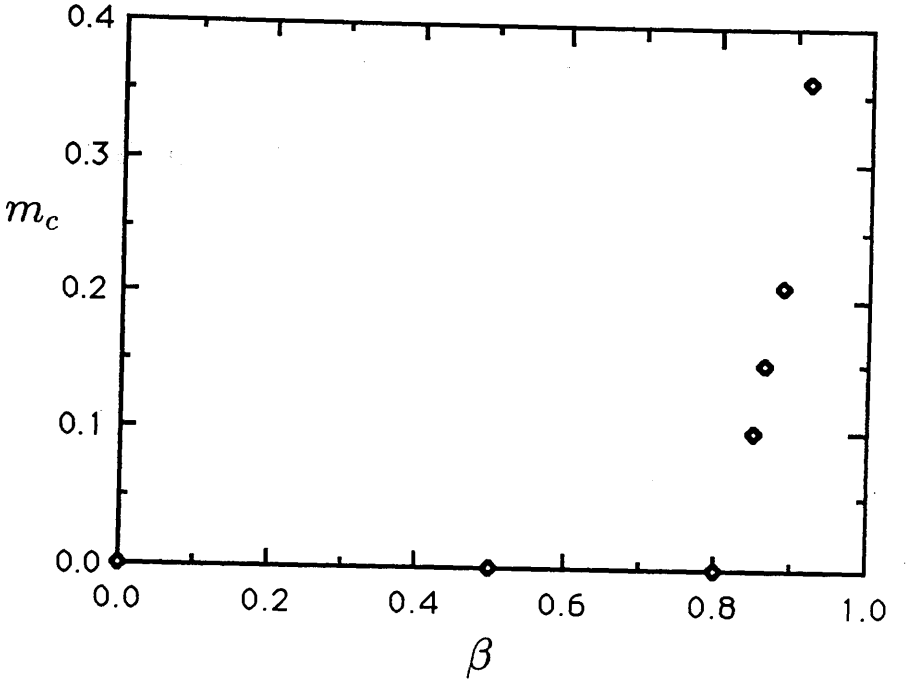

Figure 6.5 : The critical mass for $U(1)$ with staggered fermions as β is increased. *i.e.*the real part of the zero closest to the real axis.

Chapter 7

QCD at finite chemical potential

7.1 Introduction

The QCD phase transition between confined hadronic matter and the deconfined chromoplasma phase may be induced by two mechanisms. The temperature may be increased to a critical value, T_c — This is the mechanism driving the transition in previous chapters — or else the density of the quark matter may be systematically increased. As the quarks are forced closer together the short distance, asymptotically free behaviour may take over from the confining potential which dominates at long distances. The baryonic matter may then undergo a phase transition at a temperature below T_c. It is through a combination of these effects that heavy ion collision experiments are hoped to produce deconfined quark matter.

Lattice simulations of QCD usually have a net baryon number density of zero since matter is always produced as a quark/antiquark pair. Finite baryon number density may be produced by introducing a chemical potential, μ, for the production of quarks. As in statistical mechanics, the chemical potential is the Lagrange mutiplier for the constraint on the particle number, N. The Grand

Canonical Partition Function is given by

$$Z(T,\mu) = \mathrm{Tr}(e^{-(\mathcal{H}-\mu N)}) \tag{7.1}$$

where $\mathcal{H}$ is the Hamiltonian of the system.

7.2 Lattice QCD at finite chemical potential

Finite chemical potential is introduced in the QCD lattice action by multiplying forward timelike links by a factor $e^{\mu a}$ and backward links by $e^{-\mu a}$ [50]. This has the effect of encouraging forward propagation of quarks and inhibiting backward propagation of antiquarks, resulting in a non-vanishing net fermion number density on the lattice.

We now have

$$Z = \int \mathcal{D}U \mathrm{Det}(M(U,\mu)) e^{-S_g(U)} \tag{7.2}$$

$$\begin{aligned} M(U,\mu) &= ma\delta_{x,y} + \frac{1}{2}\sum_{\nu=x,y,z}(U_\nu(x)\eta_\nu(x)\delta_{y,x+\nu} - \text{h.c.}) \\ &+U_\tau(x)\eta_\tau(x)e^{\mu a}\delta_{y,x+\tau} - U_\tau^\dagger(y)\eta_\tau(y)e^{-\mu a}\delta_{y,x-\tau} \end{aligned} \tag{7.3}$$

The gauge part of the action, S_g, is unaffected by the introduction of the chemical potential since it always involves timelike links in pairs, one forwards and one backwards. In general the only loops which will pick up a contribution from the chemical potential are those which wind completely round the lattice in the timelike direction. It is easy to see that these loops correspond to particles which propagate infinitely in time and so contribute to a net particle number. In contrast, closed loops which do not wind round the lattice pick up no contribution and correspond to quark/antiquark creation and annihilation.

The result of adding a chemical potential to our action is that the fermion determinant becomes complex. The interpretation of $\mathrm{Det}(M)$ as a probability in our Monte Carlo integration therefore becomes difficult. It has been shown that it is the presence of this complex phase in $\mathrm{Det}(M)$ which causes quenched calculations at finite chemical potential to show incorrect behaviour[51,53]. This phase also causes great difficulty in methods which use $|\mathrm{Det}(M)|$ in the importance sampling. [52]The phase, ϕ, is moved from the update weight into the observable. This is a well defined process which should produce correct answers. The expectation value of the observable becomes

$$\langle O \rangle = \frac{\left\langle O e^{i\phi} \right\rangle}{\left\langle e^{i\phi} \right\rangle} \tag{7.4}$$

where the averages on the right hand side are over configurations generated using $|\mathrm{Det}(M)|$ in the importance sampling.

The trouble comes from the fact that, in the interesting region, $\left\langle e^{i\phi} \right\rangle$ becomes very small due to large fluctuations in the phase. This makes the calculation of $\langle O \rangle$ almost impossible. Simulations are only feasible at very large or very small chemical potential, where $\left\langle e^{i\phi} \right\rangle \simeq 1$.

The expansion of the Grand Canonical Partition Function has the great advantage that the behaviour of the system may be examined over a range of chemical potential while we can avoid the difficulties described above by updating the lattice at $\mu = 0$.

7.3 The Expansion of the Grand Canonical Partition Function.

Using our freedom to normalise the partition function as we please, we may write the grand canonical partition function for QCD at finite chemical potential as

$$Z = \frac{\int \mathcal{D}U \ \mathrm{Det}(M(U,\mu)) e^{-S_g(U)}}{\int \mathcal{D}U \ \mathrm{Det}(M(U,\mu=0)) e^{-S_g(U)}} \tag{7.5}$$

$$= \frac{\int \mathcal{D}U \, \frac{\mathrm{Det}(M(U,\mu))}{\mathrm{Det}(M(U,\mu=0))} \det(M(U,\mu=0)) e^{-S_g(U)}}{\int \mathcal{D}U \, \mathrm{Det}(M(U,\mu=0)) e^{-S_g(U)}} \tag{7.6}$$

$$= \left\langle \frac{\mathrm{Det}(M(U,\mu))}{\mathrm{Det}(M(U,\mu=0))} \right\rangle_{\mu=0} \tag{7.7}$$

This looks very similar to the expression for the partition function as a function of the quark mass given in Chapter 4. However, since the chemical potential does not lie on the diagonal of the fermion matrix, we must introduce one more level of complication before we may proceed.

The matrix $M(U,\mu)$ may be written as

$$iM = G + Ve^{\mu} + V^{\dagger}e^{-\mu} + im \tag{7.8}$$

where G contains all the spacelike gauge links, V the forward timelike links , and $V^{\dagger}$ the backward timelike links.

$$\mathrm{Det}(i\mathcal{M}) = \mathrm{Det}(G + Ve^{\mu} + V^{\dagger}e^{-\mu} + im) \tag{7.9}$$

We may now define the fermion propagator matrix [54].

$$P = \begin{pmatrix} -GV - imV & V \\ -V & 0 \end{pmatrix} \tag{7.10}$$

The determinants of P and M are related.

$$\mathrm{Det}(P - e^{-\mu}) = \mathrm{Det}(GVe^{-\mu} + imVe^{-\mu} + e^{-2\mu} + V^2) \tag{7.11}$$

$$= \mathrm{Det}((Ge^{-\mu} + ime^{-\mu} + V^{\dagger}e^{-2\mu} + V)V) \tag{7.12}$$

$$= e^{-\mu N} \mathrm{Det}(G + Ve^{\mu} + V^{\dagger}e^{-\mu} + im) \tag{7.13}$$

Since $\mathrm{Det}\, V = 1$ and

$$V^{\dagger}V = VV^{\dagger} = 1 \tag{7.14}$$

This gives us the result

$$\mathrm{Det}(iM) = e^{\mu N}\,\mathrm{Det}(P - e^{-\mu}) \tag{7.15}$$

where $N = n_s^3 n_\tau n_c$ is the size of the matrix.

Since we now know Det M in terms of the determinant of a matrix which is diagonal in $e^{\pm\mu}$, we may use the method described in Chapter 4 to expand Det M as a polynomial in e^{μ}. *i.e.*we expand the grand canonical partition function in terms of the canonical partition functions for fixed particle number on the lattice.

$$\mathrm{Det}(P - e^{-\mu}) = \sum_{n=0}^{2N} w_n e^{-n\mu} \tag{7.16}$$

From this expansion we may derive an expression for the grand canonical partition function.

$$Z = \sum_{n=-N}^{N} Z_n e^{nn_\tau\mu} \tag{7.17}$$

By considering the inverse of the propagator matrix one can derive an expression similar to (7.16) which leads to [56]

$$\mathrm{Det}(P - e^{-\mu}) = \mathrm{Det}(e^{\mu} - P^{-1}) = e^{-2N\mu}\sum_{n=0}^{2N} w_n^* e^{n\mu} \tag{7.18}$$

This leads to

$$w_n = w_{2N-n}^* \tag{7.19}$$

A check on our method is possible since one can formally calculate the coefficients in the expansion in terms of traces of powers of the propagator matrix using the following recurrence relation.

$$\mathrm{Tr}(P^n) + \sum_{j=1}^{n-1} w_j\,\mathrm{Tr}(P^{n-j}) + nw_n = 0 \tag{7.20}$$

$w_0 = 1$ and $w_1 = -\,\mathrm{Tr}\,P$.

Since the propagator matrix causes a step forward in time, only those traces of P^n with n an integer multiple of n_τ will be non-zero. The recurrence relations

now give

$$\omega_0 = w_0 = 1 \tag{7.21}$$

$$\omega_1 = w_{n_\tau} = -\frac{1}{n_\tau}\,\mathrm{Tr}\,P^{n_\tau} \tag{7.22}$$

$$\omega_2 = w_{2n_\tau} = -\frac{1}{2n_\tau}\left(\mathrm{Tr}\,P^{2n_\tau} - \frac{1}{n_\tau}(\mathrm{Tr}\,P^{n_\tau})^2\right) \tag{7.23}$$

$$\omega_3 = w_{3n_\tau} = -\frac{1}{3n_\tau}\left(\mathrm{Tr}\,P^{3n_\tau} - \frac{3}{2n_\tau}\,\mathrm{Tr}\,P^{2n_\tau}\,\mathrm{Tr}\,P^{n_\tau} + \frac{1}{2n_\tau^2}(\mathrm{Tr}\,P^{n_\tau})^3\right) \tag{7.24}$$

etc.

ω_n gives the coefficient for a lattice with n fermions missing. The Z_n will be the expectation values of the ω_n.

$$Z_n = \langle \omega_{2N-n} \rangle \tag{7.25}$$

Since in $SU(N_c)$ we have N_c equivalent vacua related by $Z(N_c)$ rotations and since tunneling is always possible between these vacua on a finite lattice, our canonical partition functions must be invariant under a change of variables which describes this tunneling. A rotation between $Z(N_c)$ vacua corresponds to the introduction of an imaginary part to the chemical potential. This leads to

$$Z_n = e^{2\pi i n/N_c} Z_n \tag{7.26}$$

which means that the Z_n must be zero unless n is a multiple of N_c.

This result can also be seen from the expressions for the ω_n. Since P involves only forward timelike links the functional integrations over link variables will result in a non-zero answer only if the trace corresponds to a loop which winds around the lattice a multiple of N_c times.

$$\omega_n = 0 \qquad n \neq 0(\mathrm{Mod}N_c) \tag{7.27}$$

$$\omega_n \neq 0 \qquad n = 0(\mathrm{Mod} N_c) \tag{7.28}$$

$$\tag{7.29}$$

If the Z_n are to be interpreted as canonical partition functions then they must be real and positive. Our final expression for the partition function is thus

$$Z = \sum_{n=0}^{N} (Z_n e^{nN_c n_\tau \mu} + Z_n^* e^{-nN_c n_\tau \mu}) \tag{7.30}$$

$$Z = \sum_{n=0}^{N} Z_n \cosh(nN_c n_\tau \mu) \tag{7.31}$$

where we have absorbed a factor of 2 into the definition of Z_n in the second equation.

In strong coupling we can perform the functional integrations over gauge fields analytically. The ratio of the canonical partition functions for a full lattice and for a lattice with two fermions missing was calculated for $SU(2)$ at strong coupling on a 4^4 lattice both analytically and by Monte Carlo simulation.

$$\frac{\omega_2}{\omega_0}(\text{analytical}) = e^{9.13} \tag{7.32}$$

$$\frac{\omega_2}{\omega_0}(\text{Monte Carlo}) = e^{9.075} \tag{7.33}$$

These results are within the statistical errors in the numerical calculation.

7.4 Results

In this section results obtained in previous simulations of QCD at finite chemical potential are reviewed and the expansion of the partition function is reanalysed by studying the zeros in the complex fugacity (e^μ) plane. The results obtained from the partition function zeros are compared with those obtained directly from the partition function.

7.4.1 Strong Coupling Results

Simulations were performed at strong coupling ($\beta = 0$) on a 2^4 lattice by I.M. Barbour, C.T.H. Davies and Z.A. Sabeur[55]. The coefficients of the expansion were found by a different method in this case. The fermion determinant may be expanded as

$$Re(\mathrm{Det}\, iM(\mu)) = c_0 + \sum_{n=1}^{n_{max}} (c_n + c_{-n}) \cosh(3nn_t\mu a) \tag{7.34}$$

Gauge fields are generated with weight e^{-S_g} in the importance sampling. The left hand side of Equation(7.34) is evaluated at several complex values of the chemical potential, resulting in a set of simultaneous equations which may be solved for the c_n. These c_n are then averaged over many configurations to give the expansion of the grand canonical partition function.

The simulation was repeated using $\mathrm{Det}(M(\mu = 0))e^{-S_g}$ in the update weight. This gave results which agreed to within statistical errors with the results from pure gauge updating.

The canonical partition functions were found, to a good approximation to satisfy

$$c_n = e^{\alpha_n} \tag{7.35}$$

$$\alpha_n = a + bn \tag{7.36}$$

Using this form, and the numerical result for b, the zeros of the partition function were obtained for $ma = 0.1$, 0.2, 0.3 and 0.4. These zeros were found to lie on circles in the e^{μ} plane with the radius giving a value for μ_c, the critical chemical potential for the phase transition. (Figure (7.1))

A value for μ_c may also be obtained by noting that due to the form of the coefficients (Equation(7.36)) a value of the chemical potential exists such that all the terms of the polynomial have the same weight. If we define the critical chemical potential to be this value we have

$$e^{3\mu_c n_t} = e^{-b} \tag{7.37}$$

$$\mu_c = \frac{-b}{3n_t} \tag{7.38}$$

These two definitions of μ_c give results which are in agreement at all four values of the bare quark mass. The values of μ_c are seen to vary linearly with ma and a linear fit gives $\mu_c = 0.58$ at $ma = 0$.(Figure(7.2)) This is clear evidence that the full theory, including the effects of fermions, will give results which are different from those obtained using the quenched approximation which indicate that $\mu_c \to 0$ as $ma \to 0$.

7.4.2 Results at intermediate couplings

Simulations were performed by I.M. Barbour and Z.A. Sabeur [56] on a 4^4 lattice at two values of β and two quark masses. The partition function was expanded in terms of the canonical partition functions using the propagator matrix formalism.

Simulations at $\beta = 4.9$ and $ma = 0.05$ and 0.025 are in the confined phase at $\mu = 0$. These simulations show a clear signal for a phase transition at a non-zero value of the chemical potential.

Assuming positivity and continuity of the canonical partition functions, the number density may be evaluated as a function of μ.

$$\rho = \frac{1}{V}\frac{\partial}{\partial\mu}\ln Z \tag{7.39}$$

$$= \frac{1}{V}\frac{\sum_{n=1}^{N} Z_n n n_t \sinh(3nn_t\mu)}{\sum_{n=0}^{N} Z_n n n_t \cosh(3nn_t\mu)} \tag{7.40}$$

Plots of number density against chemical potential show an abrupt change of slope at a value of μ around 0.3. The lattice then fills over a range of μ up to about 1.0 .(Figures (7.3 a & b))

We may also define μ_c as the value of the chemical potential when the lattice is as likely to have three fermions as it is to be empty :

$$Z_0 = Z_3 \cosh(3n_t\mu_c) \tag{7.41}$$

This gives $\mu_c = 0.35$ at $ma = 0.05$ and $\mu_c = 0.30$ at $ma = 0.025$. This is in agreement with the values obtained from the density function.

In this study we extend the investigation to the examination of the zeros of the partition function. The partition function may be expressed as a polynomial in $e^{n_t\mu}$ which may be solved for the zeros. In Figures (7.4 a & b) a plot is shown of the zeros in the complex e^{μ} plane. The zeros form two rings (corresponding to μ and $-\mu$) and approach the real axis over a range of values which starts from around μ_c as calculated above and extends over the region in which the transition takes place.

At $\beta = 5.05$ we are already in the deconfined phase at $\mu = 0$. We do not, therefore, expect to see any signal for a phase transition at finite chemical potential in this case. The density function varies smoothly from zero at $\mu = 0$ till the lattice fills, with no sharp change in slope. (Figure (7.5))

The zeros of the partition function have a markedly different distribution from that of the zeros at $\beta = 4.9$. The zeros still have absolute values which cover the transition region.This is to be expected since we expect the distribution to vary smoothly as we increase β. In this case, however, the zeros do not approach the real axis. (Figure (7.6))

7.5 Conclusions

The examination of partition function zeros is a very effective method in the stydy of QCD at finite chemical potential. The distribution of zeros gives a clear indication of the presence or otherwise of a phase transition, the zeros approaching the real axis only for temperatures below T_c, the critical temperature at zero chemical potential. This signal is much clearer than that obtained from the baryon number plots. The critical chemical potential for the phase transition may be estimated from the distribution of zeros or calculated from the original

polynomial.

The method has the disadvantage that the propagator matrix is neither hermitian nor antihermitian. This means that the Lanczos vectors must be reorthogonalised during the tridiagonalisation. We cannot avoid this as we do in the mass zeros case since there is no analogue of Sturm Sequences in the case of complex eigenvalues. The storage space required for all the Lanczos vectors limits the size of lattice to which this method may be applied.

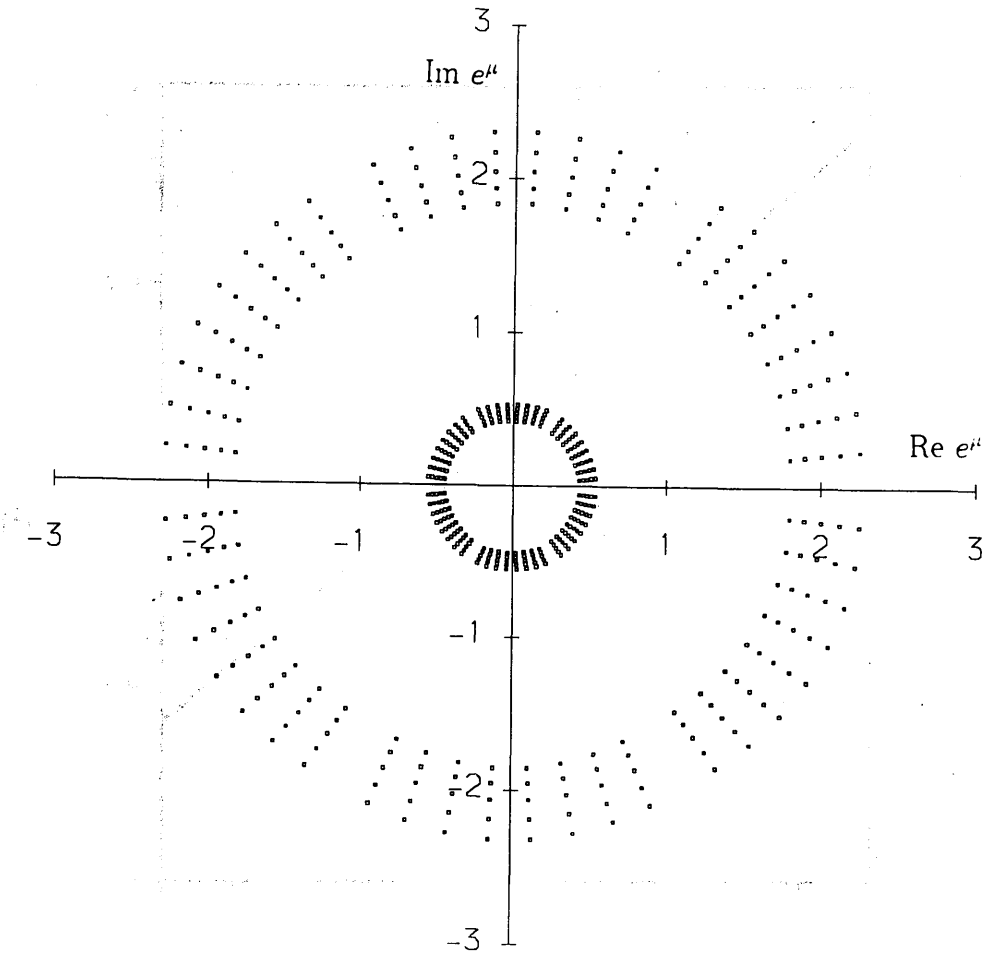

Figure 7.1 : Zeros of the partition function in the e^{μ} plane at $\beta = 0.0$ on a 2^4 lattice. The five circles of zeros correspond to $ma = 0.0, 0.1, 0.2, 0.3, 0.4$. The $ma = 0.0$ result comes from a linear extrapolation of b.

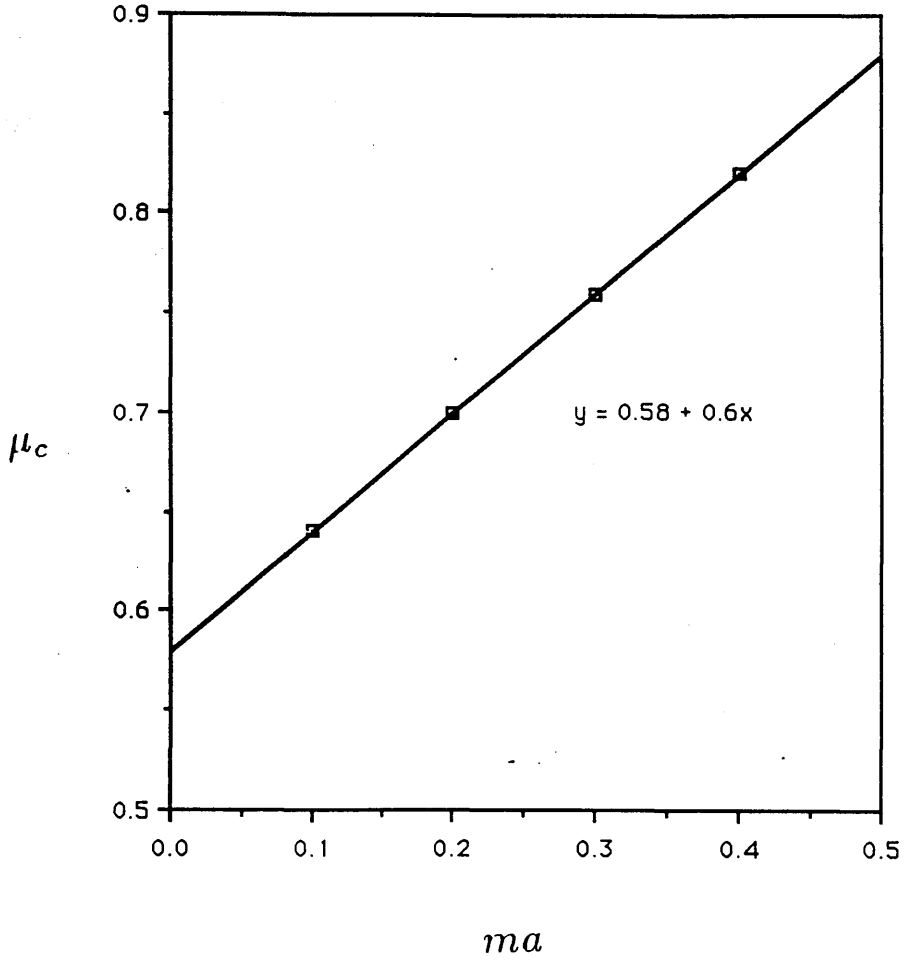

Figure 7.2 : Linear fit to μ_c on the 2^4 lattice as a function of ma. This shows the linear extrapolation to $ma = 0.0$.

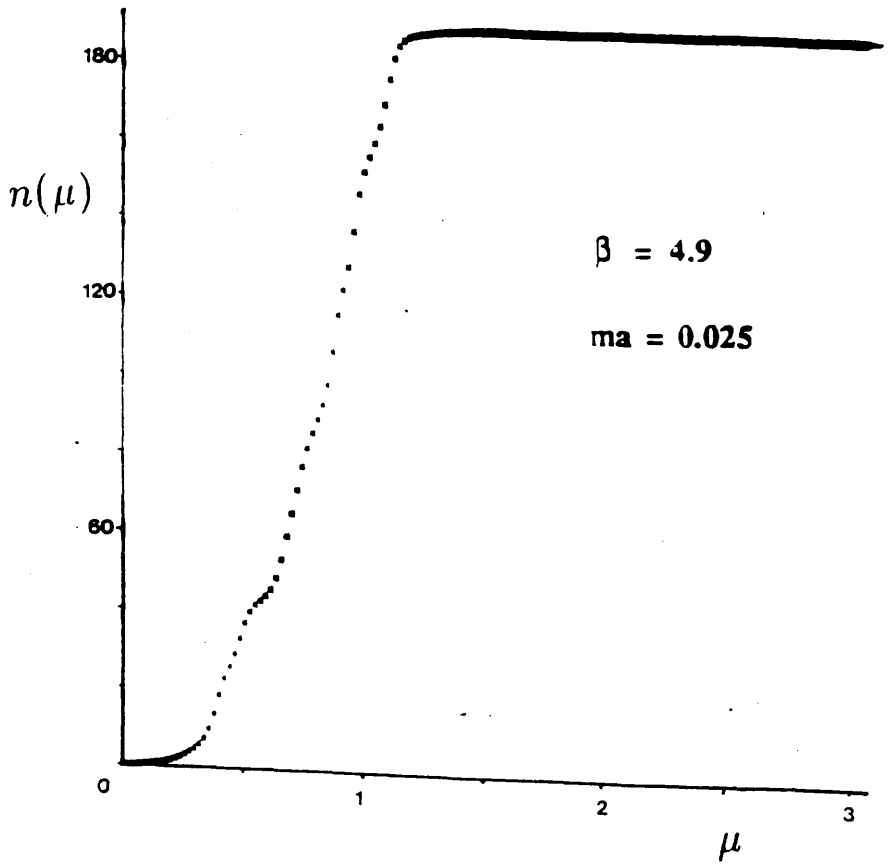

Figure 7.3a : The baryon number density as a function of μ at $\beta = 4.9$ and $ma = 0.025$. The kink at $\mu \sim 0.5$ is non-physical and is due to the higher coefficients in the expansion being less well determined. Figure taken from reference [56].

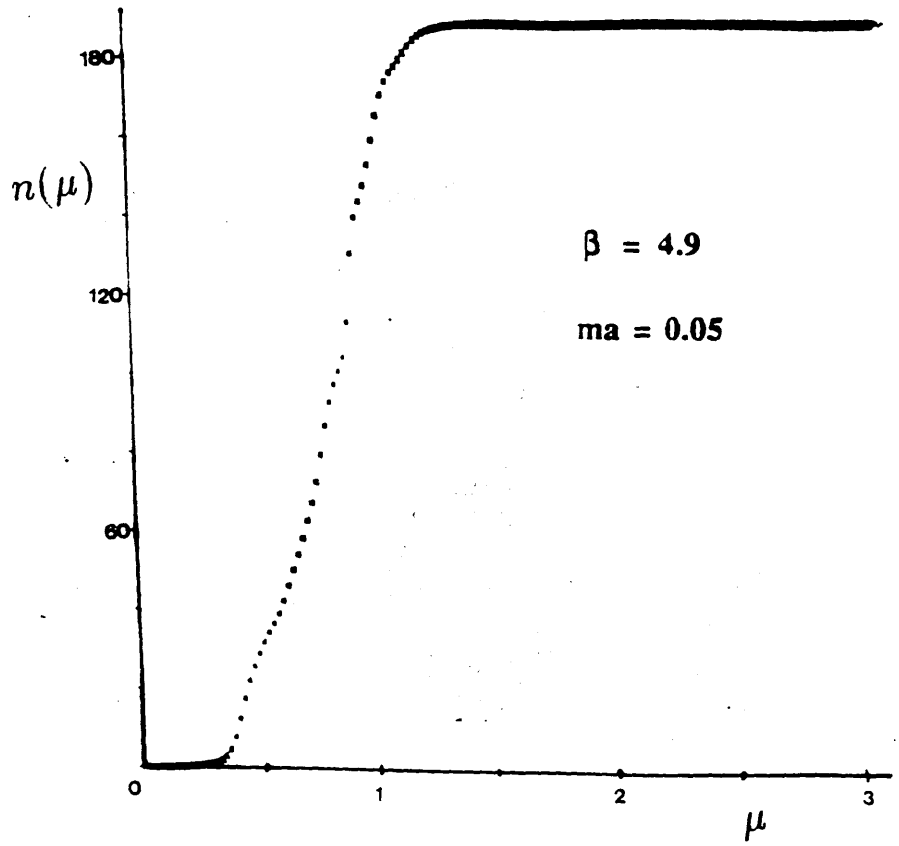

Figure 7.3b : The baryon number density as a function of μ at $\beta = 4.9$ and $ma = 0.05$. Figure taken from reference [56].

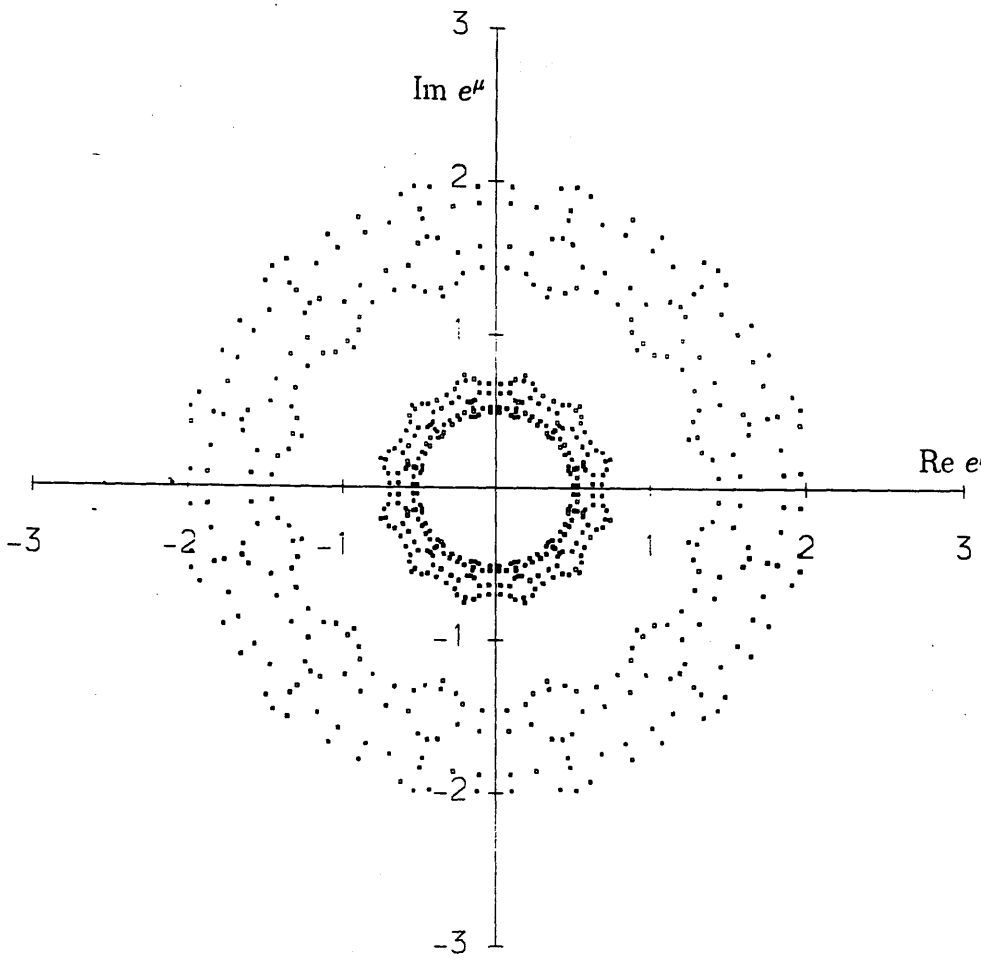

Figure 7.4a : Partition function zeros in the e^{μ} plane for $\beta = 4.9$ and $ma = 0.025$.

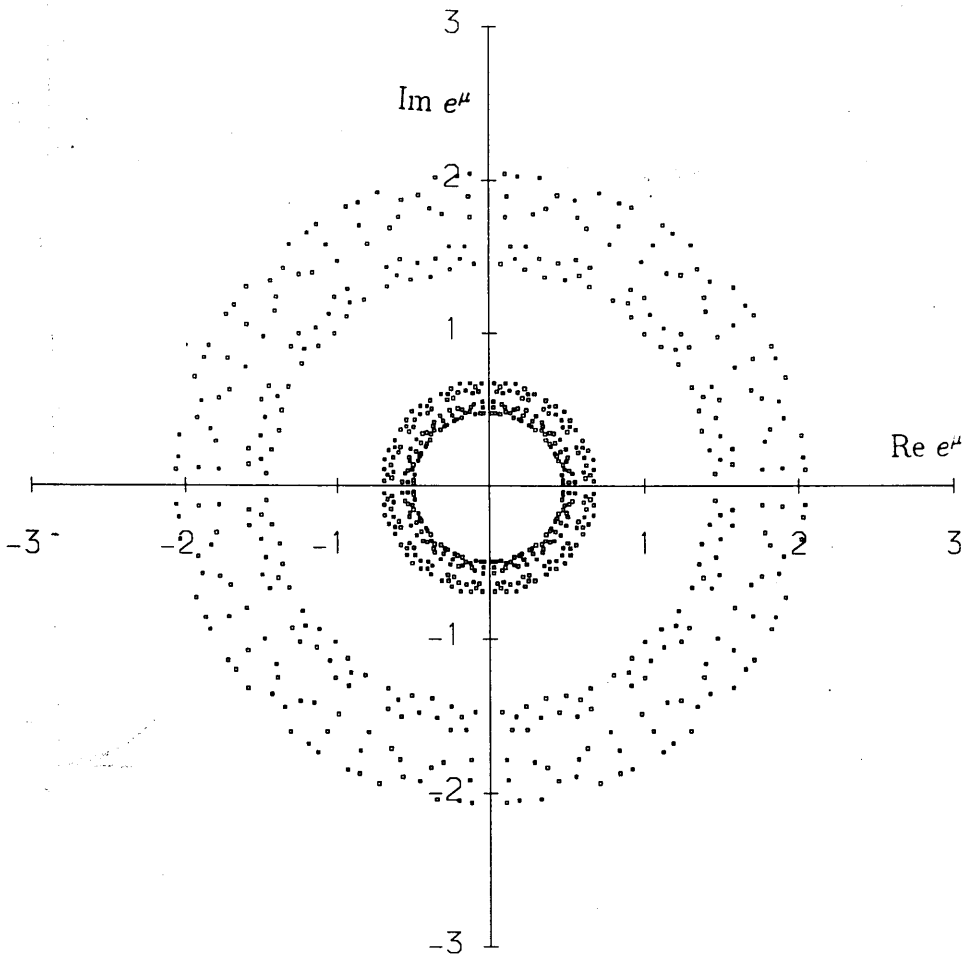

Figure 7.4b : Partition function zeros in the e^{μ} plane for $\beta = 4.9$ and $ma = 0.05$.

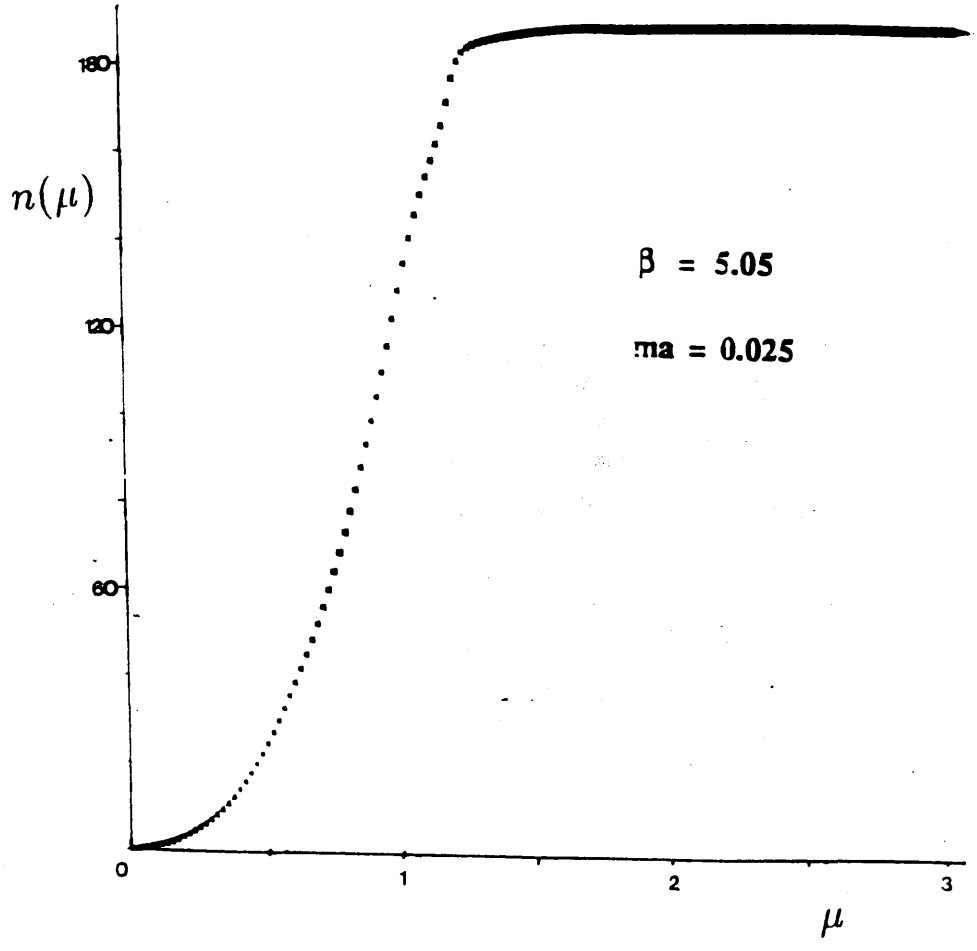

Figure 7.5 : The baryon number density as a function of μ at $\beta = 5.05$ and $ma = 0.025$. Figure taken from reference [56].

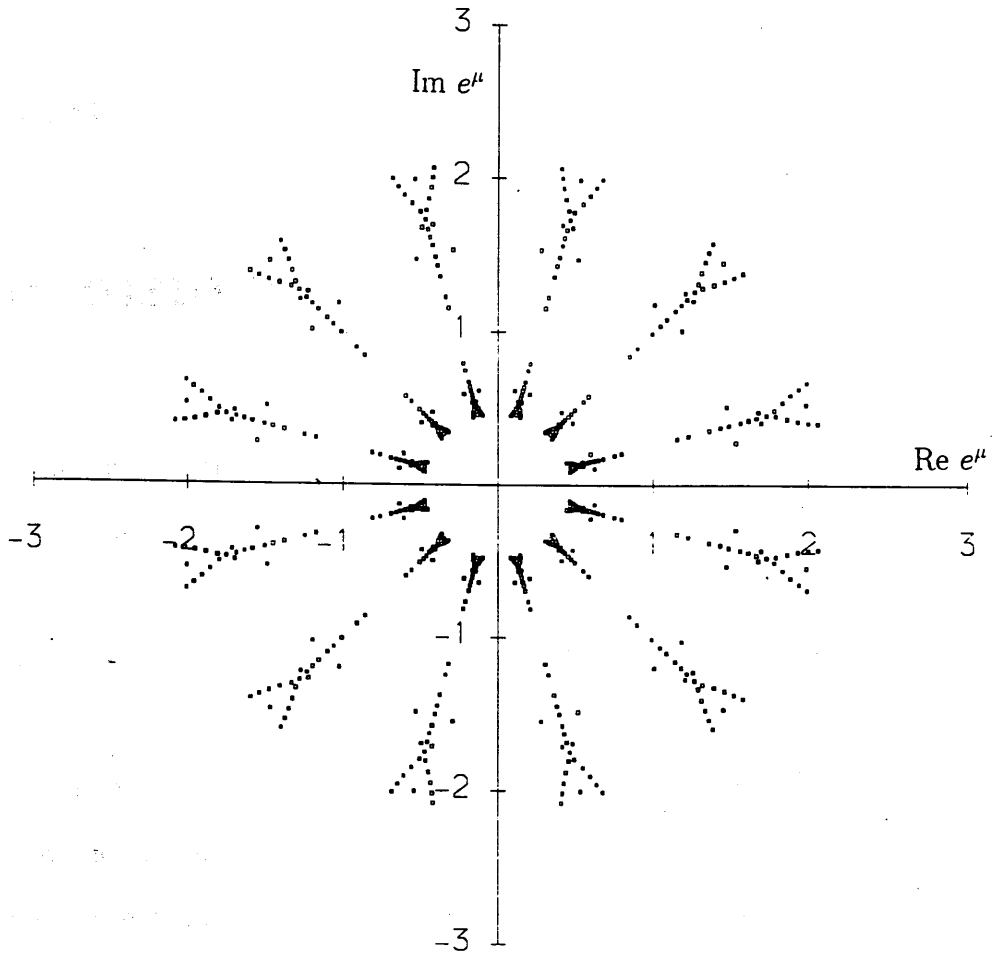

Figure 7.6 : Partition function zeros in the e^{μ} plane for $\beta = 5.05$ and $ma = 0.025$.

Chapter 8

Conclusions

We have shown that the study of partition function zeros is a powerful tool in the investigation of the phase structure of lattice field theories with staggered fermions.The method is useful both in the case of QCD at finite baryon number density and for the study of the effects of a finite bare mass on the chiral phase transition.

Unfortunately, the computing power available to this study did not permit the continuation to very large lattices for lattice QCD. It is hoped that the work on $U(1)$ will be extended to larger lattices, both in the compact and non-compact formulations. The study of the scaling behaviour of the zeros, especially those closest to the real axis, will yield important information regarding the order of any phase transition.

8.1 Other applications

The work of Lee and Yang is applicable to any statistical mechanics system. The method proposed here may be used in the study of fermionic systems in which the partition function can be expressed as the expectation value of a determinant. If one can arrange that a particular variable appears only on the diagonal of the matrix in question, then the characterisic polynomial, in that variable, can be

averaged and used to find the partition function zeros. This work is currently being applied to two such systems. These systems are described below. No results are quoted since my involvement in the work extended only to the initial setting up and the provision of some of the computer code. The purpose of the following sections is to show the wider applicability of the previously described work.

8.1.1 Wilson Fermions

In this thesis we have applied the theory of Lee and Yang to gauge theories with staggered fermions. The method is equally applicable to the Wilson formulation of lattice fermions where the expansion is performed in powers of $\frac{1}{\kappa}$, κ being the hopping parameter which determines the mass of the fermions.

The action for Wilson fermions is

$$\begin{aligned} S &= \sum_x \overline{\psi}(x)\psi(x) \\ &\quad -\kappa \sum_x \sum_\mu \left(\overline{\psi}(x)(1-\gamma_\mu)U_\mu(x)\psi(x+\mu) + \overline{\psi}(x+\mu)(1+\gamma_\mu)U_\mu^\dagger(x)\psi(x) \right) \\ &= \overline{\psi}(1-\kappa \not{D})\psi \end{aligned} \tag{8.1}$$

If one multiplies through by $1/\kappa$, the hopping parameter may be moved onto the diagonal and we may proceed in the same way as for staggered fermions.

The fermion determinant for Wilson fermions, $\det M = \det(1-\kappa \not{D})$, is real since $\gamma_5 M^\dagger \gamma_5 = M$, but not positive definite. In order to interpret the determinant as a probability density we must use $\det(M^\dagger M)$ as the update weight. Thus, HMC simulations of dynamical Wilson fermions is restricted to multiples of two degenerate flavours. Since $\not{D}$ is not an antihermitian matrix one might expect that the expansion of the characteristic polynomial will have both odd and even powers of κ. However, since the eigenvalues come in sets of four, λ, $-\lambda$, λ^* and $-\lambda^*$, we may write

$$\det M = \prod_{i=1}^{N}(1-\kappa\lambda_i) \tag{8.2}$$

$$= \prod_{i=1}^{N/2}(1-\kappa^2\lambda_i^2) \tag{8.3}$$

Since $\det M$ is real, $\det M^\dagger = \det M$ and the update weight is

$$\text{update weight} = (\prod_{i=1}^{N/2}(1-\kappa^2\lambda_i^2))^2 \tag{8.4}$$

$$= (\det(1-\kappa^2 \not{D}^2)_e^2 \tag{8.5}$$

where the determinant is over only even (or odd) sites.

The expansion which we want to make is thus

$$\tilde{Z}(\kappa) = (\det(\not{D}^2 - (\frac{1}{\kappa})^2))^2 \tag{8.6}$$

$$= \sum_{i=1}^{N/2} a_i \kappa^{-2i} \tag{8.7}$$

This system is currently being studied, at strong coupling and on small lattices, by a collaboration involving physicists at Glasgow and Edinburgh, using Maxwell, the UKQCD parallel supercomputer. An investigation is also being carried out of partition function zeros for both one and two flavours of Wilson fermions using pure gauge updating. Since the partition function is insensitive to the overall multiplicative factor which is introduced by the average sign of the determinant, it is also planned to simulate a single flavour of Wilson fermions using $|\det M|$ in the updating procedure. The usually quoted value for the critical value of κ which gives zero mass quarks, $\kappa_c = 0.25$ at $\beta = 0.0$, is calculated in the quenched approximation. It is hoped that the study of partition function zeros will indicate the value of κ_c in the presence of dynamical quarks.

8.2 The Hubbard Model

The Hubbard model is the simplest model for electrons in a metal. The hamiltonian for the model is given by [57]

$$H = -t \sum_{\langle i,j\rangle,\sigma} c_{i,\sigma}^\dagger c_{j,\sigma} + U\sum_i (n_{i+} - \frac{1}{2})(n_{i-} - \frac{1}{2}) - \mu \sum_i (n_{i+} + n_{i-}) \tag{8.8}$$

where $\langle i, j \rangle$ denotes nearest neighbour lattice sites, σ denotes the spin degree of freedom and $n_{i\sigma}$ the electron number operator $c\,\dagger_{i\sigma}\, c_{i\sigma}$. The constant t is the hopping parameter which allows electrons to move from site to site, and U represents the on-site Coulomb repulsion.

The numerical simulation of the Hubbard model with a finite electron density has attracted much attention due to the suggested relation between the 2-D Hubbard model and high T_c superconductivity. Since this problem is essentially non-relativistic, many problems, such as fermion doubling, are avoided. However, the inherent difficulties of simulating fermions at finite density can not be avoided completely.

We have already seen that in the case of QCD at finite chemical potential the fermionic determinant becomes complex and any importance sampling based on this determinant ceases to be well defined in terms of probability densities.

In the Hubbard model, the partition function is always real. In the case of the half-filled Hubbard model (one electron per site) the partition function can be expressed as the product of the determinants of a matrix and its complex conjugate and is thus positive definite.

$$\begin{aligned} Z(\mu = 0) &\propto \left\langle \det M \det M^{\dagger} \right\rangle \\ &= \langle (\det M)(\det M)^{*} \rangle \end{aligned} \tag{8.9}$$

However, if a real, finite chemical potential is introduced for the impurities (holes) then this positivity is lost and we can have configurations with real, negative determinants. Two solutions to this problem are currently being investigated [58].

Since the update action contributes only a multiplicative constant to the partition function, we can follow the same route as in the QCD case and update at $\mu = 0$. The partition function can then be expanded as a polynomial in $e^{\mu\beta}$, where β is the inverse temperature. This temperature is introduced by extending the

2-D lattice in a third, imaginary time, direction and relating β to the temporal extent by $\beta = n_\tau\ \delta t$ where n_τ is the number of time slices and δt is the time-step. The resulting polynomial expression for the partition function can then be solved for the partition function zeros. Alternatively, differentiation with respect to μ will give the hole density as a function of μ.

Another approach is to choose the updating chemical potential, μ_0, such that the first few terms in the polynomial are of similar magnitude: if one updates at $\mu = 0$, then all other terms are small compared to the first and are therefore more susceptible to fluctuations. The lattice can then be updated using the absolute value of the weight function in the updating procedure and the first few coefficients, corresponding to the lowest excitations, can be determined reliably.

Preliminary results using both the above methods are encouraging and in good agreement both with each other and with previous studies [59].

It is probable that this method will prove useful in future studies of theories involving lattice fermions, both in lattice field theories and in non-relativistic Hubbard type models.

References

1. R. P. Feynman and A.R. Hibbs, *Quantum Mechanics and Path Integrals* (McGraw-Hill 1965)

2. K.G. Wilson, Phys. Rev. D10 (1974) 2445

3. D. Gross and F. Wilczec, Phys. Rev. Lett. 30 (1973) 1343
   H.D. Politzer, Phys. Rev. Lett. 30 (1973) 1346

4. C. Callan, Phys. Rev. D2 (1970) 1541
   K. Symanzik, Comm. Math. Phys. 49 (1970) 424

5. W. Caswell, Phys. Rev. Lett. 33 (1974) 244
   D.R.T. Jones, Nucl. Phys. B75 (1974) 531

6. B.J. Pendleton, in *'Computational Physics'*: Proceedings of SUSSP 1987, edited by R.D. Kenway and G.S. Pawley.

7. G. Schierholz, in *'Fundamental Forces'*: Proceedings of SUSSP 1984, edited by D. Frame and K.J. Peach.

8. M. Creutz, *'Quarks, Gluons and Lattices'*, (Cambridge U. P. 1983)

9. H.B. Nielsen and M. Ninomiya, Nucl. Phys. B193 (1981) 173
   H.B. Nielsen and M. Ninomiya, Phys. Lett. B105 (1981) 219

10. K.G. Wilson, in *'New Phenomena in Subnuclear Physics'*, ed. A. Zichichi (Plenum 1977)

11. L. Susskind Phys. Rev. D16 (1977) 3031
N. Kawamoto and J. Smit, Nucl. Phys. B192 (1981) 100

12. N. A. Metropolis, M.N. Rosenbluth, A.M. Rosenbluth, E. Teller, J. Teller, J. Chem. Phys. 21 (1953) 1057

13. G.G. Batrouni, G.R. Katz, A.S. Kronfeld, G.P. Lepage, B. Svetitsky, K.G. Wilson, Phys. Rev. D32 (1985) 2736

14. D.J.E. Callaway and A. Rahman, Phys. Rev. Lett. 49 (1982) 613

15. J. Polonyi and W.H. Wylde, Phys. Rev. Lett. 51 (1983) 2257

16. S. Duane, Nucl. Phys. B257[FS14] (1985) 652
S.Duane and J.B. Kogut, Nucl. Phys. B275 (1986) 398

17. S. Duane, A.D. Kennedy, B.J. Pendleton, D. Roweth, Phys. Lett. B195 (1987) 216

18. J. Kuti, in *'Computational Physics'*: Proceedings of SUSSP 1987, edited by R.D. Kenway and G.S. Pawley.

19. S. Gottlieb, W. Liu, D. Toussaint, R.L. Renken, R.L. Sugar, Phys. Rev. D35 (1987) 2531

20. A.D. Kennedy and B.J. Pendleton, Nucl. Phys. B(Proc. Supl.)20 (1991) 118.Proceedings of the 1990 Conference on Lattice Field Theory, Tallahassee, Florida.

21. R. Gupta, G.W. Kilcup, S.R. Sharpe, Phys. Rev. D38 (1988) 1278

22. K. Bitar, A.D. Kennedy, R. Horsely, S. Meyer, P. Rossi, Nucl. Phys. B313 (1989) 377

23. P.B. Mackenzie, Phys. Lett. B226 (1989) 369

24. P.B. Mackenzie, Nucl. Phys. B(Proc. Supl)17 (1990) 103
Proceedings of the 1989 Symposium on Lattice Field Theory, Capri, Italy.

25. C. Lanczos, J. Res. Nat. Bur. Stand. 49 (1952) 409

26. P. Gibbs, *'Applications of the Lanczos algorithm to Lattice QCD'*. Glasgow University thesis 1985.

26a. A.N. Burkitt and A.C. Irving, Phys. Lett. B205 (1988) 69

27. C.T.H. Davies, D.S. Henty & R. Setoodeh, Nucl. Phys. B337 (1990) 487

28. C.N. Yang and T.D. Lee, Phys. Rev. 87 (1952) 404

29. C.N. Yang and T.D. Lee, Phys. Rev. 87 (1952) 410

30. M. Fisher, in *Lectures in Theoretical Physics* vol. 12C p.1 (University of Colorado Press, Boulder, 1965)

31. C. Itzykson, R.B. Pearson & J.B. Zuber, Nucl. Phys. B220[FS8] (1983) 415

32. M. Karliner, S.R. Sharp, Y.F. Chang, Nucl. Phys. B302 (1988) 204

33. G. Bhanot, S. Black, P. Carter & R. Salvador, Phys. Lett. B183 (1987) 331
G. Bhanot, K. Bitar, S. Black, P. Carter & R. Salvador, Phys. Lett. B187 (1987) 381
G. Bhanot, K. Bitar & R. Salvador, Phys. Lett. B188 (1987) 246

34. V. Azcoiti, A. Cruz, G. Di Carlo, A. Taracón, Nucl. Phys. B(Proc. Supl)17 (1990) 727
Proceedings of the 1989 Symposium on Lattice Field Theory, Capri, Italy.

35. T. Jolicoeur, H. Kluberg-Stern, A. Morel, M. Lev, B. Petersson, Nucl. Phys. B235[FS11] (1984) 455

36. E.V.E. Kovacs, D.K. Sinclair and J.B. Kogut, Nucl. Phys. B290 (1987) 431

37. S. Gottleib, Nucl. Phys. B(Proc. Supl.)20 (1991) 247
Proceedings of the 1990 Conference on Lattice Field Theory, Tallahassee, Florida.

38. A. Vaccarino, Nucl. Phys. B(Proc. Supl.)20 (1991) 263
Proceedings of the 1990 Conference on Lattice Field Theory, Tallahassee, Florida.

39. S. Gottlieb, W. Liu, D. Toussaint, R.L. Renken, R.L. Sugar, Phys. Rev. D35 (1987) 3972

40. R. Gupta, G. Guralnik, G.W. Kilcup, A. Patel, S. Sharpe, Phys. Rev. Lett. 57 (1986) 2623

41. R. Gupta, G. Guralnik, G.W. Kilcup, A. Patel, S. Sharpe, Phys. Lett. B201 (1988) 503

42. K. Bitar, A.D. Kennedy, R. Horsely, S. Meyer, P. Rossi, Nucl. Phys. B313 (1989) 348

43. R. Gupta, G.W. Kilcup & S.R. Sharpe, Phys. Rev. D38 (1988) 1288

44. J.B. Kogut, Nucl. Phys. B270[FS16] (1986) 169

45. D.K. Sinclair, Nucl. Phys. B(Proc. Supl)17 (1990) 554
Proceedings of the 1989 Symposium on Lattice Field Theory, Capri, Italy.
J.B. Kogut and D.K. Sinclair, Phys. Lett. B229 (1989) 107

46. M. Fukugita and A. Ukawa, Phys. Rev. D38 (1988) 1971

47. C. DeTar and J.B. Kogut, Phys. Rev. D36 (1987) 2828

48. J.B. Kogut and E. Dagotto, Phys. Rev. Lett. 59 (1987) 617
E. Dagotto and J.B. Kogut, Nucl. Phys. B295 (1988) 123

49. V. Azcoiti, G. Di Carlo and A.F. Grillo, Phys. Rev. Lett. 65 (1990) 2239
V. Azcoiti, A. Cruz, G. Di Carlo, A.F. Grillo and A. Vladikas, Nucl. Phys. B(Proc. Supl.)20 (1991) 650.Proceedings of the 1990 Conference on Lattice Field Theory, Tallahassee, Florida.

50. P. Hasenfratz and F. Karsch, Phys. Lett. B215 (1983) 308

51. P.E. Gibbs, Phys. Lett. B182 (1986) 369

52. A. Vladikas, Nucl. Phys. B (Proc. Suppl.)4 (1988) 322
Proceedings of the International Symposium on Field Theory on the Lattice, Seillac, France, 1987

53. C.T.H. Davies and E.K. Klepfish Phys. Lett. B256 (1991) 68

54. P.E. Gibbs, Phys. Lett. B172 (1986) 53

55. I.M. Barbour, C.T.H. Davies & Z.A. Sabeur, Phys. Lett. B215 (1988) 567

56. I.M. Barbour and Z.A. Sabeur Nucl. Phys. B342 (1990) 269
Z.A. Sabeur, *'Lattice QCD at finite density with dynamical fermions'* Glasgow University Thesis,1990

57. S.R. White, D.J. Scalapino, R.L. Sugar, E.Y. Loh, Jr., J.E. Gubernatis and R.T. Scalettar, Phys. Rev. B40 (1989) 506and references therein.

58. I.M. Barbour and E. Klepfish, *paper in preparation.*

59. A. Moreo, Talk presented at Canadian Workshop in Theoretical Physics, Kingston, Ontario, July 1991.